https://doi.org/10.57634/RCR5072

Low-dimensional group IV – VII transition metal polychalcogenides and chemical aspects of their applications

Ekaterina D. Grayfer,[a, b]* Sofya B. Artemkina,[a] Mariia N. Ivanova,[a] Konstantin A. Brylev,[a] Vladimir E. Fedorov [a]

[a] *Nikolaev Institute of Inorganic Chemistry, Siberian Branch of the Russian Academy of Sciences, Prosp. Academika Lavrentieva 3, 630090 Novosibirsk, Russian Federation*
[b] *Skolkovo Institute of Science and Technology, Bolshoy bulv. 30, stroenie 1, 121205 Moscow, Russian Federation*

This review systematizes literature data on polymeric polychalcogenides of group IV – VII transition metals (TiS_3, VS_4, $NbSe_3$, MoS_x, ReS_4, *etc.*). It covers the structural characteristics of crystalline compounds and the proposed structural models of amorphous phases. The latest advances in the synthesis of these low-dimensional materials at the nanoscale are presented. Their chemical properties are discussed, in particular, those arising from the presence of the dichalcogenide bonds. It is emphasized that the properties of the S – S (or Se – Se) groups largely determine the distinctive features of polychalcogenides and the unusual phenomena observed in them. In particular, these groups play an important role in the performance of electrode materials in metal-ion batteries, photo- and electrocatalysts for hydrogen evolution reaction, and mercury vapour sorbents based on transition metal polychalcogenides, which is also addressed in this review.
The bibliography includes 304 references.

Contents

1. Introduction

Metal polychalcogenides are inorganic compounds where anions are formed by interconnected chalcogen atoms of the $(Q-Q)^{2-}$ type, where Q = S, Se, Te. Such linkage is well known for elemental sulfur and selenium, the structure of which comprises stable chains and cycles (S_8, S_6, S_4, Se_4), and also for Li_2S_x-like alkali metal ionic polysulfides (S_8^{2-}, S_6^{2-}, S_4^{2-}, S_2^{2-}),[1–3] for organic[4] and biological[5] systems. Transition metal complexes containing Q_x ($x = 2–6$) moieties as chelate and bridging ligands (Fig. 1 *a*,*b*) are also very numerous.

Key molecular representatives of polychalcogenides have been considered in detail in earlier reviews[14–22] prepared by our scientific group and other researchers. A critical view on polychalcogenide anions is presented in the review.[23]

This review addresses low-dimensional group IV – VII transition metal polychalcogenides (TMPC) (TiS_3, VS_4, $NbSe_3$, MoS_x, ReS_4, *etc.*), which are compounds with extended structures (quasi-1D, -2D). They are composed of covalently bonded chains or layers that interact with each other *via* van der Waals forces (Fig. 1 *c*–*g*).

The family of low-dimensional group IV – VII metal polychalcogenides comprises crystalline MQ_3 trichalcogenides (M = Ti, Zr, Hf, Nb, Ta; Q = S, Se, Te)[12,24–83] (see Fig. 1 *f*), MQ_4 tetrachalcogenides (VS_4,[8,84–111] NbS_4,[112] $NbTe_4$,[113,114] $TaTe_4$[113,115]) (see Fig. 1 *c*), M_2Se_9 dimetal nonaselenides (V_2Se_9 (see[116,117]) and Nb_2Se_9 (see[118])) (see Fig. 1 *d*) and a variety of the $MQ_{\approx 3}$-type amorphous phases (M = Cr, Mo, W; Q = S, Se)[68,119–142] (Fig. 2), MoS_4,[142–

Received 1 November 2022

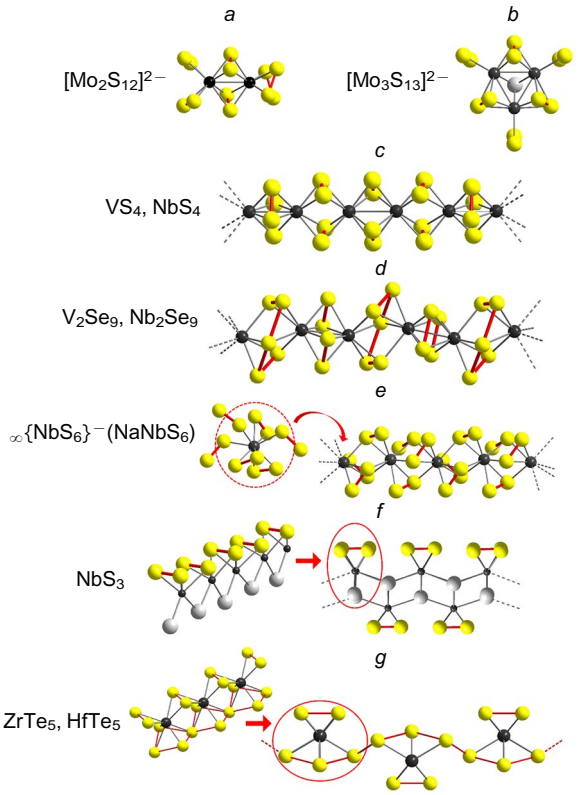

Figure 1. Structure of crystalline transition metal polychalcogenides. Cluster anions: $[Mo_2S_{12}]^{2-}$ (*a*),[2–6] $[Mo_3S_{13}]^{2-}$ (*b*).[2–7] Chain structures: MS_4 (M = V, Nb) (*c*),[8] M_2Se_9 (M = V, Nb) (*d*);[9,10] an example of ternary polychalcogenide: polysulfide $NaNbS_6$ — the structure comprises $_\infty\{NbS_6\}^-$ infinite chains, where Nb^{5+} ions are in a coordination environment of $(S_2)_3(S)_3$ disulfide groups (*e*).[11] Structures combining the properties of chain and layered compounds: NbS_3 (*f*),[12] MTe_5 (M = Zr, Hf) (*g*).[13] Here and below, transition metal atoms are marked in black; chalcogen atoms in an oxidation state of −2 are marked in light-grey; chalcogen atoms in an oxidation state of −1 (in Q–Q units) and higher (in longer chalcogen chains) are marked in yellow. Red colour indicates the 'chalcogen–chalcogen' bonds, the presence of which in the compound allows it to be assigned to the class of transition metal polychalcogenides.

[148] TiS_4,[149–151] MoS_5,[142,152,153] WS_5,[143,154] MoS_6,[142,152] $MoSe_{\approx 5}$, $WSe_{\approx 6-7}$,[155] $NbS_{\approx 2.5}$,[156] and also $MoSe_3$S-type chalcogen-mixed or metal-mixed phases,[157,158] $Nb_{1+x}V_{1-x}S_5$,[159] $Zr_{1-x}Ti_xS_3$ ($0 < x < 0.33$),[160,161] $Ti_{1-x}Nb_xS_3$,[162,163] $Nb_{1-x}Ta_xS_3$.[164] Moreover, $(Q_x)^{2-}$ chains ($x = 2–6$) are an important structural unit of such an interesting class of objects as MoS_x-type chalcogenide gels,[165–169] in which polychalcogenide chains are linked by metal ion bridges. Finally, there are ternary and quaternary polychalcogenides, whose structure is stabilized by halide ions or metal cations, most often, alkaline ones (see Fig. 1 *e*).[11,170]

It seems timely to systematize and generalize the latest data on TMPCs accumulated in recent years, since in the 2000s, these studies have evolved to a new stage. A large number of works have appeared on the preparation of these compounds at the nanoscale. Structures of amorphous phases have been refined, and in 2020–2022, novel polychalcogenides were prepared, previously thought to be nonexistent such as crystalline CrS_3,[175] NbS_4 [112] and WS_3.[176] However, practically-oriented research develops especially fast. On the one hand, these are applications in the new-generation electronics and optoelectronics devices based on TiS_3 and related materials,[28,29,39,40,42,50–52,59,61,65,67,69,80] in which the physical properties of TMPCs are important. On the other hand, these are areas, where chemical processes play an important role: electrodes of high-capacity metal-ion batteries, catalysis of hydrogen evolution reaction, photocatalytic decomposition of organic molecules, and sorption of toxic vapours. To a large extent, these functional properties

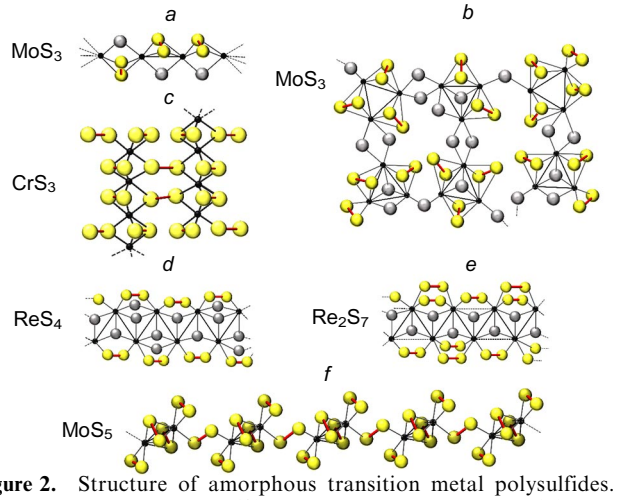

Figure 2. Structure of amorphous transition metal polysulfides. Chain model for MoS_3 (*a*),[123] cluster model for MoS_3 (*b*),[171] CrS_3 (*c*),[172] ReS_4 (*d*),[173] Re_2S_7 (*e*),[173] MoS_5 (*f*).[174] The Figure was prepared by the authors using original data from the cited publications.

E.D.Grayfer. PhD in Chemistry, Executor of the Project of RSF 21-13-00274 of the NIIC SB RAS.
E-mail: grayfer@niic.nsc.ru
Current research interests: carbon nanomaterials, transition metal chalcogenides, composite materials based on layered and chain chalcogenide compounds.
S.B.Artemkina. PhD in Chemistry, Senior Researcher at the Laboratory of the Synthesis of cluster compounds and materials of the same Institute.
E-mail: artem@niic.nsc.ru
Current research interests: metallocluster complexes, transition metal chalcogenides, composite materials based on layered and chain chalcogenide compounds.
M.N.Ivanova. PhD in Chemistry, Researcher at the same Laboratory.
E-mail: kozlova@niic.nsc.ru
Current research interests: transition metal chalcogenides, composite materials based on layered and chain chalcogenide compounds.
K.A.Brylev. Doctor of Chemical Sciences, Professor of RAS, Director of the same Institute.
E-mail: brylev@niic.nsc.ru
Current research interests: metallocluster complexes, coordination chemistry, transition metal chalcogenides.
V.E.Fedorov. Doctor of Chemical Sciences, Professor, Laureate of the L.A. Chugaev RAS Prize, Honored Scientist of the Russian Federation, Chief Researcher of the same Laboratory.
E-mail: fed@niic.nsc.ru
Current research interests: carbon nanomaterials, coordination chemistry, metallocluster complexes, transition metal chalcogenides and chalcohalides, low-dimensional (1D and 2D) compounds, including composite materials based on layered and chain chalcogenide compounds.

Translation: N.M.Vinogradova

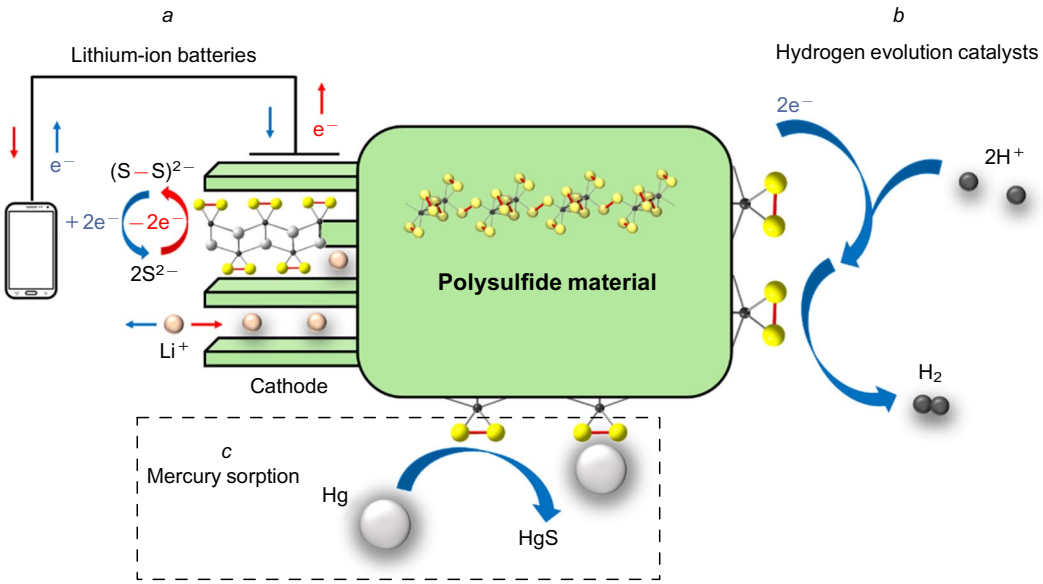

Figure 3. Schematic of several practically relevant processes, in which polysulfide materials are explored: cathode materials for lithium-ion batteries (*a*); catalysts for hydrogen evolution reactions (can act as photo-, electro- and photoelectrocatalysts) (*b*); mercury vapour sorbents (*c*). The $(S-S)^{2-}$ groups of the material, which are involved in reversible redox transformations, play a special role.

depend on the structure and chemical properties of materials, in particular, on transformations in di- or poly-chalcogenide anions. It is proved that $(S-S)^{2-}/(Se-Se)^{2-}$ groups are involved in redox processes occurring in the electrodes of lithium-ion batteries [68, 90, 105, 108, 109, 140, 142, 169, 177–180] or in electrocatalysts (Fig. 3).[53, 125, 126, 128, 133, 136, 138, 181, 182]

Thus, during charge/discharge of a battery, an anionic disulfide group in the electrode material undergoes a reversible redox transformation: $S_2^{2-} + 2e^- \rightleftarrows 2S^{2-}$ (Fig. 3 *a*).[177] As a result, the involvement of both cations and anions in the redox processes on the electrode makes it possible to accomplish multielectron reactions and hence, to achieve higher capacities. At the same time, layered or chain structures of the electrode material can potentially contribute to stable cycling. Disulfide units $(S-S)^{2-}$ are also involved in electrocatalytical processes, *e.g.*, in the hydrogen evolution reaction (HER), which is important from the practical point of view and is now being actively studied. Much evidence suggests that it is the $(S-S)^{2-}$ groups that act as active centres in the electro- and photocatalysts like FeS_2, MoS_3 and ZrS_3 (Fig. 3 *b*). Moreover, it is interesting that their important role in electrocatalysis is observed not only for polysulfide materials,[53, 181] where all sulfur exists as S_2^{2-}, but also for the edge disulfide centres of nanosized MoS_2, which is not a polysulfide but contains terminal sulfur dimers.[7, 183–185] Numerous proofs of this fact have been obtained using molecular models [186] (clusters like $[Mo_2S_{12}]^{2-}$ (Ref. 6) and $[Mo_3S_{13}]^{2-}$ (Ref. 7), see Fig. 1 *a*,*b*), which once again illustrate the intimate connection between the chemistry of molecular and non-molecular polychalcogenides. The above examples show that diverse structurally distinct polychalcogenides have in fact many common properties due to the presence of polysulfide groups S_n. Therefore, it is worth considering low-dimensional TMPCs as a separate class of compounds and to summarize recent related data accordingly.

Most of the reviews on polychalcogenides were written more than 20 years ago.[24, 170, 187–192] Some recent reviews have focused on specific members of the TMPC family: in 2007–2022, papers were published regarding amorphous molybdenum polysulfides [119–121] and group IV metal trichalcogenides (TiS_3, ZrS_3, *etc.*),[26–29, 82] however, they highlighted mainly electronic properties and prospects for applying such materials in electronics.

In this review, we consider a wide range of polychalcogenide materials trying to demonstrate their similarity, and emphasize more their chemical properties and the applications they define, in particular as electrocatalysts and electrode materials (the concept of their functioning we have recently summarized [177]). We will focus on the structural features of TMPCs, methods for the synthesis of their nanostructures, chemical properties, present latest advances in the use of these materials as electrodes in metal ion batteries, photo- and electrocatalysts, *etc.*, and describe our views on the further development of their chemistry and applications. The review will largely discuss sulfides, since most of the results accumulated in the literature apply to them; at the same time, if possible, data on selenides and tellurides will be presented.

2. Structures of transition metal polychalcogenides

Since the family of low-dimensional transition metals polychalcogenides includes a large number of representatives with different structures and compositions, it is useful to distinguish several groups. For instance, pure polychalcogenides containing chalcogen atoms only as $(Q_2)^{2-}$ groups such as VS_4, MoS_5, CrS_3, NbS_4, $NbTe_4$, $TaTe_4$, $ZrTe_5$ can be considered separately. Mixed polychalcogenides, such as layered trichalcogenides MQ_3, contain both dichalcogenide and monochalcogenide groups. It is possible to classify TMPCs in a different way and to consider separately crystalline materials, which structures have been determined, and purely amorphous materials, for which no crystalline analogues have been obtained, and whose structures have been determined using a combination of indirect data from various methods. Section 2 of this review is based on the latter classification. (1D/2D) layered-chain crystal structures characteristic of metal trichalcogenides MQ_3, linear chain (1D) structures of VS_4 and also structures of several amorphous metal polychalcogenides will be discussed briefly below.

2.1. Structures of crystalline transition metal polychalcogenides

Crystal structures of low-dimensional transition metal polychalcogenides are diverse (see Fig. 1), since chalcogens can serve as bridging and terminal ligands Q^{2-} and $(Q_2)^{2-}$, and V–VII group metals can form metal–metal bonds (metal cluster complexes). The structures in question are defined by 1) the formation of strong dichalcogenide units with short Q–Q bond lengths (~2.0–2.1, 2.3–2.9 and 2.8–3.0 Å for Q = S, Se and Te, respectively) and 2) the presence of weakly bonded layers or chains (van der Waals solids). Several structural types characteristic of low-dimensional transition metal polychalcogenides can be distinguished.

Trichalcogenides of IV and V group metals of general formula MQ_3 (M = Ti, Zr, Hf, Nb, Ta; Q = S, Se, Te) make up a family of compounds with slightly different structures,[12,24–81] which can be considered as derivatives of $ZrSe_3$ structure (monoclinic syngony, $P2_1/m$ space group). These structures are composed of the $MQ_{6/2}$ trigonal prismatic columns, which in turn are made up of MQ_6 elementary prisms sharing their triangular faces and extending along the b-axis (see Fig. 1*f*). In a triangular base of the prisms, two chalcogen atoms are bonded into dichalcogenide groups [*e.g.*, d_{S-S} = 2.04 Å (TiS_3), d_{Se-Se} = 2.34 Å ($ZrSe_3$)], while one chalcogen ligand is a sulfide or selenide ion (S^{2-} or Se^{2-}). Since chalcogen atoms in MQ_3 structures are in two electronic states, the formula for trichalcogenides can be represented as $M^{4+}Q^{2-}Q_2^{2-}$. Shape and packing of prisms differ for various trichalcogenides. Polymorphism of NbS_3 is addressed in a recent study.[12] Covalently bonded columns in MQ_3 structures determine their quasi-1D nature. On the other hand, there is also strong covalent bonding between the prisms from neighbouring columns, connecting the chains into layers (quasi-2D structure), which in turn are linked by van der Waals contacts. Thus, trichalcogenides are characterised by the combined properties of 1D/2D materials.

The recently synthesized crystalline chromium trisulfide[175] (Fig. 4) differs significantly in structure from crystalline trisulfides of groups IV and V transition metals: its structure is three-dimensional, derived from the structure of marcasite FeS_2. Crystalline CrS_3 contains only disulfide sulfur: in its structure, Cr_2S_{10} dimers are interconnected through disulfide bridges. In these dimers, two CrS_6 octahedrons share an S–S edge.

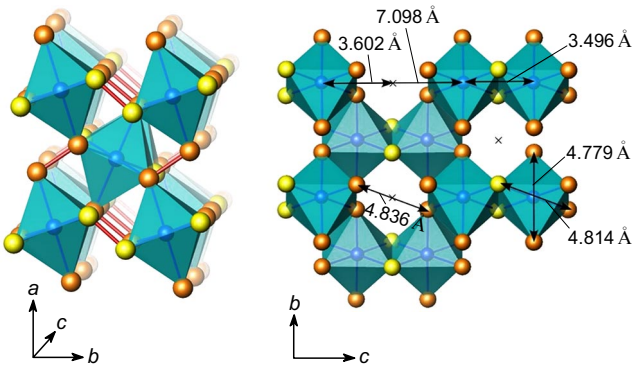

Figure 4. Crystal structure of CrS_3.[175] Reprinted with the permission of the American Chemical Society.

Vanadium tetrasulfide VS_4 ($V^{4+}(S_2^{2-})_2$) (see Fig. 1*c*) crystallizes in the monoclinic space group $C2/c$, and its structure is a packing of infinite $\{VS_4\}_\infty$ chains. The chains of V^{4+} ions run along the c axis, the vanadium atoms being linked in pairs by short V–V (d = 2.84 Å) bonds, while the distances between V_2 pairs are significantly longer (3.21 Å). Such structure is characteristic of a Pierels insulator, which is typical of d^1 chain compounds. The distance between V···V chains is >6.1 Å, therefore, they interact weakly, which determines the 1D nature of the structure. Each vanadium atom is surrounded by eight sulfur atoms. All sulfur atoms are bonded into $(S_2)^{2-}$ groups with short S–S distances (d = 2.03–2.04 Å). Rectangular S_4 planes perpendicular to the axis of the metal chains define the tetragonal-antiprismatic coordination of the vanadium atoms.[8] A recently prepared crystalline niobium tetrasulfide NbS_4[112] is isostructural with VS_4.

Binary tetraselenides MSe_4 are unknown, but $(MSe_4)_xA_y$ ionic compounds with infinite chains $\{MSe_4\}_\infty$ and halide ions or anionic halide complexes (A) have been obtained: $(NbSe_4)_3I$,[193] $(NbSe_4)_{10}I_3$,[194] $(NbSe_4)_4Br_2$,[195] $(TaSe_4)_2I$,[196] $(TaSe_4)_2TaBr_6$.[197] Similar ionic compounds were also reported for tellurium: $(NbTe_4)I$, $(TaTe_4)I$,[198] $(TaTe_4)_4I_2TaI_6$ (Ref. 199) and $(TaTe_4)_6I_4TaI_6$,[200] but simple binary tetratellurides $NbTe_4$ and $TaTe_4$ are also known. Unlike tetrasulfides, infinite MTe_4 chains comprise clusters composed of three metal atoms. In $NbTe_4$ chains,[114] niobium atoms form Nb_3 clusters with Nb–Nb bond lengths of 3.07–3.28 Å, separated by Nb···Nb distances of 3.90–3.93 Å. Another structural feature of MTe_4 is the covalent Te–Te bonding between neighbouring $\{MTe_4\}$ chains (in $NbTe_4$, distances are d_{Te-Te} = 2.91–2.94 Å).

Two representatives are known for the stoichiometric MQ_5, both being tellurides — $ZrTe_5$ and $HfTe_5$ ($M^{4+}(Te_2^{2-})(Te_3^{2-})$, where M = Zr, Hf).[13,201] Their crystal packings consist of infinite layers, which in turn are composed of trigonal-prismatic infinite columns cross-linked by polytelluride bridges (see Fig. 1*g*).

Infinite M_2Se_9 chains appear in V_2Se_9 and Nb_2Se_9 compounds. In these, binuclear $\{M_2Se_4\}$ clusters alternate with polyselenide bridging Se_5 ligands: $\ldots-M_2Se_4-Se_5-M_2Se_4-Se_5-\ldots$ (see Fig. 1*d*). In V_2Se_9 chains ($(V^{5+})_2(Se_2^{2-})_4(Se^{2-})$),[117] the V–V bond lengths in V_2Se_4 clusters are 2.84 Å, and those between the clusters are $d_{V\ldots V}$ = 3.65 Å.[9] Nb–Nb bond lengths in Nb_2Se_9 are 2.88(3) and 2.89(3) Å in Nb_2Se_4 clusters, while long Nb···Nb distances are equal to 3.76(3) Å.[10]

Electron-rich rhenium forms a crystalline polytelluride having an unusual structure: in a cage (3D) structure of Re_6Te_{15} ($(Re^{3+})_6(Te^{2-})_8(Te_7)^{2-}$)), $\{Re_6Te_8\}^{2+}$ cluster cores are bridged by polytelluride $(Te_7)^{2-}$ groups.[202]

2.2. Structures of amorphous metal polychalcogenides

For a number of amorphous metal polysulfides and polyselenides crystalline analogues are unknown. Amorphous chalcogen-rich group VI TMPCs (MoS_3, WS_3, CrS_3, $MoSe_3$, $CrSe_3$, MoS_{5-6}, $MoSe_{5-6}$, WSe_5) are particularly diverse, but the structures of amorphous group IV (TiS_4) and group VII (ReS_4 and Re_2S_7) TMPCs are also being studied. The lack of translational symmetry hampers the elucidation of their structures. They were studied by extended X-ray absorption fine structure (EXAFS-spectroscopy), analysis of the radial distribution function, X-ray photoelecron spectroscopy (XPS), Raman spectroscopy, *etc.*, and also by an indirect method of chemical excision

of structural units in chemical reactions [122] and the reverse Monte Carlo method.[123] Various models for structures of such polychalcogenides were proposed, and discussions in the literature on this issue are ongoing (see Fig. 2 *a*,*b*). For example, it is likely that the structures of MoS_3 samples obtained by different methods may differ and there may be polymorphism/isomerism inherent in Mo/S fragments bearing sulfide and disulfide groups.[119]

The two most commonly discussed structural models for MoS_3, WS_3 and similar compositions are the chain and cluster models,[123, 139, 171] variants of which are shown in Fig. 2 *a*,*b*. The chain model (see Fig. 2 *a*) suggests the formation of octahedral $Mo^{V}S_6$ units sharing their *trans*-faces, with pair bonds between molybdenum atoms (Mo—Mo). In the cluster model (see Fig. 2 *b*), molybdenum atoms are assembled in triangular structures Mo_3^{IV}. Recent density functional theory (DFT) calculations show that different structures can coexist depending on MoS_3 particle size.[171] At smaller sizes, structures formed by triangular clusters are more energetically favourable, and as the size increases, chain structures begin to prevail; it is emphasised that these chains are bent.

The structural model of amorphous CrS_3 is made up of chains, which are additionally linked together by the S—S groups (CN (Cr) = 6) (see Fig. 2 *c*).[172] At the same time, the recently synthesized crystalline chromium trisulfide (see Fig. 4) [175] differs significantly in structure from the amorphous CrS_3: it has a three-dimensional structure, derived from the structure of marcasite FeS_2. Therefore, the structure of this compound differs from that of both its amorphous counterpart and the other crystalline trichalcogenides (*e.g.*, trichalcogenides of Nb, Ta, Ti, Zr, Hf, having a structure like the one depicted in Fig. 1 *f*).

Sulfur-rich amorphous polychalcogenides such as $MoS_{4.7}$, MoS_5, $MoS_{5.6}$ and MoS_6, are obviously similar in structure to MoS_3. New S—S bridges may incorporate into the chains shown in Fig. 2 *a*. Since MoS_3 is amorphous, there are no structural restrictions that could hamper such chain growth. In fact, one managed to prepare amorphous polysulfides MoS_x with a wide range of compositions ($x = 3-6$) and this not be the limit, as the S_4^{2-} units are known and found in thiomolybdates.[119, 152, 174] In polymeric materials MoS_x, sulfur exists in different states such as bridging $(S-S)^{2-}$ groups, terminal S^{2-}, S_2^{2-} groups, *etc.*[124–127, 138, 203] The large number of bridging $(S-S)^{2-}$ units between building blocks explains why sulfur-rich polysulfides exist only as amorphous phases and form in an unusual morphology. Thus, in MoS_5, dimers M_2S_8 ($[(M^{5+}-M^{5+})(S-S)_4^{2-}]^{2+}$) are linked by disulfide bridges into infinite chains, which bend like the classical polymeric chains and are arranged in such a way that the MoS_5 and WS_5 particles have a globular morphology, as shown experimentally and confirmed by simulations using DFT and DFT molecular dynamics methods.[174] For this reason, sulfur-rich TMPCs can only be produced in an amorphous state. The corresponding amorphous selenides $MoSe_3$,[204] $CrSe_3$, $MoSe_{5-6}$ (Ref. 143) and WSe_5 have also been reported.[205]

The data from the pair distribution function (PDF), XPS, Re LIII edge EXAFS and sulfur K-edge XANES for two related rhenium polysulfides ReS_4 and Re_2S_7 also suggest their chain-type structure with a zig-zag arrangement of the Re—Re bonds [173] (see Fig. 2 *d*,*e*). Apart from bridging S^{2-} and S_2^{2-} in different ratios, both structures contain μ_3-sulfur atoms.

For amorphous TiS_4, the PDF analysis and DFT modelling data indicated a three-dimensional network-like structure in which titanium ions are linked by bridging polysulfide ions (S_2^{2-}, S_3^{2-}, *etc.*) rather than the chain structure. The average S—S and Ti—S bond lengths are 2.09 and 2.46 Å, respectively, and the average coordination number of Ti is 6.9. In this case, the structure switches into the chain one by the intercalation of lithium ions in the electrochemical process.[150, 151]

Based on the literature data, it can be concluded that great progress in the study of amorphous TMPCs is due to the use of theoretical modelling, and it is clear that in the coming years it will be an integrated approach, including modern experimental and computational methods, that will allow further advances in the understanding of the structure of amorphous TMPCs.

2.3. Features of electronic structures

Features of crystal structure of TMPCs are associated with several interesting properties, which have been developed in studies on electrochemistry and the exploration of the electro-physical properties of one-dimensional systems. Most TMPCs are of the semiconductor or metallic conductivity type. For example, NbS_3 of I and II structural types are semiconductors at room temperature, NbS_3(III) is a semimetal, $NbSe_3$, $TaSe_3$ (rhombic and monoclinic) have a metallic conductivity, while $(TaSe_4)_2I$ and $(NbSe_4)_{10}I_3$ have a semi-metallic conductivity. When considering the electronic structure of TMPCs, the electronic structure of the conduction bands is of the greatest interest because it can explain the features of the electrophysical behaviour. This is important for many applications, particularly in the use of TMPCs in electrochemical and photocatalytic processes (see Section 5).

A description of the calculated electron densities of states of TMPCs can be found in the monograph [206] or in later works. The contribution of s- and p-states of chalcogen, d-bands of metal atoms to the blocks of the energy spectrum, as well as their mutual location and overlapping near the Fermi level and the filling of bands with electrons constitute the principal features of the electronic structure of TMPCs. For example, first three bands below the Fermi level for NbS_4 are represented by the following blocks (Fig. 5): from −0.5 to −1.0 eV, Nb4d states, responsible for the overlapping of Nb4d orbitals and the formation of Nb—Nb covalent bonds, prevail; the band from −1 to −3 eV corresponds to the overlapping of the S3p and Nb4d states and the formation of the Nb—S bonds; two bands from −3 to −3.5 and from −3.5 to −7 eV consist mainly of S3p states responsible for the formation of S_2 covalent bonds, which coordinate covalently bound Nb_2 pairs in the$\{NbS_4\}_\infty$ infinite chains. The theoretical value of the band gap is 1.07 eV, which is in line with the experimental value of 1.1 eV derived from spectral data.[112]

The current computational studies show that the electronic structure of TMPCs can be altered under the influence of various factors, namely, through bulk-to-nano transition, doping,[207] tensile strain,[208] exposure to high pressure.[209, 210] For example, the O-doping or S-vacancy in VS_4 narrows the band gap (Fig. 6).[211] Moving from crystalline VS_4 to its nanowire, the valence band maximum and the conduction band minimum are formed by the overlapping of S2p orbitals and V3d levels, but compared to the crystal, S2p orbitals make a greater contribution, and vanadium contributes the $d_{xy} + d_{x^2-y^2}$ orbitals.[212] Metal

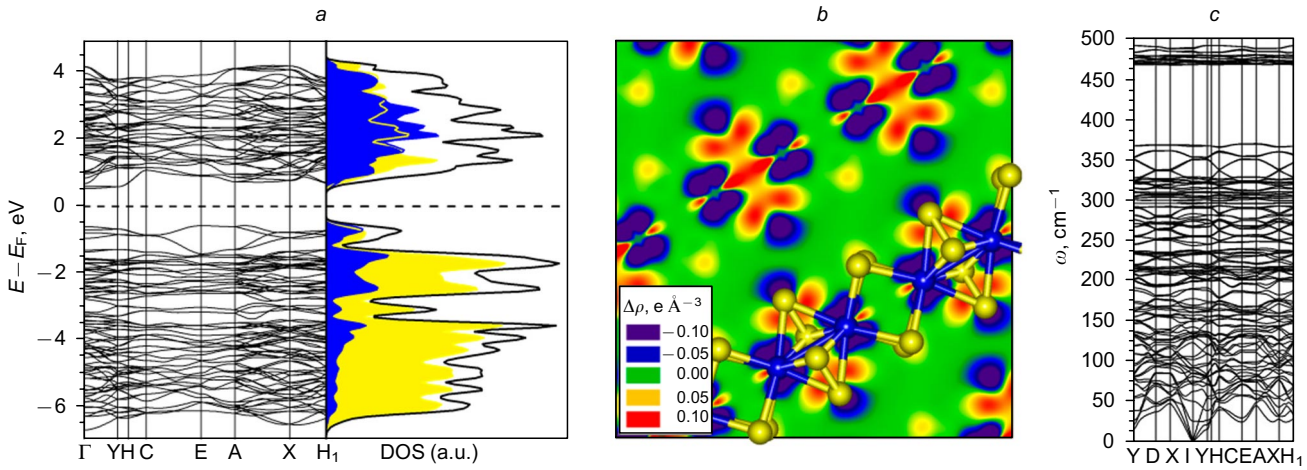

Figure 5. Calculation of the electron density of crystalline NbS_4 in DFT:[112] electronic band structure, total and selected partial density of states (DOS) (*a*). Total DOS is represented by a solid black line, Nb4d and S3p valence states are marked in blue and yellow respectively; electron density difference map in the plane (010), passing through the NbS_4 molecular chain (*b*); phonon band structure (*c*). Reprinted with the permission of the American Chemical Society.

polychalcogenides are often referred to as electron reservoirs due to the presence of $(Q_2)^{2-}$ dichalcogenide groups, which can serve both as an electron donor and an electron acceptor.[189] In TMPCs, chalcogen p orbitals overlap with metal d orbitals to form hybrid d/p orbitals near the Fermi level, which allows the electron density transfer from metal atoms to the dichalcogenide group thus forming an electron reservoir.[177]

When describing electrophysical properties by single-particle electron processes, TMPCs are seminconductors or metals. There is a number of publications devoted to the study of electrophysical properties of TMPCs, for which the relationship with their quasi-one-dimensional structure is clearly seen, and anomalies in electrical conductivity are discussed in terms of a collective state (electron-hole condensate movement) along a preferred direction. Compounds MS_4, M_2Se_9, MTe_5 belong to one-dimensional van der Waals structures, *i.e.*, including infinite chains, which form van der Waals interactions with neighbouring chains, while MQ_3, $NbTe_4$, $TaTe_4$ are quasi-one-dimensional: in their structures infinite chains of metal atoms can be distinguished, which assemble into infinite layers *via* interatomic bonds stronger than van der Waals forces.

Studies of electrophysical properties of trichalcogenides such as NbS_3,[213] $NbSe_3$,[214] TaS_3,[215] $TaSe_3$,[216] ionic compounds with infinite chains $(NbSe_4)_{10}I_3$,[217] $(TaSe_4)_2I$,[218]

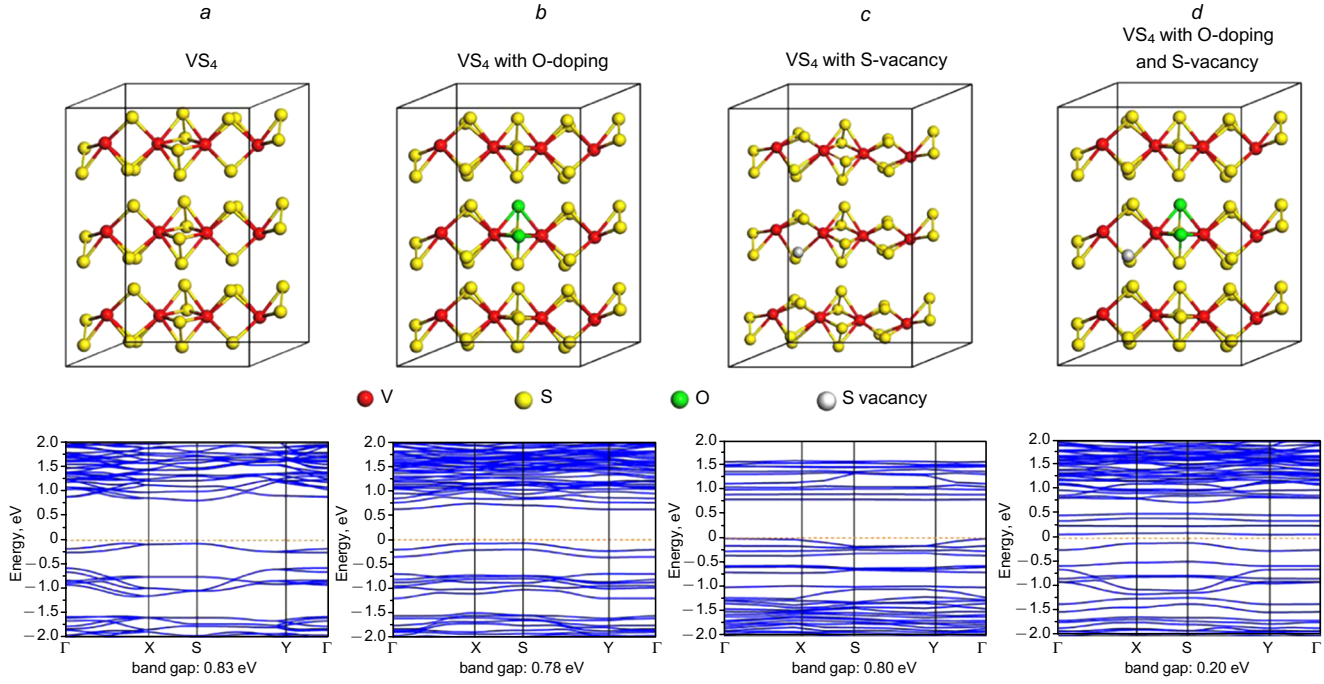

Figure 6. Simulation models of electronic structure for crystalline VS_4 (*a*), VS_4 with O-doping (*b*), VS_4 with S-vacancies (*c*), VS_4 with O-doping and S-vacancies at the same time (*d*).[211] Reprinted with the permission of the American Chemical Society.

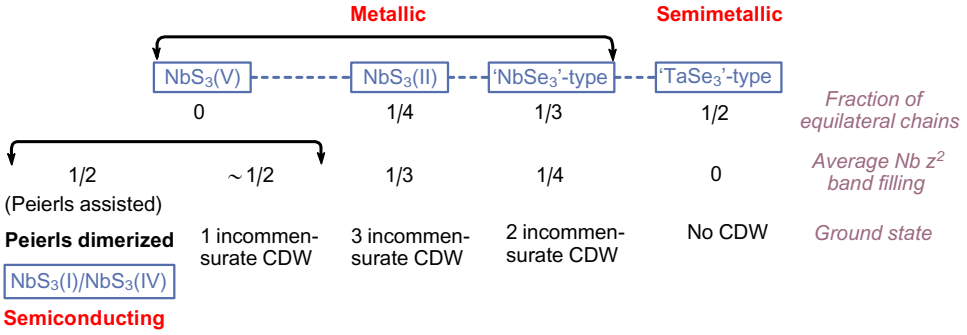

Figure 7. Summary of electrophysical properties of NbS_3 polymorphs.[12] Reprinted with the permission of the American Chemical Society.

and also tetrachalcogenides $NbTe_4$ and $TaTe_4$[113] contributed much to the discussion on electrophysical properties of one-dimensional and quasi-one-dimensional compounds.

In the $[MQ^{2-}(Q_2)^{2-}]_\infty$ infinite chains in MQ_3 and $[M(Q_2)_2]_\infty$ infinite chains in MQ_4, metal atoms can shift along the chains under certain conditions, according to the Peierls theorem on the instability of one-dimensional crystals consisting of evenly spaced atoms with one unpaired electron.[219,220] In the Peierls transition, the chain under consideration converts to an insulating state. For example, the Nb···Nb distances of 3.04 and 3.69 Å alternate in the $[NbS^{2-}(S_2)^{2-}]_\infty$ chains of compound NbS_3(I), which characterizes an insulating state of these chains at room temperature. A large number of polymorphs are known for NbS_3, but the difficulty of crystallizing most of them prevents their experimental study. In a theoretical work,[12] models of electronic structure of seven stable polymorphs are compared, four of them being experimentally obtained ones and the three others being unreported ones which were refined in the structures of $NbSe_3$, TiS_3 and $TaSe_3$. It was shown that structural differences of these polymorphs stem from the differences in their conductivities and electron transport[12] (Fig. 7). Thus, for NbS_3(I), linkages between infinite chains in pairs of chains of the same type are quite strong compared to other polymorphs. Further, NbS_3(V), NbS_3(II) and 'NbSe$_3$' phases exhibit metallic properties with incommensurable charge density waves (CDW), which is associated with different partial occupation of the Nb d_{z^2} band of the trigonal prismatic chains by half, one-third and one-quarter, respectively.

In TMPC crystals, a nonohmic character of electrical conductivity is observed: anomalies in the dependences of electrical conductivity on temperature, pressure or exposure to electromagnetic radiation are accompanied by a periodic modulation of the electron density — charge density waves.[221] The emergence and dynamics of CDW, the state of superconductivity, and related phenomena at TMPCs have been studied since the 1960s, as reflected in several monographs;[206,222] the research has also continued in recent years.[223]

3. Methods for the synthesis of transition metal polychalcogenides

Synthetic approaches and theoretical foundation of preparing such materials were laid as early as the 1980–1990s[189] and were detailed in earlier papers,[24,27–29,187] so here we will discuss recent publications addressing their synthesis, with a focus on obtaining nanomaterials. Polychalcogenide crystals feature anisotropic morphology in the form of ribbons, rods or wires growing along the *b* axis, *i.e.* parallel to the infinite chains (more pronounced growth occurs along the *a* axis with increasing temperature[41]) and, often, one (or more) of the crystal sizes is in the nanoscale range.Therefore, many of the polychalcogenide samples discussed here can be micro-or nanocrystals (or amorphous particles). Theoretical calculations also supported the possibility of stabilization and predicted interesting physical properties of various nanostructures of polychalcogenides, including monolayers.[37,62,65–67,71,77,79] The main synthetic approaches to various crystalline and amorphous TMPCs are listed in Tables 1 and 2.

3.1. Synthesis from elements

Transition metal polychalcogenides are prepared from elements at moderately high temperatures: the upper limit of the reaction temperature is generally limited by the formation of more stable dichalcogenides. For the synthesis of monocrystalline samples the chemical vapour transport technique is used: a transport agent such as iodine, bromine or a chalcogen chloride is introduced into the reaction medium. Sulfur/selenium, taken in excess, can also act as transport agents, producing MQ_x intermediates responsible for mass transfer.[26,41,187] In these cases, smaller crystals are obtained due to less active material transport.[187] The procedure consists of three steps:[26,41] evaporation of the solid reactants, transport of gaseous substances, condensation on a surface accompanied by the crystal growth.

For the synthesis of TiS_3, the following mechanism is proposed:[29,40,61] at a temperature of 450 °C, sulfur turns into a gaseous state, precipitates on the titanium surface and reacts with it to generate unstable gaseous intermediates such as TiS_x. Next, TiS_x reacts with S in the gaseous phase and the resulting stable TiS_3 phase is again deposited on the titanium surface, becoming the centre of crystallisation and growth of TiS_3 (nano)fibres from the gaseous phase through further interactions between TiS_x and S. Probably, ZrS_3 and HfS_3 nanoribbons are also formed in a similar way.[41] This mechanism is evidenced by the pointed shape of the ends of trichalcogenide nanocrystals.[29] Thus, the direction of growth is determined by the competition among the growth rates of the different crystallographic faces. Growth will occur towards the edge with the highest free energy, *i.e.*, the most reactive (the least stable) face.

In the process of the synthesis, parameters such as vapour pressure, heating and cooling rates, reaction time, reaction temperature and temperature gradient along the length of the ampoule can be varied. The growth temperature and temperature gradient have the most significant impact on the characteristics of the resulting samples.[36,41,61,81] In the case of TiS_3, crystals displayed a morphology of nanoribbons at 500 °C, nanosheets at

Table 1. Main methods for the synthesis of crystalline and amorphous IV – VI group transition metal trichalcogenides.

Compound	Starting material	Reaction conditions	Comments, product properties	Ref.
TiS_3	Metal + chalcogen	Chemical vapour transport technique	Crystalline samples	29, 40, 61, 187
	Metal oxide + sulfur + boron	Heating the reaction mixture in a vacuum-sealed ampoule	Reduced synthesis temperature due to the B_2O_3 formation, 400 °C	224
	Metal sulfide + sulfur	Mechanochemical activation of the mixture in an inert atmosphere	Amorphous samples	44, 225, 226
ZrS_3	Metal + chalcogen	Chemical vapour transport technique	Crystalline samples	29, 41, 187, 227
	Metal sulfide + sulfur	Heating the reaction mixture in a vacuum-sealed ampoule	Crystalline samples (nanoribbons)	227
	$ZrCl_4$ + thiourea	Heating the solution in hexane in an autoclave, 230 °C, 48 h	Nanocrystalline ZrS_3 sheets Photoluminescence at rt, 598 and 637 nm (probably due to surface defects in nanocrystallites)	33
HfS_3	Metal + chalcogen	Chemical vapour transport technique	Crystalline samples, nanoribbons	51, 187
NbS_3	Metal + chalcogen	Chemical vapour transport technique	Crystalline samples	29, 187
	NbS_2 + sulfur	Mechanochemical activation of the mixture in an inert atmosphere	Amorphous samples	228
	Metal oxide + sulfur + boron	Heating the reaction mixture in a vacuum-sealed ampoule	Reduced synthesis temperature due to the B_2O_3 formation, 350 °C	224
$ZrSe_3$, $HfSe_3$	Metal + chalcogen	Chemical vapour transport technique	Crystalline samples	29, 187
	$ZrCl_4$ ($HfCl_4$) + Se	Oleylamine, 300°, 1 h	Nanocrystals	229
MTe_3 (M = Ti, V, Nb, Ta)	Metal + tellurium in the presence of multiwalled carbon nanotubes	Chemical vapour transport technique, 600 – 900 °C, 3 days	Telluride species are encapsulated within multiwalled carbon nanotubes with a diameter of 1 – 10 nm	230, 231
CrS_3, $CrSe_3$	$Cr(CO)_6$ + S (Se)	Boiling 1,2-dichlorobenzene (180 °C, 2 h)	Amorphous samples	143, 155
	Cr_3S_4 + sulfur	Cr + S, 800 °C, amorphous samples 13 GPa, 2 h	Microcrystals. First obtained in 2020	175
MoS_3	Thiometallate salts $(NH_4)_2MoS_4$	Thermal decomposition, acidification, electrodecomposition from solutions	Amorphous samples	124, 138, 203, 232 – 235
	MoF_6 + $[(CH_3)_3Si]_2S$	Exothermic reaction at room temperature or chemical vapour deposition (CVD) at 150 – 400 °C	Amorphous samples	236, 237
	$Mo(CO)_6$ + S	Boiling 1,2-dichlorobenzene, 2 h	Amorphous samples	143, 144
	MoO_3 (or $Mo_6O_{24}^{6-}$) + S(Se), Na_2S, H_2S (H_2Se)	Solvothermal synthesis or reaction with H_2S (H_2Se) on heating	Amorphous samples, films	126, 127, 148
WS_3	$(NH_4)_2WS_4$	Thermal deconposition, acidification, electrodecomposition from solutions	Amorphous samples	137, 232 – 234, 238
	$WO_3 \cdot 0.33\,H_2O$ + thioacetamide	Solvothermal synthesis, DMF, 200 °C, 12 h	Nanocrystalline microspheres, 1 – 10 μm, first obtained in 2022	176
$MoSe_3$	Sodium molybdate + Se	Solvothermal synthesis, hydrazine solution, 180 °C, 12 h	Amorphous	204

400 °C, and at 450 °C, a sample of a mixed morphology was formed.[61] It was noted that titanium trisulfide microparticles are formed in a temperature range from 400 to 550 °C for 24 h, with the morphology of the resultant microparticles depending on the synthesis temperature — from broad thin ribbons (400 °C) to narrow ribbons (500 – 550 °C).[81] The growth temperature for TiS_3 should not exceed 632 °C, since TiS_2 is stable at higher temperatures.[28, 61, 81] Zirconium trisulfide is stable at even higher temperatures, and it was also noted[83] that upon increasing the temperature of the ampoule synthesis from Zr and S from 350 to 650 °C, the morphology of the resultant ZrS_3 changed from thin fibres to nano- and microribbons (Fig. 8).

Niobium triselenide in the form of nanoribbons and nanowires begins to grow from a stoichiometric mixture of elements at temperatures above 610 °C, with samples of the

Table 2. Main methods for the synthesis of crystalline and amorphous chalcogen-rich (MQ_x, $x > 3$), and also metal- or chalcogen-substituted IV – VII group transition metal polychalcogenides.

Compound	Starting material	Reaction conditions	Comments, product properties	Ref.
TiS_4	TiS_2 + sulfur	Mechanochemical activation of the mixture in an inert atmosphere	Amorphous samples	149, 150, 225, 226, 239
NbS_4	NbS_2 + sulfur	Mechanochemical activation of the mixture in an inert atmosphere	Amorphous samples	228
	Nb or $Nb_{1.14}S_2$ + sulfur	Heating the reaction mixture in a vacuum-sealed ampoule, 400 °C	Crystalline, first obtained in 2022	112
VS_4	Metal sulfide + sulfur	Heating the reaction mixture in a vacuum-sealed ampoule	Crystalline samples	105
	Na_3VO_4 + thioacetamide	Hydrothermal synthesis, graphite support may be present, pH 5 – 12 at 140 – 160 °C	Microcrystalline VS_4 samples	87 – 96, 99, 101 – 103, 106, 109 – 111
	Metal oxide + sulfur + boron	Heating the reaction mixture in a vacuum-sealed ampoule	Reduced synthesis temperature due to the B_2O_3 formation, 350 °C	224
	VCl_4 + sulfurizing agents	Reactions with $[(CH_3)_3Si]_2S$ or H_2S were carried out at room temperature, those with $(CH_3)_3CSSC(CH_3)_3$ or $(CH_3)_3CSC(CH_3)$ — on heating under reflux	Amorphous samples	86
	$V(amd)_3$ + H_2S (amd = *N*,*N*′-diisopropyl-acetamidinate)	Atomic layer deposition at 200 °C	Deposited atomic VS_4 film, amorphous or weakly crystallized	100
ReS_4	Thiometallate salts, Et_4NReS_4	Electrodeposition of polysulfides from solutions Oxidation with iodine or ferrocenium salt $(Cp_2Fe)PF_6$ in acetonitrile	ReS_4 precipitates from a MeCN solution at +0.6 V (*vs* Ag/AgCl) for 2 min Rapid formation of black ReS_4 precipitate	173
NbS_5	Metal sulfide + sulfur	Mechanochemical activation of the mixture in an inert atmosphere	Amorphous samples	228
MoS_5, MoS_6, $MoSe_5$; WS_5,	$(NH_4)_2Mo_2S_{12}$ solutions	In different media (acetone, DMF, aqueous HCl)	Amorphous samples	145, 146, 152, 240
WSe_{6-7}	Metal sulfide + sulfur	Mechanochemical activation of the mixture in an inert atmosphere	Amorphous samples	142
	$M(CO)_6$ + S (Se)	Boiling 1,2-dichlorobenzene, 2 h	Amorphous $ReSe_{6-7}$ can be prepared from $Re_2(CO)_{10}$	143, 144, 155
V_2Se_9, Nb_2Se_9, MTe_4 (M = Nb, Ta), MTe_5	Metal + chalcogen	V_2Se_9 330 °C, Nb_2Se_9 500 – 600 °C, 3 days, MTe_4 900 °C, 0.5 – 7 days MTe_5 500 °C, 7 days	V_2Se_9, Nb_2Se_9 Single crystals of $NbTe_4$, $TaTe_4$ $ZrTe_5$, $HfTe_5$	116, 118 113, 115 13
Chalcogen-substituted	$(NH_4)_2MoO_4$ + H_2Se + H_2S	Reaction 10 h, annealing at 280 – 300 °C, 6 h	$MoSe_3S$	157
Metal-substituted	Metal mixture or alloy + chalcogen	Chemical vapour transport technique	$Nb_{1+x}V_{1-x}S_5$, $Zr_{1-x}Ti_xS_3$ ($0 < x < 0.33$), $Ti_{1-x}Nb_xS_3$, $Nb_{1-x}Ta_xS_3$, $Cr_2Nb_2Se_{10}$	159 – 164, 241

highest purity being obtained at 630 – 700 °C.[36] The cross-section area of nanostructures increases with increasing synthesis temperature. A sample of $NbSe_3$ fabricated at 700 °C, has a fibre morphology up to a few millimetres long and 20 – 700 nm wide.[36, 42, 43] At temperatures beyond this range, *i.e.* both below 610 °C and above 700 °C, other niobium selenides, Nb_2Se_9 and $NbSe_2$, are formed, respectively. Nanoribbons of ZrS_3 and HfS_3 prepared at 600 °C,[41] and TaS_3 prepared at 650 °C[47] possessed a morphology and dimensions similar to those of $NbSe_3$, however in the case of HfS_3, a thin amorphous layer with a thickness of 2 – 20 nm and a significant content of TaS_2 was also found on the surface of the particles, which leads the authors to classify these structures as the 'core – shell' architecture.

Careful control of experimental conditions allows the growth of nanostructures of transition metal trichalcogenides of very different and sometimes unusual morphology: in the form of ring-shaped structures ($NbSe_3$[242] and $TaSe_3$ (Ref. 32)), Möbius strips ($TaSe_3$[32] and $NbSe_3$ (Ref. 31)), 'flowers' (TiS_3)[45] and other complex structures.[25, 26, 31] Such

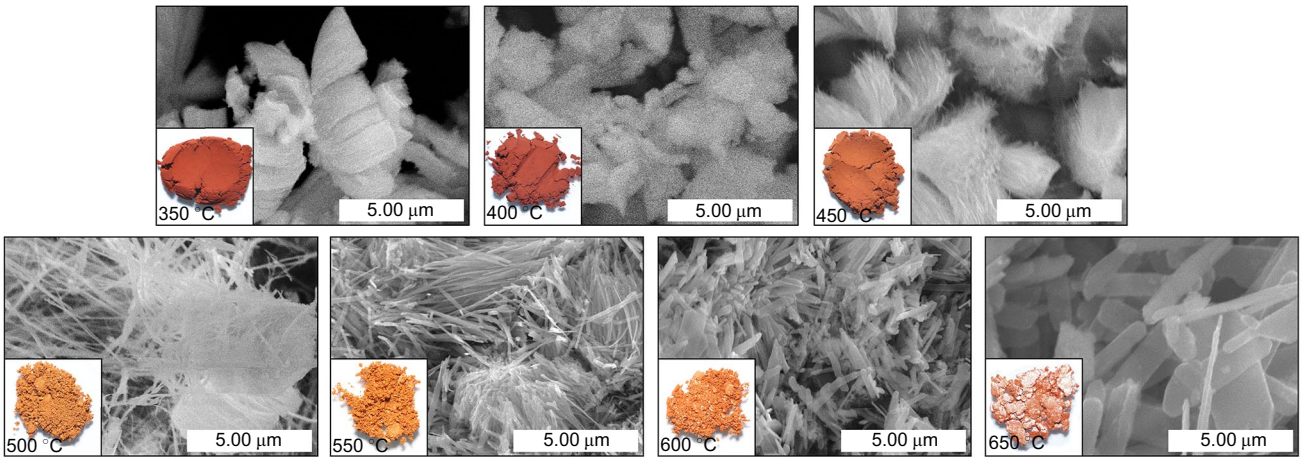

Figure 8. Temperature dependence of the morphology of ZrS_3, microcrystals obtained from elements in the range from 350 to 650 °C.[83] Reprinted with the permission of Elsevier.

structures are formed due to a temperature gradient.[31] Under strongly non-equilibrium conditions, selenium simultaneously exists as vapour, aerosol and liquid droplets, which act as templates: growing trichalcogenide filamentary crystals are 'wrapped' around them.

There are also reports of binary niobium and vanadium polyselenides of the stoichiometric composition M_2Se_9 (M = V or Nb) prepared from the elements. Divanadium nonaselenide V_2Se_9 is formed on heating a mixture of 2 V + 12.6 Se (molar ratio) at a temperature of up to 330 °C,[116] and Nb_2Se_9 — on heating a mixture of Nb + 200 Se (molar ratio) at a temperature of 500–600 °C in 3 days.[118]

Tetratellurides of niobium [113] and tantalum [113, 115] MTe$_4$ (M = Nb, Ta) can be produced on prolonged heating of a mixture of elements in an almost stoichiometric ratio at 900 °C. Zirconium and hafnium pentatellurides MTe$_5$ (see Fig. 1 *g*) [13] were prepared from elements at a significantly lower temperature (500 °C) in 7 days.

The synthesis of trichalcogenides from elements can also give products with partial substitution of the metal or chalcogen atoms, similarly to the synthesis of transition metal dichalcogenides, which allows to adjust the electronic properties of the material.[243] Thus, in a study,[160] in the synthesis of crystalline ZrS_3 nanolayers, zirconium was partially replaced by titanium. The (Ti,Zr)S_3 solid solutions were obtained by the reaction of an Ti/Zr alloy and sulfur vapour at 800 °C. As a result, the samples with the morphology of microribbons were obtained, which is typical of transition metal trichalcogenides. The solid solutions had the $ZrSe_3$ structural type (monoclinic). Interestingly, with molar ratios of zirconium and titanium Zr/Ti from 20/80 to 80/20, the stoichiometry of the resultant solid solutions was close to $Zr_{0.8}Ti_{0.2}S_3$. The formation of solid solutions with close stoichiometry is probably influenced by the difference in stabilities of di- and trisulfides for titanium and zirconium: ZrS_3 is stable up to 800 °C,[161] whereas TiS_3 decomposes to TiS_2 and elemental sulfur at a temperature above 630 °C.[244] At 800 °C, zirconium only formed trisulfides while titanium, when used in excess, formed TiS_2. Nanolayers of substituted zirconium trisulfide were fabricated by scotch-tape exfoliation of the crystals, and their electrotransport properties were examined. The synthesis of a number of solid solutions $Ti_{1-x}Nb_xS_3$ (x = 0.05, 0.07, 0.10) from stoichiometric quantities of metals and sulfur at 550 °C is reported;[162] for the obtained materials, temperature-dependent electrical resistivity and the Seebeck coefficient value were studied.

3.2. Synthesis from lower chalcogenides or metal oxides

Not all polychalcogenides can be obtained from the elements in good yield — many amorphous polychalcogenides were prepared from metal compounds and various sulfurizing agents. The formation of crystalline VS_4 and NbS_4 tetrasulfides from the elements is kinetically hampered. The synthesis of VS_4 from metal vanadium and sulfur takes 10 days at 400 °C, and NbS_4 is formed from the elements in a very low yield. At a temperature >450 °C these tetrasulfides are unstable. In both cases, the yield of MS_4 increases significantly using metal sulfide and excess sulfur as reactants. Thus, VS_4 can be produced in quantitative yield by heating a mixture of V_2S_3 + 6 S (molar ratio) in an evacuated sealed glass tube at 400 °C for 24 h;[105] similarly, NbS_4 is obtained from a mixture of $Nb_{1.14}S_2$ + 11.4 S at 440 °C in 60 h in 85% yield.[112] The study [227] showed that ZrS_3 nanoribbons are produced *via* the reaction of ZrS_2 with sulfur in a nitrogen atmosphere at 550 °C in a sealed tube for 2 h. This conversion is probably facilitated by the higher pressure (due to the addition of nitrogen) compared to the vapour pressure of sulfur when synthesised from the elements. In the above instances, sulfide ions were oxidized with sulfur to S^- along with the partial metal oxidation in the case of vanadium and niobium.

Carrying out the high-temperature synthesis also at elevated pressure allows to obtain polychalcogenides that differ in structure from the known analogues, as well as polychalcogenides with previously unknown metal–chalcogen combinations. For example, chromium trisulfide CrS_3 was recently obtained for the first time as a crystalline product from Cr_3S_4 and sulfur at 800 °C and a pressure of 13 GPa (see Fig. 4) [175] (CrS_3 is also formed from Cr and S under similar conditions). The structure and physical properties (superconductivity) of TiS_3 at pressures up to 100 GPa were theoretically predicted. At 20 GPa denser structures (layered, corresponding to the experimentally obtained phase II) and cubic (cage) structures at 80 GPa) are suggested.

An alternative way of activating the reaction mixture is to treat them mechanochemically in an inert atmosphere. It is commonly used to prepare amorphous polysulfides of titanium and niobium. Amorphous TiS_3 [44, 225, 226] and TiS_4 [149, 150, 225, 226, 239] were obained from a stoichiometric mixture of TiS_2 and S. During a rather short synthesis time (several hours to tens of hours), X-ray amorphous products were formed that, according to their XRD patterns, did not contain the pristine crystalline TiS_2 and S. In a similar way, a number of amorphous niobium polysulfides were prepared such as NbS_3, NbS_4 and NbS_5.[228] The study [151] showed that the Ti 2p XPS spectrum of amorphous TiS_4 corresponds to Ti^{4+}, and in the S 2p spectrum, sulfur atoms in three charge states were found, namely, S^{2-}, S^-, and S with a small negative charge due to inner position within the $(S-S-S)^{2-}$ bridging groups.

Interestingly, mechanochemical synthesis also makes available amorphous MoS_3 and other sulfur-rich polysulfides starting from MoS_2 and sulfur,[142] which do not react on conventional, even prolonged, heating. A series of amorphous molybdenum polysulfides MoS_x ($x = 3-7$) is formed *via* the prolonged (180 h) mechanochemical synthesis from crystalline MoS_2 and elemental sulfur in an argon atmosphere. These polysulfides were produced as a mixture with partially amorphized MoS_2; resulting mixtures were then explored as cathode materials in solid-state sodium-ion batteries. Noteworthy that according to the XPS data for the obtained samples, the binding energy of the Mo 3d 5/2 electrons is in the narrow range of 228.9–229.0 eV, which is very close to MoS_2 (229.1 eV), and it can be assumed that using this synthetic method, molybdenum retains its Mo^{4+} oxidation state. The S 2p 3/2 XPS data confirm the polysulfide nature of the obtained materials: there are both S^{2-} (161.8–162.1 eV) and S_2^{2-} (163.0–163.2 eV).

An example when one polychalcogenide is prepared from another is the transformation of niobium polyselenides. When Nb_2Se_9 crystals were heated in an evacuated sealed tube at 600–630 °C for 3–6 h, the formation of $NbSe_3$ crystals was observed.[242] Niobium triselenide is considered to be a stable phase in this temperature range, and this transition is in agreement with the Nb–Se phase diagram. A fascinating feature of this transformation was the organisation of the resulting crystals into perfect rings.

Apart from sulfides, oxides can also serve as starting materials to prepare certain TMPCs. Crystalline trisulfides of titanium and niobium as well as vanadium were derived from Ti (TiO_2), V (V_2O_5), Nb (NbO, Nb_2O_5) oxides, which reacted with sulfur and bromine in the high-temperature ampoule process.[224] The reactions are driven by the formation of thermodynamically favourable B_2O_3, with boron sulfides (B_2S_3 and BS_2) generated *in situ* being sulfidation agents along with sulfur; metal in the process can be oxidized (NbO) or reduced (V_2O_5, Nb_2O_5). Using this procedure, polysulfides TiS_3, VS_4, NbS_3 and various disulfides were obtained at 350–400 °C. Finally, the solvothermal reaction between $WO_3 \cdot 0.33\,H_2O$ and thioacetamide has recently been used to prepare the first microcrystalline WS_3.[176]

3.3. Synthesis from salts and molecular precursors

Methods for obtaining IV–VII group metal polychalcogenides in solutions, as well as methods of vapour deposition using salts or complex metal compounds, have also been developed. As starting metal-containing compounds, one can use tetrachlorides (to prepare TiS_3, ZrS_3 and VS_4 [33, 86]), thiocomplexes (MoS_3), carbonyls $M(CO)_6$ [143, 144, 155] (polychalcogenides of Cr, Mo, W) and other coordination compounds. The products of such syntheses are generally X-ray amorphous.

The reaction of $ZrCl_4$ with thiourea $CS(NH_2)_2$ under solvothermal conditions (160–230 °C) produces ZrS_3 nanocrystallites.[33] It is assumed that one stage in the production of ZrS_3 is the formation of an intermediate complex *via* the coordination of the thiourea S atom with the Zr^{IV} atom. In this regard, it was noted that the synthesis was successful only in solvents having no coordination ability towards zirconium atoms, such as n-hexane, toluene and cyclohexane, while pyridine or ethylenediamine, capable of complex formation with Zr^{IV}, hampered the reaction with thiourea. When sulfur or carbon disulfide was used instead of thiourea, the reaction did not proceed.

As sulfurizing agents in the syntheses from halides at a temperature of $\leqslant$160 °C, bis(trimethyldisil)thiane, di-*tert*-butyl disulfide, di-*tert*-butyl sulfide and hydrogen sulfide are also used. The following equations describe the synthesis of amorphous VS_4 [86] and MoS_3 [236, 237] using bis(trimethyldisil)thiane:

$$VCl_4 + 4(CH_3)_3-Si-S-Si-(CH_3)_3 \longrightarrow$$
$$\longrightarrow VS_4 + 4(CH)_3SiCl + 2(CH_3)_3Si-Si(CH_3)_3$$
$$MoF_6 + 3(CH_3)_3-Si-S-Si-(CH_3)_3 \longrightarrow$$
$$\longrightarrow MoS_3 + 6(CH_3)_3SiF$$

Sulfurization reaction using di-*tert*-butyl disulfide $(CH_3)_3C-S-S-C(CH_3)_3$ is outlined in a quite detailed study on the synthesis of amorphous and crystalline titanium sulfides.[245] Thus, crystalline TiS_3 was prepared by a two-step procedure: first, a precipitate of amorphous titanium sulfide was obtained by reacting $TiCl_4$ with di-*tert*-butyl disulfide, then, it was heated with excess sulfur in an evacuated sealed ampoule; pure TiS_3 was formed in a temperature range of 300–500 °C.

Reacting the same reactants, $TiCl_4$ and di-*tert*-butyl disulfide, under chemical vapour deposition (CVD) conditions afforded amorphous titanium sulfide TiS_3 at a temperature below 260 °C.[246] Interestingly, the reaction of other sulfur sources with $TiCl_4$ yielded TiS_2.

Preparation of amorphous VI group metal polysulfides MS_3 (M = Cr, Mo, W), $MoS_{4.7}$, WS_5 can be achieved by solvent chemical methods and electrochemical deposition on various surfaces (see reviews [119, 121, 191]). A well-known procedure to prepare trisulfides MoS_3 [124, 138, 203, 232–235] and WS_3,[232–234, 238] and also MoS_x [136, 139] comprises thermal decomposition of $(NH_4)_2MS_4$ (M = Mo, W) or acidification of their aqueous solutions:[119]

$$(NH_4)_2MoS_4 \longrightarrow MoS_3 + 2\,NH_3 + H_2S$$
$$MoS_4^{2-} + 2\,H^+ \longrightarrow MoS_3 + H_2S$$

Electrodeposition method allows to obtain MoS_3 film samples of tens or hundreds of nanometres thickness from MoS_4^{2-} solutions on various surfaces (indium–tin oxide (ITO), fluorine-doped tin oxide (FTO), glassy carbon).[124, 131, 138] For example, 20–30 nm thick MoS_3 layers were fabricated *via* oxidation of an aqueous solution of $(NH_4)_2MoS_4$/KCl at a potential of +0.11 V (*vs* RHE) for 100 s:[138]

$$MoS_4^{2-} \longrightarrow MoS_3\downarrow + S + 2e^-$$

Similarly, it was shown [173] that various amorphous ReS_4 species can be produced by electrodeposition of a Et_4NReS_4 solution in acetonitrile (at 0.6 V *vs* AgCl/Ag) for 2 min, this reaction being reversible: at −900 mV, the precipitated solid dissolved to give $(ReS_4)^-$. In the same study, amorphous ReS_4 was prepared by oxidation of Et_4NReS_4 with iodine and ferrocenium salt $(Cp_2Fe)PF_6$ in acetonitrile. Based on a set of methods, ReS_4 is shown to be a superposition of two states, $Re^V(S^{2-})(S_2^{2-})_{1.5}$ and $Re^{VI}(S^{2-})_2(S_2^{2-})_1$. It was also found out that a commercial product Re_2S_7 (Aldrich), related to tetrasulfide ReS_4, is a superposition of two states such as $Re^{IV}(S^{2-})_{0.5}(S_2^{2-})_{1.5}$ and $Re^V(S^{2-})_{1.5}(S_2^{2-})_1$. Therefore, the Re^{7+} ion in thioperrhenate $Re^{VII}S_4^-$, in which it is stabilized by four terminal sulfide groups, acting as strong π-donors, is reduced in these reactions allowing some of the sulfide groups to oxidize to disulfide ones.

Sulfur-rich molybdenum polysulfides MoS_5, $MoS_{5.6}$ and MoS_6 in the form of amorphous solids were derived from solutions of $(NH_4)_2Mo_2S_{12}$ in various media (acetone, I_2/DMF, aqueous HCl).[145, 146, 152, 240] Interestingly, under hydrothermal conditions, the species of non-stoichiometric polysulfide $MoS_{5.6}$ grew in the original morphology of hollow spheres, which is probably due to the slow steps of nucleation and particle growth.[152]

Also, TMPCs derived from $(NH_4)_2MoS_4$ were produced in the form of aerogels, which are fluffy porous structures.[167] For this purpose, a solution of $(NH_4)_2MoS_4$ in formamide/DMF was treated with iodine to afford amorphous molybdenum polysulfide as a paste. The precipitate was allowed to age for a month, washed repeatedly with a water–alcohol mixture and then with alcohol and dried in supercritical CO_2 at 42 °C and a pressure of 1400 psi (≈95 atm). As a result, chalcogenide aerogel (chalcogel) MoS_x ($x \approx 3-4$) was formed. According to PDF and XPS data, the aerogel is a network having a residual negative charge; its structure consists mainly of trinuclear $[Mo_3S_{13}]^{2-}$ clusters and the aerogel formula was determined as $(NH_4)_{0.2}MoS_4$. The product features high specific surface area (up to 370 $m^2\ g^{-1}$) and porosity, hence, exhibits good sorption capacity towards iodine, mercury and several gases. This study is a continuation of a cycle of publications on the synthesis and investigation of chalcogels of other transition metals.[165]

Several procedures to prepare molybdenum polychalcogenides from molybdenum(VI) oxygen compounds have been reported. For instance, MoS_3 was prepared by reacting MoO_3 with Na_2S in an acidified aqueous solution.[127] The study[126] used ammonium heptamolybdate $(NH_4)_6(Mo_7O_{24})\cdot 4H_2O$ and Na_2S as a sulfur source to produce MoS_3. An alternative approach is to use sulfur: heating a mixture of $(NH_4)_6Mo_7O_{24}\cdot 4H_2O + S_{ex}$ in propylene carbonate furnished $MoS_{\approx 3}$ and $MoS_{\approx 4}$ nanoparticles of 15–29 nm size.[148] Apparently, under these conditions, both sulfur and the solvent *per se* had reductive properties. Potato starch was used as a particle growth inhibitor. A mixed amorphous tetrachalcogenide $MoSe_3S$ was prepared by bubbling a mixture of hydrogen sulfide and hydrogen selenide through a solution of ammonium molybdate in aqueous ammonia.[157]

Sodium molybdate was also used in the reaction with elemental selenium to produce amorphous molybdenum triselenide $MoSe_3$.[204] Reactants were heated under hydrothermal conditions in 80% aqueous hydrazine at 180 °C for 12 h. The Se 3d XPS spectrum of amorphous $MoSe_3$ showed peaks corresponding to Se^{2-} and Se_2^{2-} in a ratio of 1/1, which allowed the triselenide formula to be defined as $Mo^{4+}(Se^{2-})(Se_2^{2-})$. Heating of purified $MoSe_3$ in a dynamic vacuum at 450 °C gave crystalline $MoSe_2$, which demonstrates the similarity of the chemical behaviour of this substrate with other metal trichalcogenides.

Sulfur-rich amorphous polysulfides CrS_3, MoS_5 and WS_5 and their polyselenide analogues are produced when treating carbonyls $M(CO)_6$ with an excess of sulfur and selenium, respectively, in 1,2-dichlorobenzene at 160 °C (see Fig. 2*f*).[143, 144, 155, 174]

3.4. Synthesis of nanosized transition metal polychalcogenides using templates and surfactants

It is of particular interest to develop synthetic approaches to produce TMPC materials on the nanoscale. Carbon templates are often used in the synthesis, which help to stabilize the metal polychalcogenides on the surface and also affect the composition of the product and sometimes even facilitate the formation of novel compounds in the form of nanostructures.

Recently, nanosized tellurides $TaTe_3$,[231] $NbTe_3$, VTe_3 and $TiTe_3$,[230] were prepared, whose crystal analogues were not previously reported and whose structures were not described. These phases were stabilized as thin crystals consisting of several $\{MTe_3\}_\infty$ chains, with structures similar to that of the infinite chains in the $NbSe_3$ structure (a member of the trichalcogenide family, such as NbS_3, see Fig. 1*f*). The above compounds were synthesized within the cavity of multiwalled carbon nanotubes: they were formed on heating stoichiometric quantities of a metal and tellurium in the presence of iodine vapour and multiwalled end-opened carbon nanotubes at 520–625 °C. Single- and many-chain specimens of Ti, V, Nb tritellurides are probably stabilized by the carbon nanotube walls, which act as suitable nanoreactors.

Nanosized quasi-1D VS_4 (Ref. 87) was grown using graphitic templates (graphene, graphene oxide, carbon nanotubes, perylene-3,4,9,10-tetracarboxylic dianhydride) in the presence of Na_3VO_4 and thioacetamide C_2H_5NS under hydrothermal conditions, which has been confirmed by numerous follow-up publications.[88–90, 92–95, 99, 101–103, 110] In some cases, the method was modified, *e.g.*, by the addition of a surfactant.[109, 111] Graphene oxide was found to contribute specifically to the formation of the VS_4 phase.

However, the template-free synthesis of VS_4 accomplished under hydrothermal conditions using the same reactants, vanadate Na_3VO_4 and thioacetamide C_2H_5NS, with careful control of experimental conditions was also reported.[1, 96, 106] For example, it was shown that increasing the reaction time up to 48 h favours the formation of VS_4, and to prevent oxidation of vanadium to its oxides, it is important to reduce the reaction temperature from 180 to 140–160 °C.[91] The authors note that the change in pH of the aqueous solution from 5 to 12 has no significant effect on the crystallinity of VS_4 but is a factor in controlling morphology of the resulting particles. The study[96] also provides the method for coating VS_4 microspheres with organic polymer films. Moreover, in the absence of a structural template, VS_4 amorphous films can be produced *via* an atomic layer deposition onto aluminium oxide using vanadium(III) *tris*-(*N*,*N*′-diisopropylacetamidinate) ($V(amd)_3$) and H_2S.[100] The process occurred at a temperature <200 °C; in the first half-cycle (the pulse of a

vanadium precursor followed by nitrogen purging) the parent vanadium complex lost its organic ligands, while in the second half-cycle (the pulse of 4% H_2S/N_2 followed by nitrogen purging), hydrogen sulfide generated S_2^{2-} disulfide moieties followed by oxidation of V^{3+} to V^{4+}. At higher temperatures, V_2S_3 films were obtained.

Transition metal polychalcogenide nanomaterials are also accessible by solvent methods carried out in the presence of surfactants, as in the case with nanoparticle synthesis of many other compounds. For example, 2D nanoplates of $ZrSe_3$ and $HfSe_3$ were produced from $ZrCl_4$ and $HfCl_4$ and selenium in oleylamine, a high-boiling solvent with coordinating and stabilizing properties.[229]

$MoS_{\approx 3}$ and $MoS_{\approx 4}$ nanoparticles of 15–29 nm size were prepared by heating a solution of ammonium heptamolybdate with excess sulfur in propylene carbonate with potato starch added, which was used as a particle growth inhibitor.[148] After the process is completed, the particles were heated to 400 °C in a flow of nitrogen or hydrogen to afford highly porous MoS_2.

Nanoparticles of MoS_3 and $ReS_{\approx 5}$ of 8–110 nm size prepared from thiometallates were explored as friction modifiers for mineral lubricating oils. Several tetraalkylammonium thiometallates $(Alk)_4NMoS_4$ and $(Alk)_4NReS_4$[247] were subjected to thermosolvolysis in DMF at 155–165° in the presence of alkenyl succinimide.

3.5. Ultrasonic exfoliation of bulk to nanosized samples

Polychalcogenides in the form of nano-objects can also be produced *via* post-synthetic treatments, which enable the isolation of species of a certain dispersibility and/or possessing given properties. For example, this can be achieved through exfoliation of their bulk analogues by mechanical[28, 29, 52, 58, 59, 61, 71, 73, 77] or physicochemical[8, 53–57, 72, 75, 76, 248] means or their combinations.[69] However, it should be noted that high anisotropy of such materials (width/height ratio) makes mechanical exfoliation very difficult in practice.

Liquid-phase exfoliation results from overcoming the weak van der Waals interactions in the polychalcogenide structure and thereby separating the layers or chains that make up the bulk material. This group of methods is to a great extent based on a large body of literature data on exfoliation of other weakly bonded materials[249–251] such as graphite/graphene,[252] MoS_2-like transition metal dichalcogenides[253] and hexagonal boron nitride.[254] Generally, a layered material is treated with solvents under ultrasonication (US); to remove unexfoliated bulk materials, centrifugation is applied. As a whole, US-stimulated interaction between the material and the solvent can be represented as a following sequence: 1) immersion into the solvent, 2) exfoliation and 3) stabilisation of the colloidal solution containing the nanoplates. The width of the resultant plates, their lateral dimensions, concentration and other characteristics depend on the experiment conditions. Ultrasonication parameters, the solvent nature and the composition of the liquid medium have the greatest impact on the properties of the resultant dispersions.

In this regard, of particular interest is liquid-phase chemical exfoliation of polychalcogenides. Some of the first experiments in this direction were carried out in our laboratory with VS_4 and MQ_3 (M = Ti, Zr, Nb, Ta).[8, 54–57, 75, 83, 248] We have systematically explored the dispersion of polychalcogenides in liquid media and comprehensively characterised the resulting products by modern physicochemical methods. It was shown that under direct ultrasonication, bulk trichalcogenides NbS_3, $NbSe_3$,[54, 55, 75] TaS_3,[56] ZrS_3 (Ref. 83) and tetrachalcogenide VS_4[8] are consistently dispersed in a series of organic solvents (Fig. 9).

The most stable and concentrated colloids (up to 0.4 g L^{-1} for NbS_3 and $NbSe_3$ and up to 0.3 mg L^{-1} for VS_4) are formed in isopropanol and water-ethanol mixture, which distinguishes polychalcogenides from dichalcogenides and graphene, which are best dispersed in DMF and *N*-methylpyrrolidone. Transformation of TaS_3 into colloid occurs only in acetonitrile and DMSO.[56] According to the data of atomic force microscopy and photon correlation spectroscopy, colloidal NbS_3 and $NbSe_3$ contain thin, well-crystallized nanostructures with a high linear size ratio, which allows us to term them as 'nanoribbons' (50–200 nm length, 1–20 nm width).

Trichalcogenide nanoribbons obtained in colloids are thinner and shorter than nanoribbons synthesised from elements (the bottom up method, Section 3.1), where the thickness of $NbSe_3$ species ranged from 20–30 nm to 95 nm.[36, 42] In the case of VS_4, individual particles are shaped like rods or elongated plates several hundred nanometres long (Fig. 9 *b*,*c*).[8] Interestingly, TEM images show that VS_4 nanorods align themselves in an end-to-end fashion, which is probably due to the features of their edges, *e.g.*, dangling bonds and functional groups. Another indirect proof is that the colloidal nanostructures are charged (zeta potential is −44 mV ($NbSe_3$/alcohol),[54] −34 mV (VS_4/alcohol),[8] −12.6 mV (TaS_3/acetonitrile) and

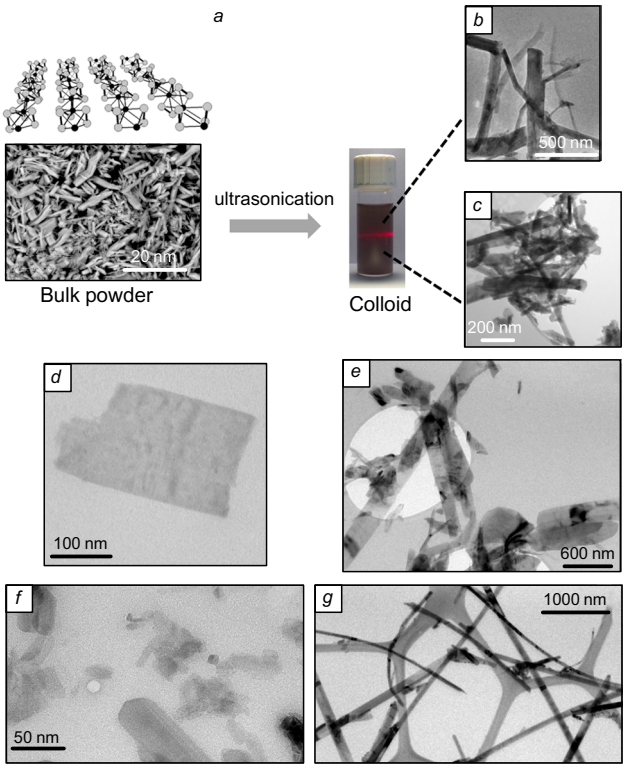

Figure 9. Schematic illustrating the process of exfoliation crystalline samples to nanoscale by the example of VS_4 (*a*),[8] and TEM images of the products obtained in the form of VS_4 nanorods (*b*, *c*);[8, 98] ZrS_3 nanosheets (*d*);[53] TiS_3 nanoribbons (*e*);[76] ZrS_3 particles (*f*, *g*).[83] Reprinted with the permission of Wiley, American Chemical Society, Royal Society of Chemistry, Springer, Elsevier.

+20.2 mV (TaS_3/DMSO)[56]). Filtration or spraying of the colloids produces textured thin films with good conductivity, volt-ampere characteristics[55] and other transport properties.[57] For example, a colloidal solution of ZrS_3 in isopropanol was used to sputter ZrS_3 on the surface of perovskite $CH_3NH_3PbBr_3$ as an electron-injection layer in an LED material.[255]

Besides the works of our scientific group, one of the few examples of obtaining polychalcogenide nanostructures in colloidal dispersions is the study[53] proposing a two-step procedure to prepare 2D ZrS_3 comprising an initial treatment of ZrS_3 with n-propylamine in an autoclave at 120 °C for 3 days followed by dispersing the washed product in a mixture of ethanol and 1-cyclohexyl-2-pyrrolidinone under ultrasonication. The resulting nanostructures have proven efficient catalysts for oxygen evolution reaction. Finally, another study made use of a sequence of chemical liquid-phase dispersion in ethanol and mechanical exfoliation of $TaSe_3$ to produce $TaSe_3$ nanowires up to several millimetres long and lateral dimensions of ~20–70 nm.[69] The obtained species were then modified with hexagonal boron nitride (*h*-BN), which prevented oxidation of the edges of the $TaSe_3$ nanostructures, and the resulting heterostructures were used in model electronic devices.

The question arises, how exactly does the transformation of the bulk MQ_3 powder into a colloid occur? Theoretically, there are three possible cutting directions for a nanocrystal (Fig. 10): (1) parallel to the plane *ab* (direction 001) — exfoliating the layers from the bulk phase, (2) parallel to the plane *bc* (direction 100) — breakage of the interchain linkages and (3) parallel to the plane *ac* (direction 010) — 'cutting' the chains length.

As thin nanoribbons are found in the colloids, it is likely that exfoliation occurs parallel to the *ab* plane as expected, given that only weak van der Waals bonds between the layers need to be overcome to separate layers in this direction. Exfoliation and stabilization of NbS_3, $NbSe_3$, ZrS_3, and also VS_4 in the form of colloidal nanoribbons (nanorods for VS_4) appear to be the result of solvent intercalation into the spaces between the columns, leading to material exfoliation and stabilization of the resulting colloids by solvent molecules with suitable surface energies. Bulk particles may also be cleaved in other directions, for example, nanoribbons may be ultrasonically cut perpendicular to the ribbon axis, breaking not only van der Waals but also stronger covalent bonds, which is most clearly observed for VS_4.[8]

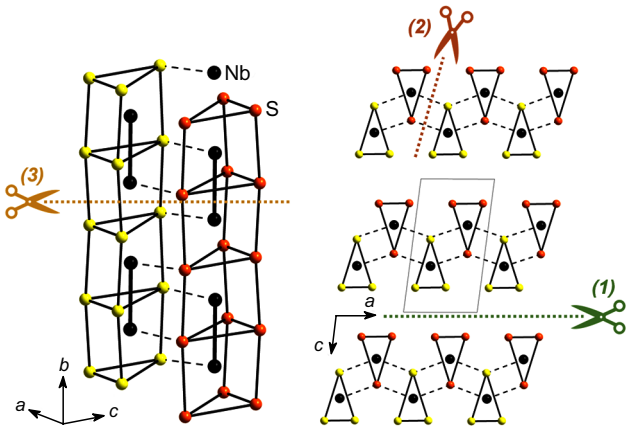

Figure 10. Schematic representation of NbS_3 crystal cutting potential directions during liquid phase exfoliation.[55] Reprinted with the permission of the Royal Society of Chemistry.

The question of which particular properties of a solvent render it capable or incapable of dispersing a layered material has been discussed from various standpoints. On the one hand, intermolecular interactions with solvent molecules, which do not provide covalent bonds but are strong enough to overcome the forces of attraction between nanosheets, are considered. On the other hand, recent studies on dichalcogenides MQ_2 (M = Mo, W, *etc.*) show that interactions at the solvent–MQ_2 interface may be of a more complex, chemical nature, determined in particular by the solvent's ability to form chemically active species during sonolysis.[256–259] Probably, the same applies to polychalcogenide materials.

Depending on how the TMPC nanoparticles are prepared, different methods are used to determine the size of the particles, in particular microscopic methods (scanning and transmission electron microscopy, sometimes atomic force microscopy). As for colloidal solutions of TMPC nanoparticles, colloidal chemistry methods usual for sols of other nanoparticles are applied. For example, particle size distributions are obtained from photon correlation spectroscopy data, possibly followed by modelling of the distributions with an idealized particle shape (*e.g.*, within the framework of Deryagin–Landau–Verwey–Overbeek theory). Since the above methods of particle shape and size characterisation are not specific to TMPCs, we did not focus on them in this review.

4. Chemical properties

Since polychalcogenide materials are very diverse, in this review we tried to summarize some of their characteristic chemical properties. Many of the interesting chemical properties of TMPCs stem from the presence of S–S fragments therein.

When heated in a vacuum, TMPCs lose some of their chalcogen atoms and eventually transform to dichalcogenides. In particular, trisulfides of Ti, Zr and Hf are directly converted to disulfides, amorphous pentasulfides first lose sulfur to give trisulfides, and then disulfides,[260] whereas Nb_2Se_9 when heated *in vacuo*, transforms to $NbSe_3$.[242] The transformation of NbS_3 nanoribbons into NbS_2 nanosheets has recently been studied in detail by *in situ* electron microscopy (Fig. 11).[261]

It is likely that on heating to 500 °C, each $(S_2)^{2-}$ loses one sulfur atom, less strongly bonded to niobium than S^{2-} (Fig. 11 *a*). The atoms then need to be rearranged so that the existing chains are transformed into layers (Fig. 11 *b*). Bonds are formed between each Nb atom and two additional S atoms from neighbouring chains, which is promoted by pre-existing Nb···S interactions. As a result, a half of the new $\{NbS_6\}$ polyhedron of the NbS_2 building block is constructed.

As these chemical changes occur, niobium sulfides 'fuse' to form continuous sheets of NbS_2 made up of $\{NbS_6\}$ polyhedrons sharing their edges.

Heating the trichalcogenide to a temperature sufficient to remove some S_2^{2-} disulfide groups but not sufficient for the complete conversion of MX_3 to MX_2, is used to create targeted defects on the disulfide groups (M = Ti,[262] Zr (Ref. 263)). For this purpose, annealing of ZrS_3 (at 700 °C) or TiS_3 (at 550 °C) in a sealed ampoule for

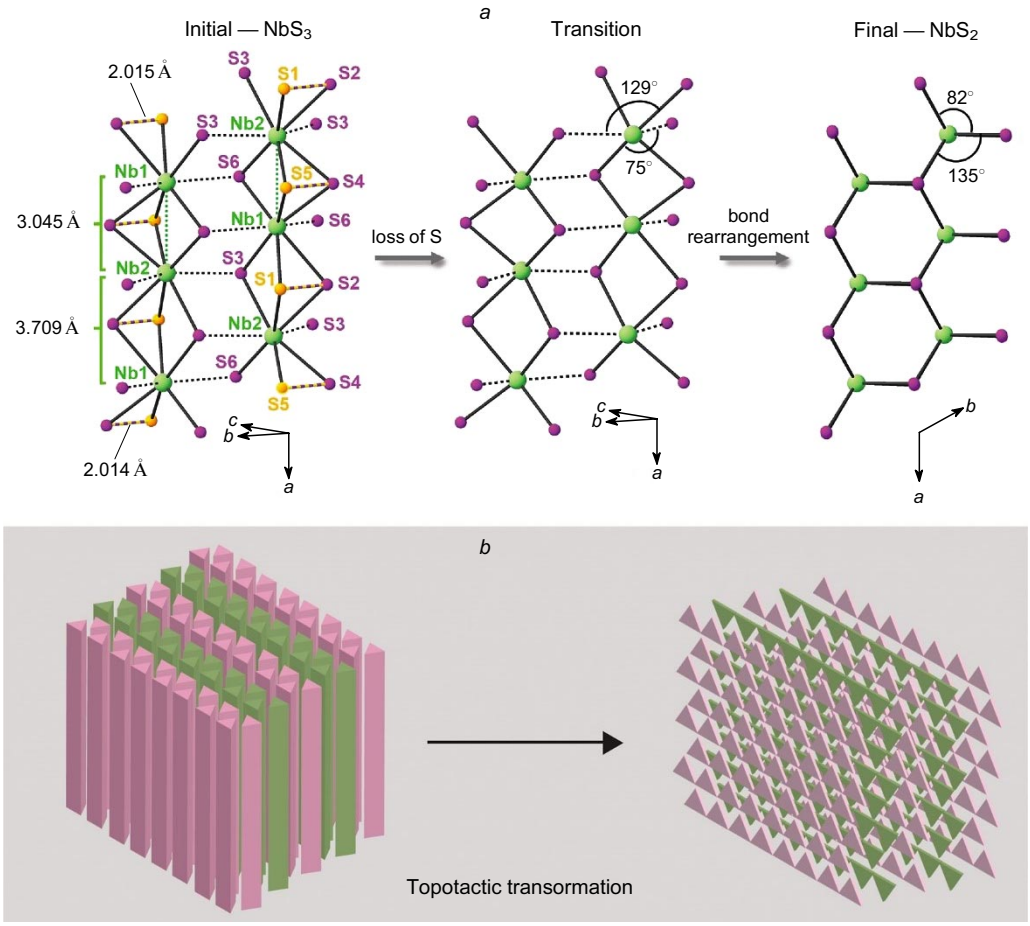

Figure 11. Structure of pristine NbS_3 (*a*). When heated *in vacuo* to 1000 °C, the loss of sulfur occurs (marked in yellow), the bonds are then rearranged, and NbS_2 is formed; schematic representation of the topotactic transformation of quasi-1D NbS_3 to quasi-2D NbS_2 (*b*).[261] Reprinted with the permission of the American Chemical Society.

10–30 min is carried out. This produces no disulfide, since to obtain TiS_2, temperature should be >600 °C,[40] while for ZrS_2 it should be 820 °C,[39] but the S_2^{2-} vacancies arise (the formula was determined as $ZrSS_{2-x}$ or TiS_{3-x}), affecting the catalytic activity of the species in the reactions of photochemical hydrogen evolution [262] or hydrogen peroxide synthesis.[263]

On heating sulfur-rich amorphous pentasulfides MoS_5 and WS_5, sulfur is lost in two steps: first, trisulfides MS_3 (M = Mo (190 °C), W (240 °C)) are formed, then poorly crystalline MS_2 disulfides of spherical morphology similar to the pristine MS_5 (M = Mo (380 °C), W (300 °C)).[260] The kinetics of their thermal decomposition was studied based on thermogravimetric analysis and it was shown that both steps are described by the Avrami–Erofeev model including random nucleation and subsequent nucleate growth. The rate-limiting step is the diffusion of sulfur from spherical MS_5 particles. Theoretical modelling results suggest that the first step of thermolysis is depolymerization of MS_5 chains to afford cluster units followed by desulfurization.

Amorphous molybdenum sulfides transform into cluster compounds through a number of chemical reactions.[122, 203, 264–268] Thus, amorphous MoS_3 reacts with an aqueous solution of sodium cyanide to give an anionic cluster complex $[Mo_3S_4(CN)_9]^{5-}$ and a small amount of $[Mo_4S_4(CN)_{12}]^{8-}$ (Refs 122, 203, 266), while the reaction of MoS_3 with ammonia or aqueous KOH affords complex $[Mo_3S_{13}]^{2-}$ (Refs 203, 265, 267). At the same time, the cluster anion salt $[Mo_3S_7Cl_6]^{2-}$ was isolated from the reaction of MoS_3 with concentrated HCl.[203] At first, these experiments were carried out to establish the structure of amorphous MoS_3: it was assumed that cluster units are excised from the polycrystalline material and therefore, MoS_3 is described by a cluster model (see Fig. 2*b*), rather than a chain one (see Fig. 2*a*). Nevertheless, there is an ongoing debate on this topic, since there may also be a sequential degradation of the chain structure and then — an assembly of cluster units in solution: for example, the fusion of two Mo_2 dimers and monomer extraction may produce a Mo_3 metal cluster.[123] In any case, the findings once again confirm the close relationship between polychalcogenide structures and molecular clusters, at least in the case of the 'Mo–S' system.

We have recently described the formation of cluster complexes from the sulfur-rich amorphous pentasulfides MoS_5 and WS_5.[268] These compounds react with molten thiuram disulfide to furnish triangular cluster complexes comprising $\{Mo_3S_7\}^{4+}$ and $\{W_3S_4\}^{4+}$ cores, and the reaction between MoS_5 or WS_5 and halogenating agents ($CHCl_3$ and Br_2) gives well-known coordination polymers $M_3S_7Hal_4$ (M = Mo, W; Hal = Cl, Br). Assuming that the parent MS_5 has a chain-like structure based on M_2S_8 dimers or M_3S_{12} trimers,[174] it can be stated that the rearrangement of clusters depends on the reaction conditions. Remarkably, molybdenum formed only clusters with $\{Mo_3S_7\}^{4+}$ core, and tungsten formed two different cluster cores depending on conditions: $\{W_3S_4\}^{4+}$ in dithiocarbamate complex and $\{W_3S_7\}^{4+}$ in coordination thiohalide polymers.

Transition metal polysulfides, like many other layered and chain compounds, are characterized by metal ion intercalation reactions, primarily the electrochemical intercalation of Li^+ in electrodes for lithium-ion batteries

(LIBs), but also other metals such as Na^+, Mg^{2+}, Zn^{2+}, Al^{3+} to create Na-ion,[93, 99, 102, 106, 107, 111] Mg-ion,[109, 269] Zn-ion [270, 271] and Al-ion [110] batteries (see Section 5.1). In intercalation reactions, the electron density is redistributed between guest and host and in the case of polychalcogenides, this means electron transfer to disulfide groups and elongation or cleavage of the Q–Q bonds: $(Q-Q)^{2-} + 2e^- \rightarrow 2Q^{2-}$. In addition to intercalation, a conversion mechanism can also take place, where the reaction is completed to form (nano)transition metal species and lithium chalcogenide. The reversibility or irreversibility of the intercalation process depends on the specific compound and the amount of inserted lithium. Recently, using $NbSe_3$ as an example, it was shown [272] that a particular reaction pathway also depends on the size of the chalcogenide species (Fig. 12). During electrochemical intercalation of lithium cations into $NbSe_3$ species with lateral sizes of several hundred nanometres, the lattice is capable of relaxation and accomodation of Li^+ ions in the interchain/interlayer space. On the surface of the particles, however, the conversion process yielding Li_2Se ($NbSe_3 + 6Li^+ + 6e^- \rightarrow Nb + 3Li_2Se$) occurs. The same happens during lithiation of particles <100 nm in size, where a nanocomposite containing Nb nanoparticles on Li_2Se is formed very rapidly.[272] It is obvious that metal ion intercalation is of direct practical interest for LIB applications, which is the subject of Section 5.1 of this review.

In addition to electrochemical intercalation of metal ions into TMPCs, intercalations of hydrazine into $TaSe_3$ (Ref. 273) and ammonia into NbS_3 were reported.[274] The intercalation of K^+, Rb^+, Cs^+ and Ca^{2+} cations into $ZrSe_3$ *via* a chemical process using alkali metal and calcium solutions in ammonia in an inert atmosphere at reduced temperatures has recently been described in detail.[275] Intercalation of alkali metal ions from NH_3 solution at -78 °C into $ZrSe_3$ furnished intercalates $K_{0.45(2)}ZrSe_3$ (space group $Cmc2_1$), $Rb_{0.41(1)}ZrSe_3$ (space group *Immm*) and $Cs_{0.42(1)}ZrSe_3$ (space group *Immm*). Compared to $ZrSe_3$, the interlayer spacing in the products increased by 16, 20 and 25%, respectively, as expected based on the large sizes of cesium and rubidium atoms. The Zr–Se distances (2.7654(2) Å for $ZrSe_3$) showed no significant changes: for example, in potassium intercalates, this value was 2.789(7) Å, and the oxidation state of Zr remained at 4+. The main change affected the Se–Se distances due to their partial reduction: in $ZrSe_3$, the Se–Se distance was 2.3441(6) Å, and in $Rb_{0.41(1)}ZrSe_3$ and $Cs_{0.42(1)}ZrSe_3$ it was 2.592(4) and 2.605(5) Å respectively. The intercalation with Ca^{2+} from the Ca/NH_3 solution proceeds with co-intercalation of ammonia molecules, so that the product formula is expressed as $Ca_{0.2}(NH_3)_{0.45(7)}(NH_2)_{0.15(7)}ZrSe_3$ and the interlayer distance is 10 % larger than in the potassium intercalate. The reaction with metal might afford not only an intercalate but, under certain conditions, a material with selectively formed sulfide ligand vacancies (S^{2-}), which was shown in a study [263] for ZrS_3, treated with lithium solution in ethylenediamine at 120 °C.

The surface properties of polychalcogenide particles differ from those of surfaces formed only by S^{2-} atoms. Thus, we observed oxidative properties of $(S-S)^{2-}$ units in the reactions of VS_4 and NbS_3 with silver particles.[98] The reduction of silver salts in the presence of 'normal' MoS_2-type sulfides (devoid of the S–S bonds) stabilizes silver metal particles (Ag/MoS_2) on the sulfide surface (*in situ* approach). Unlike MoS_2, polysulfide materials under similar conditions favour formation of Ag_2S nanoparticles. This process can proceed in two ways (Fig. 13): in a one-step (*a*) or two-step (*b*) fashion with the intermediate formation of silver metal nanoparticles. The (S_2^{2-}) disulfide groups act as oxidant in both cases. The second path (two-step) is also accomplished when mixing a colloidal polychalcogenide (VS_4, NbS_3) with pre-synthesized Ag^0 sol (*ex situ* approach).

To summarize, 'Ag/VS_4' or 'Ag/NbS_3' species cannot be obtained: the silver is stabilized as a sulfide. Ag/MoS_2, Ag_2S/NbS_3 and Ag_2S/VS_4 samples were characterized by a number of methods and it was shown that the unexpected formation of Ag_2S instead of Ag on polysulfide surfaces is probably due to complex redox processes involving S–S disulfide units, which are absent in MoS_2, but are present in VS_4 or NbS_3 structures. This observation is of interest both for a fundamental understanding of the properties of sulfur-rich surfaces and in terms of a new synthetic approach to Ag_2S nanoparticles as part of composites for various applications.

Similar observations regarding the reactivity of $(S-S)^{2-}$ groups were described by Afanasiev *et al.*[276] when studying the reactions of amorphous molybdenum polysulfides MoS_x with H_2. At room temperature, polysulfide groups irreversibly react with hydrogen, resulting in the cleavage of S–S bonds and the formation of labile –SH functional groups, which escape from the surface as H_2S in the hydrogen flow:

$$Mo-S-S-Mo \longrightarrow 2\,MoSH \longrightarrow MoS-Mo-SH_2$$

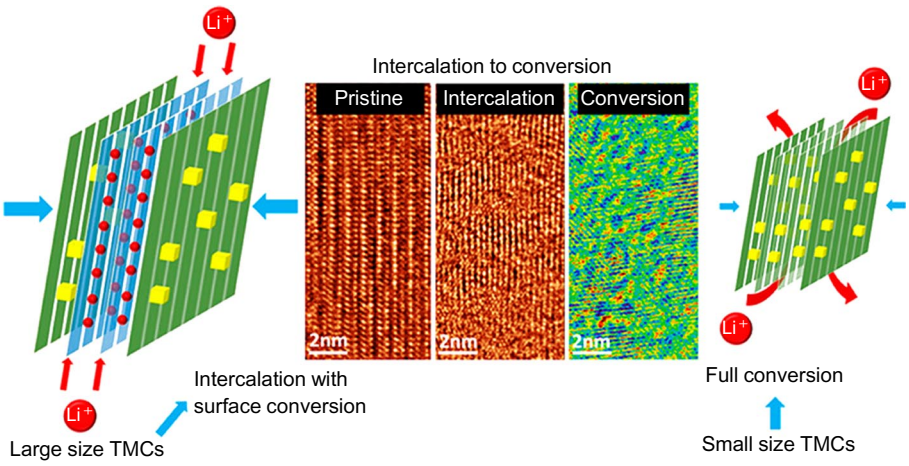

Figure 12. Different mechanisms of interaction of $NbSe_3$ with lithium cations depending on the particle size: large particle size favours intercalation, while small particle size favours conversion process (formation of $Nb + Li_2Se$).[272] TMC — transition metal chalcogenides. Reprinted with the permission of the American Chemical Society.

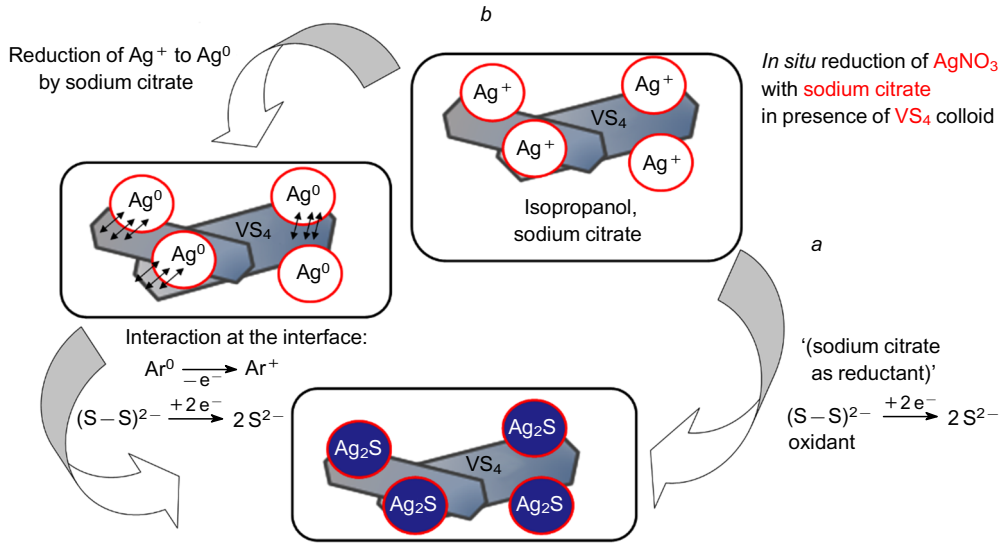

Figure 13. Schematic of two possible pathways for the formation of Ag_2S nanoparticles anchored to VS_4 nanorods: the direct formation of Ag_2S when a reducing agent is added to VS_4 colloid containing Ag^+ (*a*); a two-step process in which Ag^+ ions are first reduced by sodium citrate to form Ag^0 nanoparticles, and then oxidized to Ag_2S by disulfide groups (*b*).[98] Reprinted with the permission of Wiley.

The amount of absorbed hydrogen directly depended on the number of S–S bonds, which varied over a wide range.

In the case of MoS_3, it was shown that the surface bridging S-S groups are also able to reversibly bind water molecules, which was used to create moisture sensors.[182]

5. Potential applications

5.1. Metal-ion batteries

Ideas of using transition metal chalcogenides in lithium-ion batteries date back to the 1970–1980s, in particular to the works of M.S.Whittingham,[277] who was awarded the 2019 Nobel Prize in chemistry. Both di- and trichalcogenides were investigated then, but since the technological breakthrough came with the use of $LiCoO_2$-type oxide materials, chalcogenide materials faded into background for some time.

However, in the last 5–10 years interest in chalcogenide materials has renewed, and experimental evidence appeared that new generation electrodes with increased capacity can be developed on their basis.[1,278] Moreover, use of TMPC-based electrodes allows successfully solving the problem preventing development of Li–S batteries, namely, an escape of polysulfide anions (polysulfide shuttle effect) into liquid medium, which lead to corrosion of anodes. Metal–sulfur covalent bonds in TMPCs inhibit this process. Many state-of-the-art works use nanosized TMPCs in metal-ion batteries, but at the same time, the effect of electrode particle size on battery performance is ambiguous since, on the one hand, diffusion of lithium (or other metal) ions in the nanomaterial is facilitated, but on the other hand, side 'harmful' reactions of the electrode nanomaterial with the electrolyte are simultaneously accelerated, impairing cyclability and stability.

Among chalcogenides, both di- and polychalcogenides are studied, but it is noteworthy that when made into electrodes, they operate following remarkably different mechanisms. Under reversible intercalation of lithium ions, TiS_2 dichalcogenides form Li_xTiS_2 due to redox conversion at cationic centres: Ti^{4+}/Ti^{3+}, similarly to the way it occurs in classical oxide electrodes $LiCoO_2$, $LiMn_2O_4$, $LiFePO_4$ (Fig. 14*a*).

However, in the case of polysulfide electrodes other chemical processes are added, because anionic groups which traditionally were considered inactive are actively involved in electrochemical transformations, *e.g.*, $S_2^{2-} + 2e^- = 2S^{2-}$ (anionic redox mechanism). Such behaviour of polysulfide electrodes is due to the fact that the 3p orbitals of S atoms largely overlap with the d orbitals of transition metal atoms (Fig. 14*b*), and hence electron density may transfer between them, and therefore, the anionic redox mechanism works, for example, in $Li_{1-x}TiS_3$ but not in $Li_{1-x}TiO_2$.[177,278]

From a practical point of view, it is important that due to the anionic redox mechanism, more lithium atoms can be involved in the reaction: $2Li + TiS_3 \rightarrow Li_2TiS_3$ (as opposed to $Li + TiS_2 \rightarrow LiTiS_2$), and therefore an increase in battery capacity with such electrodes can be achieved. Below we will take a closer look at recent data on the use of various transition metal polychalcogenides as electrode components for metal-ion batteries.

In the series of TMPCs, transition metal trichalcogenides MQ_3 with quasi-layer structures were historically the first to be tested as LIB electrodes. In the 2000s, such compounds began to be re-explored both theoreti-

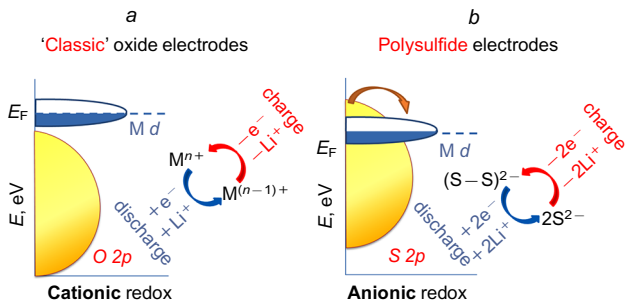

Figure 14. Two different mechanisms of redox activity of electrode materials. Schematic representation of band structure of conventional oxide electrode materials characterized by higher position of 3d orbitals of the transition metal *M* in relation to p orbitals of O anions (*a*). Schematic representation of band structure of the transition metal polysulfide (*b*). In this case, p orbitals of less electronegative S lie higher (than in O) and can overlap with the metal 3d orbitals, thus enabling the intramolecular electron transfer and triggering the anionic redox process. E_F is the Fermi level.[177] Reprinted with the permission of Wiley.

cally,[269, 279] and in practice, in particular TiS_3,[44, 68, 280] ZrS_3,[74] $NbSe_3$,[78] NbS_3.[228] The MQ_3 interlayer spacing can accommodate up to three lithium ions per MQ_3 formula unit, as exemplified by TiS_3:

$$TiS_3 + 2\,Li^+ + 2\,e^- = Li_2TiS_3$$
(accompanied by the S—S bond cleavage)

$$Li_2TiS_3 + x\,Li^+ + x\,e^- = Li_{2+x}TiS_3\ (0 < x < 1)$$

Density functional calculations show that the electron density from the absorbed lithium is largely transferred to the nearest sulfur atoms.[269, 279] The capacity of an electrode based on crystalline TiS_3 in LIB is calculated to be 339 mA h g^{-1}, while for a monolayer it is 260 mA h g^{-1}.[279] In practice, higher values are obtained, which is probably due to the use of amorphous materials: it has been observed that amorphization increases the availability of the structure for lithium ions and allows more anionic centres to be involved in the redox process.[44, 135, 149, 150, 225, 226, 228, 239] Thus, all-solid-state batteries with electrodes based on amorphous TiS_3 (particles in the micron size range) reached capacities of 400 mA h g^{-1},[44] while batteries with liquid organic electrolytes reached 350 mA h g^{-1}.[280] However, in the latter case, after a few initial cycles the capacity decreases rapidly and is set at around 50 mA h g^{-1}.[280] In the case of a solid-state battery, the results are slightly better — 300 mA h g^{-1} after 10 cycles.[44] Maintaining a high capacity during cycling is challenging, since lithium intercalation into TiS_3 is only partially reversible.

A significant part of the new research using TMPCs as electrode materials is devoted to sulfur-rich amorphous phases (MS_x, where $x \geqslant 4$). Many such materials are produced by mechanochemical synthesis from a lower sulfide, and sulfur and in this process the reagents amorphize and enter the reaction, which is accompanied by a reduction in particle size.

In a series of amorphous niobium polysulfides NbS_3, NbS_4 and NbS_5, the initial discharge capacities raised from 281 (NbS_3) and 446 mA h g^{-1} (NbS_4) to 596 mA h g^{-1} (NbS_5), which corresponded to 2.0, 3.7 and 5.6 electrons per formula unit.[228] It is assumed that both sulfur and niobium atoms are involved in the redox process, and these reactions depend on each other, since niobium and sulfur are covalently bound in NbS_x (as in other TMPCs). However, attempts to achieve stable cycling for NbS_5 have so far failed, and capacities drop significantly after the 10th cycle.

Amorphous titanium polysulfide TiS_4 has been investigated not only in Li-ion,[149–151] but also in Al- (Ref. 225) and Mg-ion batteries.[226] When switching from crystalline TiS_2 to amorphous TiS_3 and TiS_4, the capacity of LIB cathodes increased to over 500 mA h g^{-1} (TiS_4) with reversibility over 10 cycles.[149]

A 4-electron process is assumed. In-depth studies on the mechanism of the TiS_4-based electrode [150] by PDF, DFT, Ti K-edge and S K-edge XANES techniques show that the typical products of the conversion process, Ti and Li_2S, are not formed. Instead, TiS_4 is discharged to Li_4TiS_4, which is accompanied by the cleavage and reduction of the disulfide S—S bonds with a simultaneous change in the coordination number of Ti. The structure turns from a 'network' type in TiS_4 to a chain type in Li_4TiS_4 and back again.

More stable cycling of amorphous TMPC-based electrodes in all-solid-state batteries is observed: it was possible to optimize the composition of solid electrolytes and achieve stable operation of a battery with a high-capacity cathode based on TiS_4 for 100–200 cycles (507.4 mA h g^{-1}) after 100 cycles at a current density of 0.1 A g^{-1} and 350 mA h g^{-1} after 200 cycles at a current density of 1 A g^{-1}.[239]

Promising results were obtained for batteries using TiS_4-based cathodes and aluminium anodes: 206 mA h g^{-1} after 1000 cycles, which is one of the best results for Al-ion devices.[225] Its mechanism involves the anionic oxidation-reduction of $S_2^{2-} \leftrightarrow 2\,S^{2-}$, lowering the CN of Ti atoms, breaking the S—S bonds and forming Al—S bonds.

$$TiS_4 + x\,Al^{3+} + 3n\,e^- \leftrightarrow Al_xTiS_4\ (0 < x \leqslant 4/3)$$

Mg-ion batteries with TiS_4-based cathodes operate similarly, as shown by the same group of authors.[226]

In addition to amorphous titanium polysulfide, amorphous molybdenum polysulfides MoS_x ($x = 3–7$) are actively studied as electrode materials for Li- (Refs 68, 130, 135, 153, 281) and Na-ion batteries.[140, 142, 179, 180, 281] Note [281] that amorphous nanosized MoS_3 (prepared from $(NH_4)_2MoS_4$ in the presence of carbon nanotubes) has several advantages over TiS_3, TiS_4 and NbS_3 when used as a LIB cathode with liquid electrolyte: it allows operation at higher potential and is more stable under cycling (Fig. 15 *a*). In all-solid-state LIB,[68, 135] submicron-sized MoS_3 particles prepared using mechanochemical process, showed a capacity of ~670 mA h g^{-1} after 60 cycles, with the redox process affecting both sulfur and molybdenum atoms.

Amorphous MoS_x samples with sulfur content of $x > 3$ have also been studied. For example, $MoS_{5.7}$ showed a capacity of 746 mA h g^{-1} with 86% efficiency retained for 50 cycles in a liquid electrolyte-based battery.[153] It was found that the electrode operates by an unusual mechanism, as Li_2S_2 is formed in a reversible process:

$$MoS_{5.7} + 5.7\,Li^+ + 5.7\,e^- \longrightarrow Mo + 2.85\,Li_2S_2$$

In the case of all-solid-state sodium batteries, the samples of MoS_x ($x = 3–7$) synthesized by two different methods such as mechanochemical process and thermolysis from molecular precursors were compared.[142, 179, 180] It turned out that the samples obtained *via* thermolysis demonstrate higher content of disulfide groups and higher capacity of batteries using such electrodes. For example, MoS_6 produced by mechanochemical method shows capacity of 510 mA h g^{-1} while maintaining efficiency of 80% after 30 cycles, and for MoS_6 this value was 690 mA h g^{-1} while maintaining efficiency of 92%.[180] This once again confirms the important role of the anionic redox processes.

The operation mechanism of a cathode based on another related material such as molybdenum polysulfide chalcogel $MoS_{3.4}$ was studied in detail.[169] This substance is a porous amorphous network where the Mo^{4+} metal centres are linked by polysulfide chains, but are themselves chemically inactive in the electrode process. The polysulfide chalcogel features high gravimetric capacity of 578 mA h g^{-1}, maintained at 83% after 10 cycles and at 60% after 30 cycles, which is comparable to the performance of Li—S batteries. The results of XPS, EXAFS and PDF showed that upon the discharge of the battery, the S—S bonds in the polysulfide chains are cleaved and sulfur is reduced to S^{2-}, and upon its charge, S^{2-} is oxidised to form S—S bonds.[169]

Another polysulfide that has recently attracted great interest as an electrode material for metal-ion batteries is VS_4 with a quasi-chain structure, which is one of the most investigated TMPCs for battery applications: a recent

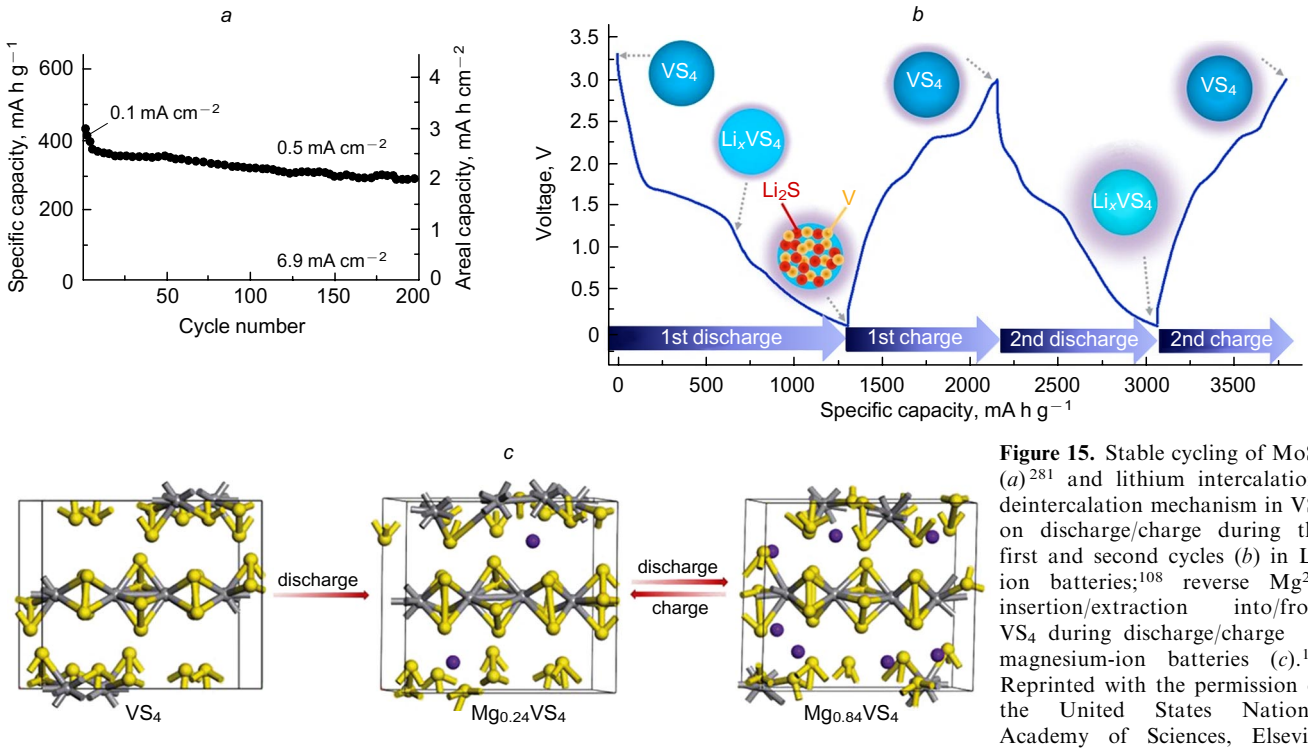

Figure 15. Stable cycling of MoS_3 (*a*)[281] and lithium intercalation/deintercalation mechanism in VS_4 on discharge/charge during the first and second cycles (*b*) in Li-ion batteries;[108] reverse Mg^{2+} insertion/extraction into/from VS_4 during discharge/charge in magnesium-ion batteries (*c*).[109] Reprinted with the permission of the United States National Academy of Sciences, Elsevier and Wiley.

review[282] is devoted entirely to electrodes based on this material. Vanadium tetrasulfide and its composites with graphene oxide were explored as electrode materials for Li-ion,[87,89,90,94,96,102,105,108] Na-ion,[93,99,102,106,107,111,283] Mg-ion,[109,284,285] Zn-ion[270,271] and Al-ion[110,286] batteries. VS_4-based electrodes (nanoparticles 50–500 nm) exhibit stable performance with high capacity: 727 mA h g^{-1} after 50 cycles even at currents up to ~3 A.[87,89] In continuation of the research by Xu *et al.*,[89] Britto *et al.*[90] carried out an in-depth study on complex and unusual redox processes occurring in VS_4-based electrodes involving both anion and cation. The products on different cycling stages were examined by solid-state NMR (^{6}Li and ^{51}V), S K-edge XANES and PDF analysis. Upon lithiation, sulfur dimers $(S-S)^{2-}$ first degrade to give an intercalated phase with a stoichiometry close to Li_3VS_4. In this compounds, formal oxidation states of V and S are 5+ and 2− respectively. Therefore, the conversion of VS_4 to Li_3VS_4 is characterized by an unusual redox reaction comprising an internal electron transfer from V^{4+} to $(S-S)^{2-}$ disulfide groups. As lithiation proceeds, once all the disulfide groups are reduced to sulfide ions, V^{5+} is partially reduced to V^{4+} in the $Li_{3+x}VS_4$ intercalate. Finally, V metal and Li_2S are formed, and the reverse reaction occurs, as upon charging, $Li_{3+x}VS_4$ is gradually formed again followed by amorphous VS_4. These interesting data show that the reversibility in this system is not exclusively due to the $Li_2S \leftrightarrow S$ reaction (which is similar to the process occurring in Li–S batteries), as previously assumed, but involves the metal V and at least partial conversion to the pristine phase.

The study[108] notes that lithiation and delithiation of VS_4 (nanoparticle size of <100 nm) in the first and subsequent cycles follow different mechanisms (see Fig. 15 *b*). Lithium sulfide is only formed in the first cycle, after which it converts back into VS_4, but now in an amorphous state, and then the following reaction occurs: $VS_4 + y\,Li^+ + y\,e^- \leftrightarrow Li_yVS_4$ ($0 < y < 8$) with reversible oxidation-reduction of the $S_2^{2-} \leftrightarrow 2\,S^{2-}$ disulfide groups. Thus, a mixed mechanism is confirmed, and not exclusively intercalation or conversion to V/Li_2S.

In contrast to Li-ion batteries, in Mg-ion devices, magnesium intercalation into VS_4 nanodendrites does not furnish alkaline-earth metal sulfide (MgS) and V metal (Fig. 15 *c*).[109] The reactions at the cathode can be represented as follows:

$$VS_4 + 0.24\,Mg^{2+} + 0.48\,e^- \longrightarrow Mg_{0.24}VS_4$$

$$Mg_{0.24}VS_4 + 0.6\,Mg^{2+} + 1.2\,e^- \longrightarrow Mg_{0.84}VS_4$$

Upon discharge, S_2^{2-} is partially reduced to S^{2-}, and V^{4+} is partially oxidized to V^{5+}. During cycling, the samples retain their morphology of nanodendrites ('sea urchins'), which affected the stable performance with a capacity of up to 74 mA h g^{-1} over 800 cycles at a high current density of 500 mA g^{-1}. This example shows that optimizing the morphology and nanostructuring of VS_4 and other TMPCs is a promising direction for the development of high-capacity and stably cyclable electrode materials. In addition, the use of novel electrodes requires optimization of electrolyte compositions and other constituents and battery operating conditions, as well as a better understanding of electrode mechanisms, but it can already be said that the potential for the use of TMPCs in this area is very high.

5.2. Electrocatalysis and photocatalysis

5.2.1. Electrocatalytic water decomposition

The hydrogen evolution reaction (HER) using various catalysts has been actively investigated in recent years,[287] when the production of green fuels has become an urgent task. In electrolysis, the surfaces of the working electrodes are coated with a layer of catalyst, which reduces the

applied potential and hence the energy consumption, and makes the process more economical. The first step in the catalytic process is the adsorption of hydrogen (H_{ads}) onto the catalyst, after which different mechanisms are possible leading to the formation of H_2 molecules, but, in any case, an effective catalyst must accelerate such adsorption processes. A plethora of materials have been studied for this purpose, in particular metal sulfides, among which various amorphous polysulfides of molybdenum (MoS_3, *etc.* (see Figs 2 *a*,*b* and 3,*b*)) and tungsten (WS_{3-x}) [137] showed promising results.[120, 121, 124, 126–128, 131–134, 136, 138, 182, 288] For catalytic applications, TMPCs in the form of nanosized samples are often used because catalysis and adsorption proceed more efficiently on materials with a developed surface and with a large number of available active sites (in this case, disulfide groups). For example, Fig. 16 compares the characteristics of various MoS_x samples. A high reaction rate can be judged by a lower initial potential and a lower overpotential with a more negative current degree.

A number of recent studies showed that the activity of MoS_x nanomaterials is largely related not to molybdenum atoms,[136] but to disulfide groups,[127, 128, 133, 134, 138] although opinions differ as to whether these are terminal [133] or bridging groups.[128–138] Thus, direct evidence of the important role of the catalyst disulfide groups in the water electrolysis reaction was obtained from *in situ* X-ray absorption spectroscopy studies of MoS_x film samples.[133] It was shown that under catalytic reaction conditions (−0.3 eV *vs* reversible hydrogen electrode (RHE)) the sample is reduced to an amorphous MoS_2 with a surface formed by terminal (η_2-S_2^{2-}) disulfide groups, which are reversibly cleaved and protonated during the catalytic process (Fig. 17).

It was also noted [124, 126, 127, 131] that the pristine MoS_3 converts to an active phase (activation of the catalyst), which is probably an amorphous MoS_{2+x} containing disulfide ligands. Based on Raman spectroscopy, H/D isotope exchange and DFT calculations, Yeo and co-workers [136] provided direct evidence for the S−H bond formation during the reaction of electrocatalytically active MoS_x films consisting of 20–30 nm particles. XPS data and density functional calculations of energy of H binding to various sites also support the involvement of disulfide centres in catalysis, although these data show that it is not the terminal, but the bridging disulfide groups that are active.[138] The correlation between the turnover frequency

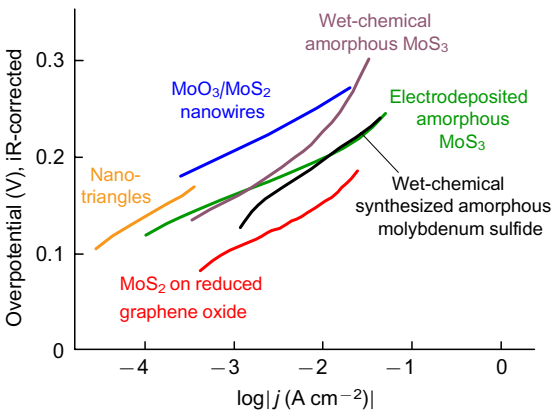

Figure 16. Comparison of Tafel curves in HER processes for different MoS_x samples.[126] Reprinted with the permission of the American Chemical Society.

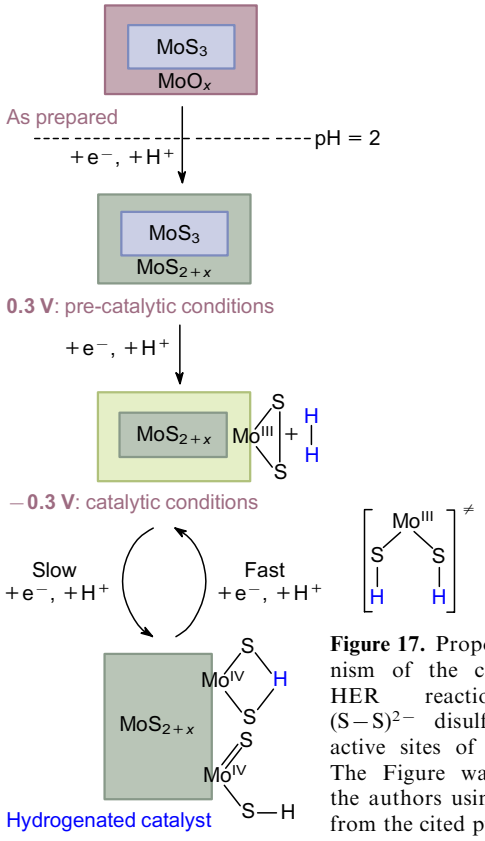

Figure 17. Proposed mechanism of the catalysis in the HER reaction involving $(S-S)^{2-}$ disulfide groups as active sites of H_2 formation. The Figure was prepared by the authors using original data from the cited publication.[133]

of the MoS_x electrocatalyst (amorphous films consisting of 20–30-nanometre particles) (Fig. 18 *a*) in the hydrogen evolution reaction, *i.e.* its activity, and the content of S atoms therein with higher binding energies (163.8/165 eV) (Fig. 18 *b*) based on the XPS data was pointed out.[138] The bridging S_2^{2-} groups and apical S^{2-} groups fall in this region of binding energies. DFT calculations of binding energies of H atoms to these centres in various configurations were performed,[134, 136, 138] and it was shown that apical S atoms (Fig. 18 *a*) bind H atoms the weakest (Gibbs binding energies of hydrogen atom adsorption $\Delta G_H > +1$ eV) and, therefore, cannot be considered as active centres (Fig. 18 *b*). At the same time, S atoms in terminal S_2^{2-} ligands (see Fig. 2 *b*) bind atomic H too strongly, causing passivation and consequently low HER catalytic activity of these centres. Optimal values close to $\Delta G_H = 0$ were obtained for bridging S_2^{2-} groups (see Fig. 2 *b*), which appear to be the most catalytically active centres. A possible mechanism for such a catalyst is depicted in Fig. 17.

Specific synthetic approaches have been developed to increase precisely the content of catalytically active S_2^{2-} groups. The preliminary reaction of ammonium tetrathiomolybdate with ammonium polysulfide $(NH_4)_2S_x$ was shown not only to promote the formation of a bridging S configuration but also to increase the total S atom proportion in the samples. The S/Mo = 3.5 ratio and bridging sulfur content in MoS_x of 67% of the total content (normally in a-MoS_x from $(NH_4)_2MoS_4$ these values are close to 2.8 and 47% respectively) were achieved in this way.These samples demonstrated excellent performance in the HER reaction with low onset potential (−96 mV), overpotential (−0.118 V) and Tafel slope of the polarization curve (46 mV dec^{-1}) at a current of 10 mA cm^{-2}.[235]

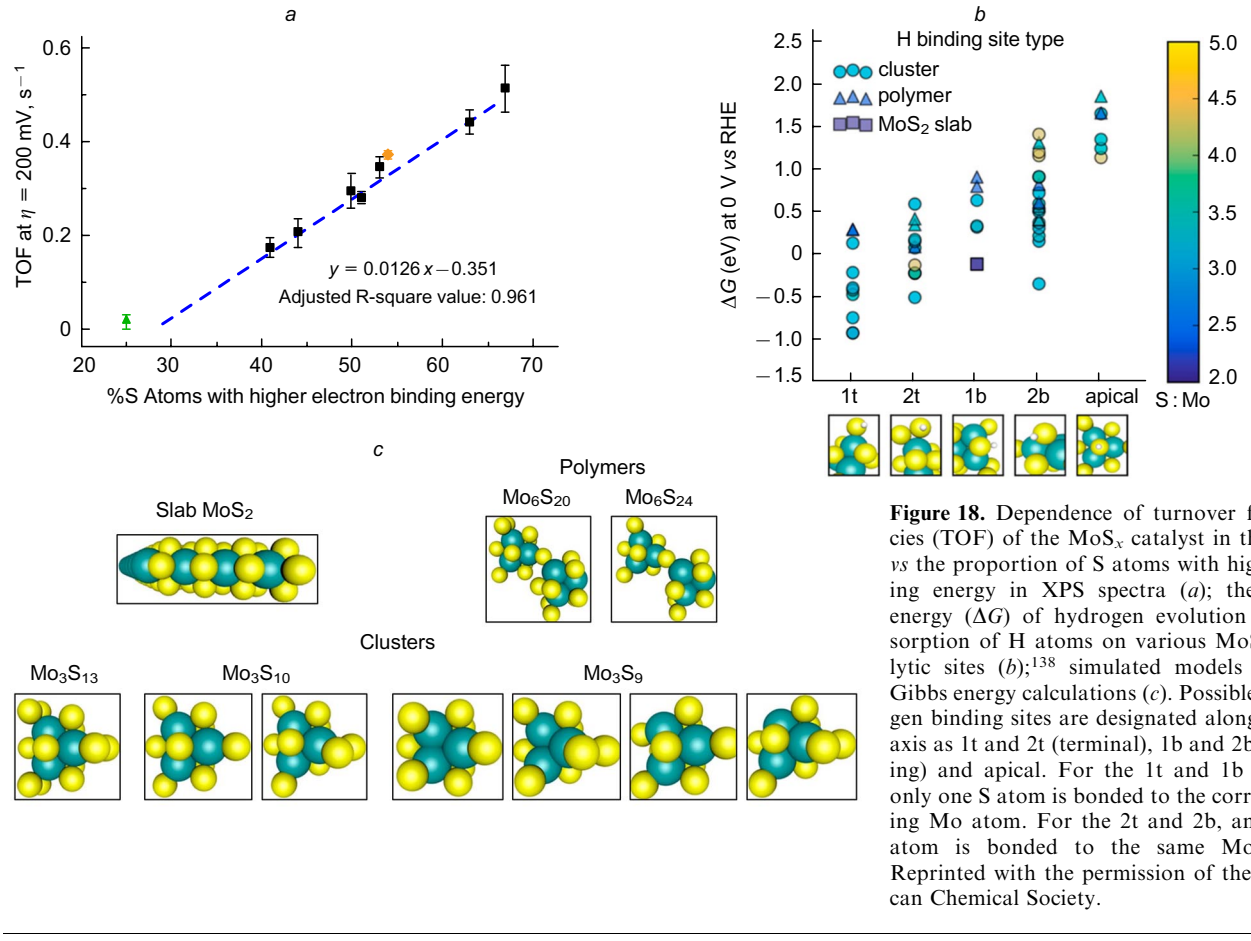

Figure 18. Dependence of turnover frequencies (TOF) of the MoS_x catalyst in the HER *vs* the proportion of S atoms with high binding energy in XPS spectra (*a*); the Gibbs energy (ΔG) of hydrogen evolution *via* the sorption of H atoms on various MoS_x catalytic sites (*b*);[138] simulated models for the Gibbs energy calculations (*c*). Possible hydrogen binding sites are designated along the X-axis as 1t and 2t (terminal), 1b and 2b (bridging) and apical. For the 1t and 1b centres, only one S atom is bonded to the corresponding Mo atom. For the 2t and 2b, another S atom is bonded to the same Mo atom. Reprinted with the permission of the American Chemical Society.

A sample for electrocatalysis with even higher sulfur content, MoS_6, was prepared by oxidation of ammonium thiodimolybdate $(NH_4)_2Mo_2S_{12}$ with iodine. The product represents amorphous particles with a diameter of ~400–800 nm. The HER with this sample proceeded at an overpotential of 130 mV (current density 10 mA cm^{-2}), while for the MoS_4 control sample, this value was higher (178 mV). The authors also attribute the good results obtained for this material to the presence of increased amounts of disulfide groups.[240]

It should be noted that the important role of disulfide groups in electrocatalysis is observed not only for polysulfide materials, where all or considerable part of sulfur exists as S_2^{2-}, but also for the extensively studied electrocatalyst MoS_2, which is not a polysulfide, but whose edge fragments can be represented by disulfide groups.[7, 183–185]

In addition to their application in the process of electrolytic hydrogen evolution reaction, TMPCs have also been investigated as electrocatalysts for the oxygen evolution reaction. Well-crystallized ultrathin ZrS_3 nanosheets with in-plane dimensions at hundreds of nanometres have proven to be efficient and stable (over 1000 cycles) electrocatalysts for this process in both alkaline and neutral solutions.[53] In strongly alkaline solutions (pH = 14), the onset overpotential was as low as 244 mV (~500 mV *vs* Ag/AgCl electrode) and a Tafel slope was 45 mV dec^{-1}, and no side reactions, which often occur using other electrocatalysts, were observed. For crystalline ZrS_3, the values of Tafel slopes of polarization curves were significantly higher (~176 mV dec^{-1}), thus indicating the importance of the dispersion degree of this material. Traditionally, transition metal cations have been considered to be catalytically active centres in water decomposition processes, but this point of view is currently under revision.[289] Xie *et al.*[53] emphasize that splitting of low-dimensional structures increases the active surface of ZrS_3 nanosheets formed by the S–S disulfide groups, which are probably the active centres of electrocatalysts. Similar observations were also made for a number of pyrites FeS_2, CoS_2, NiS_2, which were explored as catalysts for hydrogen evolution reactions.[181]

5.2.2. Photocatalytic and electrocatalytic water decomposition

Semiconducting polychalcogenide materials are also actively explored as catalysts for water decomposition reactions under visible light irradiation. In this process, an important role belongs to the light absorbing capacity of the material (*i.e.* band gap width) and a suitable arrangement of the energy bands (conduction and valence bands) according to the redox potentials of water.[288, 290–292] Based on half-reaction potentials of water oxidation and hydrogen formation, the bandgap width of a semiconductor photocatalyst should be >1.23 eV, which corresponds to near-IR wavelength $\lambda \sim 1008$ nm, and simultaneously, preferably, <3 eV (>400 nm) to provide the possibility of using not only UV radiation (4% of the solar spectrum) but also visible light (53% of the solar spectrum).[292] In reality, however, energy losses are inevitable during electron transfer, leading to kinetic overpotentials and, accordingly, the bandgap of the photocatalyst must be ~2 eV.[288, 290] On the other hand, the issue with narrow-gap semiconductors, which can absorb in the visible region, is the probability of $e^- - h^+$ rapid recombination.[88] The positions of the con-

duction and valence bands in relation to the redox potentials of water are also important:[63] for efficient reduction and oxidation of water by photo-excited electrons and holes, the width of the band gap should overlap the values of the potentials of both reactions.[291]

According to the theory calculations,[70] the transition metal trichalcogenides are characterized by the band gap widths in the range of 0.58–2.17 eV. For example, the calculated direct band gap for TiS_3 is 1.35 eV and the calculated indirect band gap is 1.21 eV (for ZrS_3, 2.16 and 2.06 eV, respectively). The results of the analysis of electronic absorption spectra showed that the absorption of light began at 0.9–1.63 eV, hence, such materials are of interest for application in photovoltaics and photocatalysis, the study of which was started back in the 1980s,[293, 294] however was actively continued only in the last few years.[46, 63, 72, 295]

The experimental results proved that *n*-type semiconductors such as TiS_3, ZrS_3 and HfS_3 can be used as photoanodes,[46, 63, 72, 293, 294] in which photo-excited holes gather on the surface and are involved in oxidation reactions, while electrons move to the counter-electrode through an external circuit and participate in reduction reactions.[292] Thus, TiS_3 nanoribbons (width of ~1–5 μm, length >100 μm, thickness of 50–200 nm) were explored as a photoanode in photoelectrochemical cell to generate hydrogen from 0.5 M solution of Na_2SO_3 (pH = 9) under visible light irradiation.[63] According to the authors, the band gap (1.1 eV) and the positions of the valence and conducting bands are thermodynamically favorable only for the evolution of hydrogen, but not oxygen, which was also confirmed by the composition of the evolved gas. The quantified hydrogen flux was 1.8 μmol H_2 min^{-1} at 0.3 V (Ag/AgCl) with a quantum efficiency of 7%. The Ti-coated pyrite FeS_2 was also studied under similar conditions and showed 2 times lower efficiency compared to TiS_3.[296] In a follow-up study,[72] the same research group tested the samples of TiS_3, ZrS_3 and HfS_3, deposited from dispersions onto supports, as photoanodes. Compared to TiS_3 nanoribbons grown on a Ti metal surface, the results were more modest and the recorded hydrogen flux was 50 times lower, probably due to insufficient electrical contact between the particles. However, this work was one of the first examples of the study of HfS_3 as a photoanode. In their follow-up study, the authors compared catalytic performance (hydrogen evolution reaction) of four trisulfides with a morphology of nanoribbons such as pure trisulfides of titanium and niobium, and two ternary trisulfides, $Nb_xTi_{1-x}S_3$ and $Ti_xNb_{1-x}S_3$.[163] It was found that niobium-doped titanium trisulfide (<10% Nb) shows slightly higher hydrogen photogeneration than the others (Fig. 19).

It was recently proposed to modify a traditional titanium dioxide (TiO_2)-based photocatalyst with a TiS_3 shell for the application in the photocatalytic water splitting. Such surface modification of a wide band gap semiconductor TiO_2 ($E_g \approx 3.2$ eV) with a narrow band gap semiconductor TiS_3 ($E_g < 1.2$ eV) facilitates the shift of the absorption of the sample towards visible region.[295] Indeed, according to the diffuse reflectance spectroscopy data, shift of the absorption onset from 3.14 eV to <2.6 eV and the absorption edge broadening are observed (Fig. 20).

Vanadium tetrasulfide has also recently been investigated as a photocatalyst for the water splitting to produce hydrogen (theoretical band gap width of VS_4 is ~1 eV).[88] It was used as a component of a nanocomposite with reduced graphene oxide, which, when applied in the optimal amount of 5 wt%, hampered the rapid $e^- - h^+$ recombination, promoted the transfer of photo-excited electrons and their interaction with H^+. The highest hydrogen evolution rate was 0.7 mmol L^{-1} h^{-1} in a photocatalytic reactor contain-

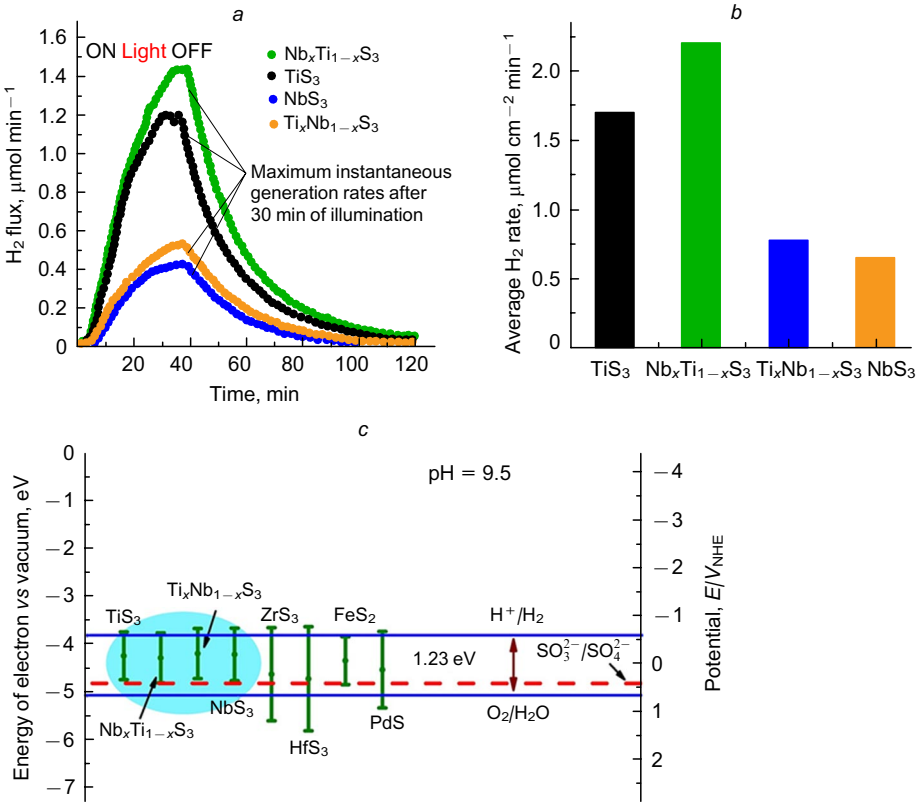

Figure 19. Generated hydrogen fluxes (*a*) and average hydrogen generation rate (*b*) obtained from various trisulfides deposited on metal plates, as photoanodes (mass-spectrometry data). The experiment was carried out in 0.5 M Na_2SO_3 aqueous solutions with pH = 9.5 using a white light source. For all trisulfides, estimated band gap value was 1 + / − 0.05 eV. Comparative scheme of energy levels of the MS_3/electrolyte interface in different sulfides (*c*).[163] Reprinted with the permission of Elsevier.

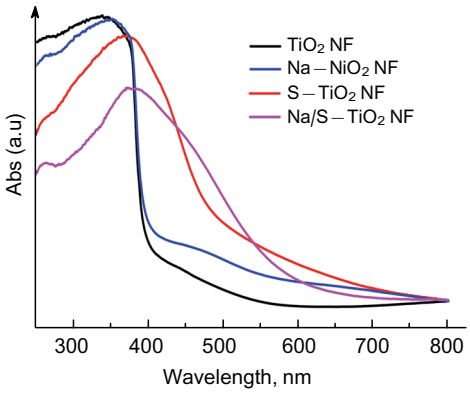

Figure 20. Diffuse reflection absorbance spectra of pristine TiO_2 nanofibres (TiO_2 NF) and samples obtained by modifying TiO_2 nanofibres with different reagents: NaOH (Na–TiO_2 NF), thioacetamide (S–TiO_2 NF) and Na_2S (Na/S–TiO_2 NF). Samples (S–TiO_2 NF and Na/S–TiO_2 NF) contain the TiS_3 phase, so there is a shift in absorption onset from 3.14 eV to < 2.6 eV and a line broadening.[295] Reprinted with the permission of the Royal Society of Chemistry.

ing 500 mL of water. The study[125] also used a composite containing polychalcogenide MoS_3 deposited on CdS/CdSe nanorods for photocatalytic decomposition of water under visible light irradiation. High values of hydrogen evolution 100 mmol h^{-1} g^{-1} and efficacy ~10% were achieved. An interesting embodiment of photocatalytic decomposition of water in gaseous phase using a combination of MoS_x nanostructure with TiO_2 was proposed.[182] The methods is based on the use of the hygroscopic nature of MoS_x: water vapour is sorbed on the material, and then decomposes with the release of hydrogen.

5.2.3. Photocatalytic decomposition of organic compounds

Polychalcogenide materials, particularly, patronite VS_4 and its composites with graphene, were also explored as photocatalysts for decolorization of dyes such as methylene blue[91,297] and methyl orange,[97,101] Rhodamine B,[297] and also phenol,[97] which were used as model compounds for water purification as well as disinfection (elimination of *E. coli*).[103] Since the band gap width of VS_4 is only 0.8–1.2 eV, such samples are promising for use in the near-infrared[101] and visible[97] regions, not just in the ultraviolet.[91,97] Vanadium tetrasulfide with a morphology of microspheres performed better in catalytic decolorization of methyl orange under near-infrared light irradiation than TiO_2 (60% *vs* 9% within 2 h).[101] The authors also studied the luminescence decay on these samples and obtained quite a long luminescence lifetime (1.99 μs), indicating relatively slow recombination, that is, efficient separation of electrons and holes in the material. Even greater efficiency can be achieved by using VS_4 nanocomposites with various carbon materials,[103] which are known for their ability to inhibit recombination of electrons and holes. Thus, nanocomposite 'reduced graphene oxide/VS_4' has proven more effective in decolorization of methylene blue under UV irradiation compared to pure VS_4.[91] It was emphasized that more active samples had a slightly higher specific surface area, which could lead to a greater availability of the active sites, but the specific surface area of these samples varied insignificantly (7–12 m^2 g^{-1}). In another study,[97] 5% C/VS_4 composites (VS_4 particle size of 50–100 nm) also had higher decolorization efficiency of methyl orange under visible light (98.8 ± 0.9% in 30 min), than carbon-free samples of VS_x (44.0 ± 1.4%). When irradiated with UV light, the photocatalytic performance decreased to 67.0 ± 3.9%, which is due to its narrow band gap width (1 eV). Under the action of sunlight, the photocatalyst decolorized 70.1 ± 3.3% of the methyl orange. Compared to other semiconductor photocatalysts (graphene oxide/TiO_2, CdS/TiO_2), which provide similar decolorization efficiency under visible light, the C/VS_4 composite has clear advantages such as short reaction time, low catalyst loading, high decolorization rate of methyl orange. For comparison, decolorization rate was 19.8 mg L^{-1} h^{-1} for 5% C/VS_4, 4.8 mg L^{-1} h^{-1} for CdS/TiO_2, and 1.4 mg L^{-1} h^{-1} for graphene oxide/TiO_2. When irradiated with UV and sunlight, the VS_4 composite is inferior in efficiency to samples such as Cu/ZnO, Co_2TiO_4 and Se/ZnS, but still outperforms them in decolorization rate. A systematic study of various factors affecting this process, such as pH, catalyst loading and dye concentration was conducted.[97] Moreover, other polysulfides were also explored as photocatalysts for dye degradation, in particular nanostructured TiS_3 in the photodegradation of methyl orange and methylene blue,[298] ZrS_3 microribbons in the degradation of methyl orange[299] and MoS_3 nanoparticles in photodecolorization of methyl red.[300]

Another example of photocatalytic properties of TMPCs includes their application in photogeneration of hydrogen peroxide.[263] Surface-modified zirconium sulfide nanoribbons (average length, width and thickness were 24 μm, 840 and 38 nm, respectively, according to atomic-force microscopy) were employed to produce hydrogen peroxide, and were compared to the non-modified ZrS_3. Samples with two kinds of modification were used — those with defects of S_2^{2-} positions and those with defects of both sulfur positions, S_2^{2-} and S^{2-}. It was shown that in the presence of all zirconium trisulfide samples photogeneration of hydrogen peroxide occurs from an aqueous solution of benzylamine through which oxygen was bubbled (with benzylamine as a sacrificial agent oxidized to benzonitrile). It was found that the performance of ZrS_3 as a photocatalyst increased with increasing concentration of sulfur point defects on the surface of trisulfide. The lifetime of photoinduced charge carriers increased with increasing defect concentration (from 0.3 (ZrS_3) to 0.69 s ($ZrSS_{2-x}$) and 0.82 s ($ZrS_{1-x}S_{2-x}$)). The electron concentration also increased, and its value was estimated by experiments on charge carrier dynamics using the Mott–Shottky method.

5.3. Other applications

Below are a few more examples of practically relevant processes in which the chemical properties of TMPC's polychalcogenide groups play a significant role.

The use of polychalcogenide materials in gas sensors is described. For example, MoS_x ($x = 3.66$) was employed as an air moisture sensor, and it turned out that water molecules reversibly bound to disulfide ligands of MoS_x porous branched material.[182] Based on TaS_3 nanofibres, NO gas sensors were created.[80]

Ternary polychalcogenides in the form of porous chalcogels performed well in sorption of radioactive isotopes of iodine (^{129}I and ^{131}I),[301] suggesting that this area will also be promising for other TMPCs. Moreover, aerogel $(NH_4)_{0.2}[MoS_4]$ was explored as adsorbent of gases (H_2, CO_2, CH_4 and C_2H_6).[167] Due to the polarizable internal

surface of the mesoporous aerogel (estimated internal surface area was 370 $m^2\ g^{-1}$), the aerogel was expected to adsorb polar molecules. The best results were obtained for C_2H_6 and CO_2, with the aerogel exhibiting pressure-independent selectivity in C_2H_6/H_2 and CO_2/H_2 pairs with fairly high selectivity factors.

Various metal chalcogenides are successfully used as sorbents of mercury vapour (see Fig. 3 *c*),[302] and it has been noted that it is polychalcogenides, such as MoS_3 and $MoSe_3$, that are extremely efficient at sorbing mercury vapour due to their S−S and Se−Se groups, respectively.[167, 204, 303] Chalcogels MoS_x captured ~2 g of mercury per gram of the sorbent.[167] The material reacted with Hg, and the S−S sites reacted with mercury to afford HgS. According to XPS data, oxidation of mercury physically adsorbed onto MoS_3/TiO_2 composites occurred on the S_2^{2-} active sites.[303] Diselenide ligands of $MoSe_3$ amorphous nanosheets also exhibit excellent affinity towards mercury,[204] with uptake capacity of this material of 1 g g^{-1}, and the uptake rate of 240 mg g^{-1} min^{-1}, which are record values compared to the performance of other sorbents, including chalcogenide ones.

To summarize, chalcogenide aerogels could be promising matrices for capturing iodine and mercury vapour, which is of interest to the nuclear power industry and environmental protection.

6. Conclusion

Low-dimensional transition metal polychalcogenides have attracted the attention of researchers following graphene and dichalcogenides. Although TMPCs have been known for a long time, in the last decade their study has reached a new level. Thus, new crystalline phases, previously thought to be non-existent, have been synthesised, as well as numerous TMPC nanomaterials. A plethora of novel amorphous phases have been obtained, and their structure is actively studied using a set of modern experimental methods and theoretical modelling. New applications have been found, and important steps have been taken to understand how these materials function.

This review shows the influence of the structure of low-dimensional TMPCs on their functional properties. The structure of these substances, which combines the properties of 1D and 2D materials, and features chalcogen–chalcogen bonds makes them efficient materials for battery electrodes, as well as electro- and photocatalysts, since it is S−S (or Se−Se) centres that show redox activity in intercalation of metal ions, catalytic activity in water splitting processes, *etc*. Lithium-, sodium-, magnesium-, and aluminium-ion batteries with promising characteristics have been designed using various, mainly amorphous, TMPCs. Meanwhile, the potential applications of TMPCs are not limited to batteries and catalysis, but new areas can be found. For example, S−S centres actively interact with mercury vapour, which has been used to create relevant sensors.

An important trend in the development of TMPC chemistry will be a further search for synthetic approaches to the preparation of new phases, both crystalline and amorphous. Thus, MQ_4I-like ternary phases can be thought of as partially oxidized polychalcogenides, which could be hypothetically converted to binary polychalcogenide phases by careful reduction. Nanostructuring and design of morphology, defects and surface chemistry will also develop, as well as further study of the chemical properties of TMPCs in various processes. To obtain colloidal dispersions of polychalcogenides, it might also be promising to explore the intercalation approach widely used to obtain aqueous MoS_2 colloids, when a Li_xMoS_2 intercalate reacts with water to form negatively charged dispersed nanosheets.[253, 304] However, although intercalates of various polychalcogenides are well known, their use as precursors for colloidal nanostructures is not reported.

Thus, in the coming years we can expect an active development of TMPC research aimed both at the synthesis of new materials based thereon and at the creation of prototype energy storage and conversion devices based on a better understanding of the mechanisms of action of these materials.

This work was funded by the Ministry of Science and the Higher Education of the Russian Federation (Project No. 121031700321-3) and Russian Science Foundation (Project No. 21-13-00274, https://rscf.ru/project/21-13-00274/).

7. List of acronyms

1D — compound with one-dimensional (chain) structure,
2D — compound with two-dimensional (layered) structure,
amd — *N*,*N*′-diisopropylacetamidinate,
CDW — charge-density wave,
CN — coordination number,
CVD — chemical vapour deposition,
d — interatomic spacing,
DFT — density functional theory,
DMSO — dimethylsulfoxide,
DMF — *N*,*N*-dimethylformamide,
DOS — density of states,
EXAFS — extended X-ray absorption fine structure,
HER — hydrogen evolution reaction,
LIB — lithium-ion batteries,
mV dec^{-1} — millivolts per decade — unit of measure of the Tafel slope of the polarization curve,
NF — nanofibers,
PDF — pair distribution function,
RHE — reversible hydrogen electrode,
TEM — transmission electron microscopy,
TMDC — transition metal dichalcogenides,
TMPC — transition metal polychalcogenides,
TOF —turnover frequency,
XANES — X-ray absorption near edge structure,
XPS — X-ray photoelectron spectroscopy,
US — ultrasonication.

8. References

1. X.Huang, B.Luo, P.Chen, D.J.Searles, D.Wang, L.Wang. *Coord. Chem. Rev.*, **422**, 213445 (2020)
2. Z.Zhipeng, L.Xingbo. *Adv. Mater. Interfaces*, **5**, 1701274 (2018)
3. L.Gaoran, W.Shun, Z.Yining, L.Matthew, C.Zhongwei, L.Jun. *Adv. Mater.*, **30**, 1705590 (2018)
4. R.Steudel. *Chem. Rev.*, **102**, 3905 (2002)
5. J.M.Fukuto, L.J.Ignarro, P.Nagy, D.A.Wink, C.G.Kevil, M.Feelisch, M.M.Cortese-Krott, C.L.Bianco, Y. Kumagai, A.J.Hobbs, J.Lin, T.Ida, T.Akaike. *FEBS Lett.*, **592**, 2140 (2018)
6. Z.Huang, W.Luo, L.Ma, M.Yu, X.Ren, M.He, S.Polen, K.Click, B.Garrett, J.Lu, K.Amine, C.Hadad, W.Chen, A.Asthagiri, Y.Wu. *Angew. Chem., Int. Ed.*, **54**, 15181 (2015)
7. J.Kibsgaard, T.F.Jaramillo, F.Besenbacher. *Nat. Chem.*, **6**, 248 (2014)
8. M.N.Kozlova, Y.V.Mironov, E.D.Grayfer, A.I.Smolentsev, V.I.Zaikovskii, N.A.Nebogatikova, T.Y.Podlipskaya, V.E.Fedorov. *Chem. – Eur. J.*, **21**, 4639 (2015)

9. S.Furuseth, B.Klewe. *Acta Chem. Scand.*, **38a**, 467 (1984)
10. A.Meerschaut, L.Guémas, R.Berger, J.Rouxel. *Acta Crystallogr. Sect. B: Struct. Sci.*, **35**, 1747 (1979)
11. W.Bensch, C.Näther, P.Dürichen. *Angew. Chem., Int. Ed.*, **37**, 133 (1998)
12. S.Conejeros, B.Guster, P.Alemany, J.-P.Pouget, E.Canadell. *Chem. Mater.*, **33**, 5449 (2021)
13. H.Fjellvåg, A.Kjekshus. *Solid State Commun.*, **60**, 91 (1986)
14. V.E.Fedorov, A.V.Mishchenko, V.P.Fedin. *Russ. Chem. Rev.*, **54**, 408 (1985)
15. M.Draganjac, T.B.Rauchfuss. *Angew. Chem., Int. Ed.*, **24**, 742 (1985)
16. A.Müller, E.Diemann. In *Adv. Inorg. Chem. Vol. 31.* (Eds H.J.Emeléus, A.G.Sharpe). (Orlando, USA: Academic Press, 1987). P. 89
17. M.A.Ansari, J.A.Ibers. *Coord. Chem. Rev.*, **100**, 223 (1990)
18. L.C.Roof, J.W.Kolis. *Chem. Rev.*, **93**, 1037 (1993)
19. T.Shibahara. *Coord. Chem. Rev.*, **123**, 73 (1993)
20. M.G.Kanatzidis, S.-P.Huang. *Coord. Chem. Rev.*, **130**, 509 (1994)
21. M.N.Sokolov, V.P.Fedin. *Coord. Chem. Rev.*, **248**, 925 (2004)
22. P.K.Dorhout, N.B.Ford, C.C.Raymond. *Coord. Chem. Rev.*, **352**, 537 (2017)
23. W.S.Sheldrick. *Z. Anorg. Allg. Chem.*, **638**, 2401 (2012)
24. S.K.Srivastava, B.N.Avasthi. *J. Mater. Sci.*, **27**, 3693 (1992)
25. G.R.Patzke. *Angew. Chem., Int. Ed.*, **42**, 972 (2003)
26. W.Shi, R.W.Hughes, S.J. Denholme, D.H.Gregory. *CrystEngComm*, **12**, 641 (2010)
27. V.Y.Pokrovskii, S.G.Zybtsev, M.V.Nikitin, I.G.Gorlova, V.F.Nasretdinova, S.V.Zaitsev-Zotov. *Physics-Uspekhi*, **56**, 29 (2013)
28. J.Dai, M.Li, X.C.Zeng. *Wiley Interdiscip. Rev. Comput. Mol. Sci.*, **6**, 211 (2016)
29. O.I.Joshua, J.M.-M.Aday, B.Mariam, B.Robert, F.Eduardo, M.C.José, R.A.José, S.Carlos, S.J.v.d.Z.Herre, D.A.Roberto, J.F.Isabel, C.-G.Andres. *2D Materials*, **4**, 022003 (2017)
30. O.C.Mantel, F.Chalin, C.Dekker, H.S.J.van der Zant, Y.I.Latyshev, B.Pannetier, P.Monceau. *Phys. Rev. Lett.*, **84**, 538 (2000)
31. S.Tanda, T.Tsuneta, Y.Okajima, K.Inagaki, K.Yamaya, N.Hatakenaka. *Nature (London)*, **417**, 397 (2002)
32. T.Matsuura, S.Tanda, K.Asada, Y.Sakai, T.Tsuneta, K.Inagaki, K.Yamaya. *Phys. B, Condens. Matter*, **329–333** (2), 1550 (2003)
33. L.Huang, K.Tang, Q.Yang, G.Shen, S.Jia. *Mater. Res. Bull.*, **39**, 1083 (2004)
34. E.Slot, M.A.Holst, H.S.J.van der Zant, S.V.Zaitsev-Zotov. *Phys. Rev. Lett.*, **93**, 176602 (2004)
35. K.Inagaki, T.Toshima, S.Tanda, K.Yamaya, S.Uji. *Appl. Phys. Lett.*, **86**, 073101 (2005)
36. Y.S.Hor, Z.L.Xiao, U. Welp, Y.Ito, J.F.Mitchell, R.E.Cook, W.K.Kwok, G.W.Crabtree. *Nano Lett.*, **5**, 397 (2005)
37. A.N.Enyashin, A.L.Ivanovskiĭ. *Phys. Solid State*, **48**, 780 (2006)
38. J.Ma, X.Liu, X.Cao, S.Feng, M.E.Fleet. *Eur. J. Inorg. Chem.*, **2006**, 519 (2006)
39. Y.-L.Zhang, X.-C.Wu, Y.-R.Tao, C.-J.Mao, J.-J.Zhu. *Chem. Commun.*, **23**, 2683 (2008)
40. X.C.Wu, Y.R.Tao, Q.X.Gao. *Nano Res.*, **2**, 558 (2009)
41. H.Jin, D.Cheng, J.Li, X.Cao, B.Li, X.Wang, X.Liu, X.Zhao. *Solid State Sci.*, **13**, 1166 (2011)
42. A.A.Stabile, L.Whittaker, T.L.Wu, P.Marley, M.S.Banerjee, G.Sambandamurthy. *Nanotechnology*, **22**, 485201 (2011)
43. S.De, C.S.Boland, P.J.King, S.Sorel, M.Lotya, U.Patel, Z.L.Xiao, J.N.Coleman. *Nanotechnology*, **22**, 285202 (2011)
44. H.Akitoshi, M.Takuya, S.Atsushi, T.Masahiro. *Chem. Lett.*, **41**, 886 (2012)
45. S.J.Denholme, P.S.Dobson, J.M.R.Weaver, I.MacLaren, D.H.Gregory. *Int. J. Nanotechnol.*, **9**, 23 (2012)
46. I.J.Ferrer, M.D.Maciá, V.Carcelén, J.R.Ares, C.Sánchez. *Energy Procedia*, **22**, 48 (2012)
47. M.O.King, M.Popland, S.J. Denholme, D.H.Gregory, D.A.MacLaren, M.Kadodwala. *Nanoscale*, **4**, 607 (2012)
48. S.G.Zybtsev, V.Y.Pokrovskii, V.F.Nasretdinova, S.V.Zaitsev-Zotov. *Physica B Condens. Matter.*, **407**, 1696 (2012)
49. I.J.Ferrer, J.R.Ares, J.M.Clamagirand, M.Barawi, C.Sánchez. *Thin Solid Films*, **535**, 398 (2013)
50. Y.-R.Tao, X.-C.Wu, W.-W.Xiong. *Small*, **10**, 4905 (2014)
51. W.-W.Xiong, J.-Q.Chen, X.-C.Wu, J.-J.Zhu. *J. Mater. Chem. C*, **2**, 7392 (2014)
52. J.O.Island, M.Buscema, M.Barawi, J.M.Clamagirand, J.R.Ares, C.Sánchez, I.J.Ferrer, G.A.Steele, H.S.J.van der Zant, A.Castellanos-Gomez. *Adv. Opt. Mater.*, **2**, 641 (2014)
53. J. Xie, R.Wang, J.Bao, X.Zhang, H.Zhang, S.Li, Y.Xie. *Inorg. Chem. Front.*, **1**, 751 (2014)
54. S.B.Artemkina, T.Y.Podlipskaya, A.I.Bulavchenko, A.I.Komonov, Y.V.Mironov, V.E.Fedorov. *Colloids Surf. A Physicochem. Eng. Asp.*, **461**, 30 (2014)
55. V.E.Fedorov, S.B.Artemkina, E.D.Grayfer, N.G.Naumov, Y.V.Mironov, A.I.Bulavchenko, V.I.Zaikovskii, I.V.Antonova, A.I.Komonov, M.V.Medvedev. *J. Mater. Chem. C*, **2**, 5479 (2014)
56. P.A.Poltarak, S.B.Artemkina, A.I.Bulavchenko, T.Y.Podlipskaya, V.E.Fedorov. *Russ. Chem. Bull.*, **64**, 1850 (2015)
57. A.I.Romanenko, V.E.Fedorov, S.B.Artemkina, O.B.Anikeeva, P.A.Poltarak. *Phys. Solid State*, **57**, 1850 (2015)
58. A.J.Molina-Mendoza, M.Barawi, R.Biele, E.Flores, J.R.Ares, C.Sánchez, G.Rubio-Bollinger, N.Agraït, R.D'Agosta, I.J.Ferrer, A.Castellanos-Gomez. *Adv. Electron. Mater.*, **1**, 1500126 (2015)
59. A.Lipatov, P.M.Wilson, M.Shekhirev, J.D.Teeter, R.Netusil, A.Sinitskii. *Nanoscale*, **7**, 12291 (2015)
60. A.S.Pawbake, J.O.Island, E.Flores, J.R.Ares, C.Sanchez, I.J.Ferrer, S.R.Jadkar, H.S.J.van der Zant, A.Castellanos-Gomez, D.J. Late. *ACS Appl. Mater. Interfaces*, **7**, 24185 (2015)
61. J.O.Island, M.Barawi, R.Biele, A.Almazán, J.M.Clamagirand, J.R.Ares, C.Sánchez, H.S.J.van der Zant, J.V.Álvarez, R.D'Agosta, I.J.Ferrer, A.Castellanos-Gomez. *Adv. Mater.*, **27**, 2595 (2015)
62. J.Dai, X.C.Zeng. *Angew. Chem., Int. Ed.*, **54**, 7572 (2015)
63. M.Barawi, E.Flores, I.J.Ferrer, J.R.Ares, C.Sanchez. *J. Mater. Chem. A*, **3**, 7959 (2015)
64. K.E.Farley, Z.Shi, G.Sambandamurthy, S.Banerjee. *Phys. Chem. Chem. Phys.*, **17**, 18374 (2015)
65. Y.Jin, X.Li, J.Yang. *Phys. Chem. Chem. Phys.*, **17**, 18665 (2015)
66. J.Kang, H.Sahin, H.D.Ozaydin, R.T.Senger, F.M.Peeters. *Phys. Rev. B, Condens. Matter*, **92**, 075413 (2015)
67. Y.Aierken, D.Cakr, F.M.Peeters. *Phys. Chem. Chem. Phys.*, **18**, 14434 (2016)
68. T.Matsuyama, M.Deguchi, K.Mitsuhara, T.Ohta, T.Mori, Y.Orikasa, Y.Uchimoto, Y.Kowada, A.Hayashi, M.Tatsumisago. *J. Power Sources*, **313**, 104 (2016)
69. M.A.Stolyarov, G.Liu, M.A.Bloodgood, E.Aytan, C.Jiang, R.Samnakay, T.T.Salguero, D.L.Nika, S.L.Rumyantsev, M.S.Shur, K.N.Bozhilov, A.A.Balandin. *Nanoscale*, **8**, 15774 (2016)
70. M.Abdulsalam, D.P.Joubert. *Phys. Status Solidi B*, **253**, 868 (2016)
71. K.Osada, S.Bae, M.Tanaka, H.Raebiger, K.Shudo, T.Suzuki. *J. Phys. Chem. C*, **120**, 4653 (2016)
72. E.Flores, J.R.Ares, I.J.Ferrer, C.Sánchez. *Phys. Status Solidi Rapid Res. Lett.*, **10**, 802 (2016)

73. J.O.Island, R.Biele, M.Barawi, J.M.Clamagirand, J.R.Ares, C.Sánchez, H.S.J.van der Zant, I.J. Ferrer, R.D'Agosta, A.Castellanos-Gomez. *Sci. Rep.*, **6**, 22214 (2016)
74. K.Giagloglou, J.L.Payne, C.Crouch, R.K.B.Gover, P.A.Connor, J.T.S.Irvine. *J. Electrochem. Soc.*, **163**, A3126 (2016)
75. S.B.Artemkina, E.D.Grayfer, M.N.Kozlova, S.G.Kozlova, M.R.Ryzhikov, I.R.Shein, V.E.Fedorov. *Spectrochim. Acta A Mol. Biomol. Spectrosc.*, **179**, 46 (2017)
76. P.A.Poltarak, A.A.Poltarak, S.B.Artemkina, T.Y.Podlipskaya, V.E.Fedorov. *J. Struct. Chem.*, **58**, 1033 (2017)
77. W.Kong, C.Bacaksiz, B.Chen, K.Wu, M.Blei, X.Fan, Y.Shen, H.Sahin, D.Wright, D.S.Narang, S.Tongay. *Nanoscale*, **9**, 4175 (2017)
78. J.Li, Q.Sun, Z.Wang, J.Xiang, B.Zhao, Y.Qu, B.Xiang. *Appl. Surf. Sci.*, **412**, 113 (2017)
79. R.Biele, E.Flores, J.R.Ares, C.Sanchez, I.J.Ferrer, G.Rubio-Bollinger, A.Castellanos-Gomez, R.D Agosta. *Nano Res.*, **11**, 225 (2018)
80. C.C.Mayorga-Martinez, Z.Sofer, J.Luxa, Š.Huber, D.Sedmidubský, P.Brázda, L.Palatinus, M.Mikulics, P.Lazar, R.Medlín, M.Pumera. *ACS Nano*, **12**, 464 (2018)
81. M.Talib, R.Tabassum, S.S.Islam, P.Mishra. *RSC Adv.*, **9**, 645 (2019)
82. N.Tripathi, V.Pavelyev, P.Sharma, S.Kumar, A.Rymzhina, P.Mishra. *Mater. Sci. Semicond. Process*, **127**, 105699 (2021)
83. P.Poltarak, A.Poltarak, S.Artemkina, T.Podlipskaya, I.Asanov, V.Fedorov. *Colloids Surf. A Physicochem. Eng. Asp.*, **579**, 123667 (2019)
84. B.Pedersen. *Acta Chem. Scand.*, **13**, 1050 (1959)
85. R.Allmann, I.Baumann, A.Kutoglu, H.Rösch, E.Hellner. *Naturwissenschaften*, **51**, 263 (1964)
86. A.Bensalem, D.M.Schleich. *Inorg. Chem.*, **30**, 2052 (1991)
87. C.S.Rout, B.H.Kim, X.Xu, J.Yang, H.Y.Jeong, D.Odkhuu, N.Park, J.Cho, H.S.Shin. *J. Am. Chem. Soc.*, **135**, 8720 (2013)
88. W.Guo, D.Wu. *Int. J. Hydrogen Energy*, **39**, 16832 (2014)
89. X.Xu, S.Jeong, C.S.Rout, P.Oh, M.Ko, H.Kim, M.G.Kim, R.Cao, H.S.Shin, J.Cho. *J. Mater. Chem. A*, **2**, 10847 (2014)
90. S.Britto, M.Leskes, X.Hua, C.-A.Hébert, H.S.Shin, S.Clarke, O.Borkiewicz, K.W.Chapman, R.Seshadri, J.Cho, C.P.Grey. *J. Am. Chem. Soc.*, **137**, 8499 (2015)
91. G.Lui, G.Jiang, A.Duan, J.Broughton, J.Zhang, M.W.Fowler, A.Yu. *Ind. Eng. Chem. Res.*, **54**, 2682 (2015)
92. S.Ratha, S.R.Marri, N.A.Lanzillo, S.Moshkalev, S.K.Nayak, J.N.Behera, C.S.Rout. *J. Mater. Chem. A*, **3**, 18874 (2015)
93. R.Sun, Q.Wei, Q.Li, W.Luo, Q.An, J.Sheng, D.Wang, W.Chen, L.Mai. *ACS Appl. Mater. Interfaces*, **7**, 20902 (2015)
94. Q.Li, Y.Chen, J.He, F.Fu, J.Lin, W.Zhang. *J. Alloys Compd.*, **685**, 294 (2016)
95. S.Ratha, S.R.Marri, J.N.Behera, C.S.Rout. *Eur. J. Inorg. Chem.*, **2016**, 259 (2016)
96. Y.Zhou, Y.Li, J.Yang, J.Tian, H.Xu, J.Yang, W.Fan. *ACS Appl. Mater. Interfaces*, **8**, 18797 (2016)
97. R.Cai, B.Zhang, J.Shi, M.Li, Z.He. *ACS Sustain. Chem. Eng.*, **5**, 7690 (2017)
98. M.N.Kozlova, E.D.Grayfer, P.A.Poltarak, S.B.Artemkina, A.G.Cherkov, L.S.Kibis, A.I.Boronin, V.E.Fedorov. *Adv. Mater. Interfaces*, **4**, 1700999 (2017)
99. S.Li, W.He, P.Deng, J.Cui, B.Qu. *Mater. Lett.*, **205**, 52 (2017)
100. M.S.Weimer, R.F.McCarthy, J.D.Emery, M.J.Bedzyk, F.G.Sen, A.Kinaci, M.K.Y.Chan, A.S.Hock, A.B.F.Martinson. *Chem. Mater.*, **29**, 2864 (2017)
101. Y.Zhou, P.Liu, F.Jiang, J.Tian, H.Cui, J.Yang. *J. Colloid Interface Sci.*, **498**, 442 (2017)
102. Y.Zhou, J.Tian, H.Xu, J.Yang, Y.Qian. *Energy Stor. Mater.*, **6**, 149 (2017)
103. B.Zhang, S.Zou, R.Cai, M.Li, Z.He. *Appl. Catal., B*, **224**, 383 (2018)
104. E.Flores, E.Muñoz-Cortés, J.Bodega, O.Caballero-Calero, M.Martín-González, C.Sánchez, J.R.Ares, I.J.Ferrer. *ACS Appl. Energy Mater.*, **1**, 2333 (2018)
105. K.Koganei, A.Sakuda, T.Takeuchi, H.Sakaebe, H.Kobayashi, H.Kageyama, T.Kawaguchi, H.Kiuchi, K.Nakanishi, M.Yoshimura, T.Ohta, T.Fukunaga, E.Matsubara. *Solid State Ion.*, **323**, 32 (2018)
106. W.Li, J.Huang, L.Cao, L.Feng, C.Yao. *Electrochim. Acta*, **274**, 334 (2018)
107. W.Li, J. Huang, L.Feng, L.Cao, Y.Liu, L.Pan. *Mater. Lett.*, **230**, 105 (2018)
108. L.Zhang, Q.Wei, D.Sun, N.Li, H.Ju, J. Feng, J. Zhu, L.Mai, E.J.Cairns, J.Guo. *Nano Energy*, **51**, 391 (2018)
109. W.Yanrong, L.Ziteng, W.Caixing, Y.Xu, C.Renpeng, M.Lianbo, H.Yi, Z.Guoyin, C.Tao, T.Zuoxiu, M.Jing, L.Jie, J.Zhong. *Adv. Mater.*, **30**, 1802563 (2018)
110. X.Zhang, S.Wang, J.Tu, G.Zhang, S.Li, D.Tian, S.Jiao. *ChemSusChem*, **11**, 709 (2018)
111. Q.Pang, Y.Zhao, Y.Yu, X.Bian, X.Wang, Y.Wei, Y.Gao, G.Chen. *ChemSusChem*, **11**, 735 (2018)
112. A.Poltarak, P.Poltarak, A.Enyashin, V.Komarov, S.Artemkina, V.Fedorov. *Inorg. Chem.*, **61**, 2783 (2022)
113. F.W.Boswell, A.Prodan, J.K.Brandon. *J. Phys. C: Solid State Phys.*, **16**, 1067 (1983)
114. H.Böhm, H.-G.v.Schnering. *Z.Kristallogr. Cryst. Mater.*, **171**, 41 (1985)
115. Y.Gao, L.Xu, Y.Qiu, Z.Tian, S.Yuan, J.Wang. *J. Appl. Phys.*, **122**, 135101 (2017)
116. S.Oh, S.Chae, B.J.Kim, K.H.Choi, W.-S.Jang, J.Jang, Y.Hussain, D.K.Lee, Y.-M.Kim, H.K.Yu, J.-Y.Choi. *RSC Adv.*, **8**, 33980 (2018)
117. W.-G.Lee, S.Chae, Y.K.Chung, W.-S.Yoon, J.-Y.Choi, J.Huh. *ACS Omega*, **4**, 18392 (2019)
118. S.Oh, S.Chae, B.J. Kim, A.J.Siddiqa, K.H.Choi, W.-S.Jang, K.H.Lee, H.Y.Kim, D.K.Lee, Y.-M.Kim, H.K.Yu, J.-Y.Choi. *Phys. Status Solidi Rapid Res. Lett.*, **12**, 1800451 (2018)
119. P.Afanasiev. *Compt. Rend. Chim.*, **11**, 159 (2008)
120. D.Merki, X.Hu. *Energy Environ. Sci.*, **4**, 3878 (2011)
121. C.G.Morales-Guio, X.Hu. *Acc. Chem. Res.*, **47**, 2671 (2014)
122. S.J.Hibble, M.R.Feaviour, M.J.Almond. *J. Chem. Soc., Dalton Trans.*, **6**, 935 (2001)
123. S.J.Hibble, G.B.Wood. *J. Am. Chem. Soc.*, **126**, 959 (2004)
124. D.Merki, S.Fierro, H.Vrubel, X.Hu. *Chem. Sci.*, **2**, 1262 (2011)
125. M.L.Tang, D.C.Grauer, B.Lassalle-Kaiser, V.K.Yachandra, L.Amirav, J.R.Long, J.Yano, A.P.Alivisatos. *Angew. Chem., Int. Ed.*, **50**, 10203 (2011)
126. J.D.Benck, Z.Chen, L.Y.Kuritzky, A.J.Forman, T.F.Jaramillo. *ACS Catal.*, **2**, 1916 (2012)
127. H.Vrubel, D.Merki, X.Hu. *Energy Environ. Sci.*, **5**, 6136 (2012)
128. Y.-H.Chang, C.-T.Lin, T.-Y.Chen, C.-L.Hsu, Y.-H.Lee, W.Zhang, K.-H.Wei, L.-J.Li. *Adv. Mater.*, **25**, 756 (2013)
129. T.-W.Lin, C.-J. Liu, J.-Y.Lin. *Appl. Catal., B*, **134**–**135**, 75 (2013)
130. Y.Shi, Y.Wang, J.I.Wong, A.Y.S.Tan, C.-L.Hsu, L.-J.Li, Y.-C.Lu, H.Y.Yang. *Sci. Rep.*, **3**, 2169 (2013)
131. H.Vrubel, X.Hu. *ACS Catal.*, **3**, 2002 (2013)
132. H.G.S.Casalongue, J.D.Benck, C.Tsai, R.K.B.Karlsson, S.Kaya, M.L.Ng, L.G.M.Pettersson, F.Abild-Pedersen, J.K.Nørskov, H.Ogasawara, T.F.Jaramillo, A.Nilsson. *J. Phys. Chem. C*, **118**, 29252 (2014)
133. B.Lassalle-Kaiser, D.Merki, H.Vrubel, S.Gul, V.K.Yachandra, X.Hu, J.Yano. *J. Am. Chem. Soc.*, **137**, 314 (2015)
134. Y.Li, Y.Yu, Y.Huang, R.A.Nielsen, W.A.Goddard, Y.Li, L.Cao. *ACS Catal.*, **5**, 448 (2015)
135. T.Matsuyama, A.Hayashi, T.Ozaki, S.Mori, M.Tatsumisago. *J. Mater. Chem. A*, **3**, 14142 (2015)

136. Y.Deng, L.R.L.Ting, P.H.L.Neo, Y.-J.Zhang, A.A.Peterson, B.S.Yeo. *ACS Catal.*, **6**, 7790 (2016)
137. S.M.Tan, M.Pumera. *ACS Appl. Mater. Interfaces*, **8**, 3948 (2016)
138. L.R.L.Ting, Y.Deng, L.Ma, Y.-J.Zhang, A.A.Peterson, B.S.Yeo. *ACS Catal.*, **6**, 861 (2016)
139. P.D.Tran, T.V.Tran, M.Orio, S.Torelli, Q.D.Truong, K.Nayuki, Y.Sasaki, Sing Y.Chiam, R.Yi, I.Honma, J.Barber, V.Artero. *Nat. Mater.*, **15**, 640 (2016)
140. H.Ye, L.Wang, S.Deng, X.Zeng, K.Nie, P.N.Duchesne, B.Wang, S.Liu, J.Zhou, F.Zhao, N.Han, P.Zhang, J.Zhong, X.Sun, Y.Li, Y.Li, J.Lu. *Adv. Energy Mater.*, **7**, 1601602 (2017)
141. Y.Gao, W.Han, X.Long, H.Nie, D.Li. *Appl. Catal., B*, **224**, 330 (2018)
142. G.Shirota, A.Nasu, M.Deguchi, A.Sakuda, M.Tatsumisago, A.Hayashi. *J. Ceram. Soc. Jpn.*, **130**, 308 (2022)
143. D.A.Rice, S.J.Hibble, M.J.Almond, K.A.H.Mohammad, S.P.Pearse. *J. Mater. Chem.*, **2**, 895 (1992)
144. S.J.Hibble, D.A.Rice, D.M.Pickup, M.P.Beer. *Inorg. Chem.*, **34**, 5109 (1995)
145. G.F.Khudorozhko, L.G.Bulusheva, L.N.Mazalov, V.E.Fedorov, I.P.Asanov, É.A.Kravtsova, G.K.Parygina, Y.V.Mironov. *J. Struct. Chem.*, **37**, 626 (1996)
146. G.F.Khudorozhko, L.G.Bulusheva, L.N.Mazalov, V.E.Fedorov, J.Morales, E.A.Kravtsova, I.P.Asanov, G.K.Parygina, Y.V.Mironov. *J. Phys. Chem. Solids*, **59**, 283 (1998)
147. S.J.Hibble, M.R.Feaviour. *J. Mater. Chem.*, **11**, 2607 (2001)
148. P.Afanasiev. *J. Solid State Chem.*, **213**, 158 (2014)
149. A.Sakuda, N.Taguchi, T.Takeuchi, H.Kobayashi, H.Sakaebe, K.Tatsumi, Z.Ogumi. *Electrochem. Commun.*, **31**, 71 (2013)
150. A.Sakuda, K.Ohara, K.Fukuda, K.Nakanishi, T.Kawaguchi, H.Arai, Y.Uchimoto, T.Ohta, E.Matsubara, Z.Ogumi, T.Okumura, H.Kobayashi, H.Kageyama, M.Shikano, H.Sakaebe, T.Takeuchi. *J. Am. Chem. Soc.*, **139**, 8796 (2017)
151. K.Shimoda, K.Kuratani, S.Kobayashi, T.Takeuchi, M.Murakami, A.Kuwabara, H.Sakaebe. *ACS Appl. Mater. Interfaces*, **14**, 33191 (2022)
152. P.Afanasiev, I.Bezverkhy. *Chem. Mater.*, **14**, 2826 (2002)
153. X.Wang, K.Du, C.Wang, L.Ma, B.Zhao, J.Yang, M.Li, X.-X.Zhang, M.Xue, J.Chen. *ACS Appl. Mater. Interfaces*, **9**, 38606 (2017)
154. S.J.Hibble, R.I.Walton, M.R.Feaviour, A.D.Smith. *J. Chem. Soc., Dalton Trans.*, 2877 (1999)
155. S.J.Hibble, D.A.Rice, M.J.Almond, K.A.H.Mohammad, S.P.Pearse, J.R.Sagar. *J. Mater. Chem.*, **2**, 1237 (1992)
156. A.Bensalem, D.M.Schleich. *Mater. Res. Bull.*, **25**, 349 (1990)
157. D.M.Pasquariello, K.M.Abraham. *Mater. Res. Bull.*, **22**, 37 (1987)
158. K.M.Abraham, D.M.Pasquariello, G.F.McAndrews. *J. Electrochem. Soc.*, **134**, 2661 (1987)
159. H.Yun, G.Ryu, S.Lee, R.Hoffmann. *Inorg. Chem.*, **42**, 2253 (2003)
160. D.S.Muratov, V.O.Vanyushin, N.S.Vorobeva, P.Jukova, A.Lipatov, E.A.Kolesnikov, D.Karpenkov, D.V.Kuznetsov, A.Sinitskii. *J. Alloys Compd.*, **815**, 152316 (2020)
161. K.Sieber, B.Fotouhi, O.Gorochov. *Mater. Res. Bull.*, **18**, 1477 (1983)
162. P.Misse, D.Berthebaud, O.Lebedev, A.Maignan, E.Guilmeau. *Materials*, **8**, 2514 (2015)
163. E.Flores, J.R.Ares, C.Sánchez, I.J. Ferrer. *Catal. Today*, **321** – **322**, 107 (2019)
164. Z.Hemmat, A.Ahmadiparidari, S.Wang, K.Kumar, M.Zepeda, C.Zhang, N.Dandu, S.Rastegar, L.Majidi, A.Jaradat, A.Ngo, K.Thornton, L.A.Curtiss, J.Cabana, Z.Huang, A.Salehi-Khojin. *Adv. Funct. Mater.*, **32**, 2205214 (2022)
165. S.Bag, I.U.Arachchige, M.G.Kanatzidis. *J. Mater. Chem.*, **18**, 3628 (2008)
166. S.Bag, A.F.Gaudette, M.E.Bussell, M.G.Kanatzidis. *Nat. Chem.*, **1**, 217 (2009)
167. K.S.Subrahmanyam, C.D.Malliakas, D.Sarma, G.S.Armatas, J.Wu, M.G.Kanatzidis. *J. Am. Chem. Soc.*, **137**, 13943 (2015)
168. J. Staszak-Jirkovsky, C.D.Malliakas, P.P.Lopes, N.Danilovic, S.S.Kota, K.-C.Chang, B.Genorio, D.Strmcnik, V.R.Stamenkovic, M.G.Kanatzidis, N.M.Markovic. *Nat. Mater.*, **15**, 197 (2016)
169. V.V.T.Doan-Nguyen, K.S.Subrahmanyam, M.M.Butala, J.A.Gerbec, S.M.Islam, K.N.Kanipe, C.E.Wilson, M.Balasubramanian, K.M.Wiaderek, O.J.Borkiewicz, K.W.Chapman, P.J.Chupas, M.Moskovits, B.S.Dunn, M.G.Kanatzidis, R.Seshadri. *Chem. Mater.*, **28**, 8357 (2016)
170. J.A.Cody, M.F.Mansuetto, S.Chien, J.A.Ibers. In *Soft Chemistry Routes to New Materials — Chimie Douce*. Vol. 152. (Eds J.Rouxel, M.Tournoux, R.Brec). (Bäch: Trans Tech Publications, 1994). P. 35
171. A.Sahu, S.N.Steinmann, P.Raybaud. *Cryst. Growth Des.*, **20**, 7750 (2020)
172. S.J.Hibble, R.I.Walton, D.M.Pickup. *J. Chem. Soc., Dalton Trans.*, **11**, 2245 (1996)
173. D.E.Schwarz, A.I.Frenkel, R.G.Nuzzo, T.B.Rauchfuss, A.Vairavamurthy. *Chem. Mater.*, **16**, 151 (2004)
174. S.B.Artemkina, A.N.Enyashin, A.A.Poltarak, A.D.Fedorenko, A.A.Makarova, P.A.Poltarak, E.-J.Shin, S.-J.Hwang, S.-J.Kim, E.D.Grayfer, V.E.Fedorov. *ChemNanoMat*, **5**, 1488 (2019)
175. H.Fukuoka, N.Kawata, M.Furuta, Y.Katakami, S.Kimura, K.Inumaru. *Inorg. Chem.*, **59**, 13320 (2020)
176. Z.Zhang, Y.Qiu, W.Yan, Z.Zhou, Y.Yao, X.Liu, J.Sun, Y.Li. *Nanoscale Advances*, **4**, (2022)
177. E.D.Grayfer, E.M.Pazhetnov, M.N.Kozlova, S.B.Artemkina, V.E.Fedorov. *ChemSusChem*, **10**, 4805 (2017)
178. G.Wei, F.Yongzhu. *En. Env. Mat.*, **1**, 20 (2018)
179. G.Shirota, A.Nasu, M.Deguchi, A.Sakuda, M.Tatsumisago, A.Hayashi. *J. Power Sources Adv.*, **10**, 100061 (2021)
180. G.Shirota, A.Nasu, M.Deguchi, A.Sakuda, M.Tatsumisago, A.Hayashi. *Solid State Ion.*, **376**, 115848 (2022)
181. M.S.Faber, M.A.Lukowski, Q.Ding, N.S.Kaiser, S.Jin. *J. Phys. Chem. C*, **118**, 21347 (2014)
182. T.Daeneke, N.Dahr, P.Atkin, R.M.Clark, C.J.Harrison, R.Brkljača, N.Pillai, B.Y.Zhang, A.Zavabeti, S.J. Ippolito, K.J.Berean, J.Z.Ou, M.S.Strano, K.Kalantar-zadeh. *ACS Nano*, **11**, 6782 (2017)
183. J.V.Lauritsen, J.Kibsgaard, S.Helveg, H.Topsøe, B.S.Clausen, E.Lægsgaard, F.Besenbacher. *Nat. Nanotechnol.*, **2**, 53 (2007)
184. J.V.Lauritsen, M.V.Bollinger, E.Lægsgaard, K.W.Jacobsen, J.K.Nørskov, B.S.Clausen, H.Topsøe, F.Besenbacher. *J. Catal.*, **221**, 510 (2004)
185. L.S.Byskov, J.K.Nørskov, B.S.Clausen, H.Topsøe. *J. Catal.*, **187**, 109 (1999)
186. H.I.Karunadasa, E.Montalvo, Y.Sun, M.Majda, J.R.Long, C.J.Chang. *Science*, **335**, 698 (2012)
187. F.Lévy, H.Berger. *J. Cryst. Growth*, **61**, 61 (1983)
188. M.G.Kanatzidis. *Chem. Mater.*, **2**, 353 (1990)
189. J.Rouxel. *Chem. – Eur. J.*, **2**, 1053 (1996)
190. M.G.Kanatzidis, A.C.Sutorik. In *Prog. Inorg. Chem.* (New York: Wiley, 2007). P. 151
191. R.R.Chianelli. *Int. Rev. Phys. Chem.*, **2**, 127 (1982)
192. W.Jaegermann, H.Tributsch. *Prog. Surf. Sci.*, **29**, 1 (1988)
193. P.Gressier, L.Guémas, A.Meerschaut. *Mater. Res. Bull.*, **20**, 539 (1985)
194. A.Meerschaut, P.Gressier, L.Guémas, J.Rouxel. *J. Solid State Chem.*, **51**, 307 (1984)
195. P.Grenouilleau, A.Meerschaut, L.Guemas, J.Rouxel. *J. Solid State Chem.*, **66**, 293 (1987)

196. P.Gressier, L.Guemas, A.Meerschaut. *Acta Crystallogr. Sect. B: Struct. Sci.*, **38**, 2877 (1982)
197. M.Sokolov, H.Imoto, T.Saito, V.Fedorov. *Polyhedron*, **17**, 3735 (1998)
198. W.Tremel. *Chem. Ber.*, **125**, 2165 (1992)
199. S.-X.Liu, D.-P.Huang, C.-C.Huang, J.-L.Huang. *Polyhedron*, **15**, 2295 (1996)
200. J.-L.Huang, D.-P.Huang, S.-X.Liu, C.-C.Huang, H.-D.Xu. *Acta Crystallogr. Sect. C: Cryst. Struct. Commun.*, **54**, 895 (1998)
201. Y.Xia, M.Li, A.Wang, X.Tang, M.He, H.Lv, L.Zhang, S.Yuan, X.Zhou, H.Zeng. *J. Lumin.*, **241**, 118487 (2022)
202. V.E.Fedorov, N.V.Podberezskaya, A.V.Mischenko, G.F.Khudorozko, I.P.Asanov. *Mater. Res. Bull.*, **21**, 1335 (1986)
203. T.Weber, J.C.Muijsers, J.W.Niemantsverdriet. *J. Phys. Chem.*, **99**, 9194 (1995)
204. Z.Yang, H.Li, J. Yang, Q.Yang, J.Zhao, J.Yang, W.Qu, Y.Feng, K.Shih. *Adv. Sci.*, **6**, 1901410 (2019)
205. S.J.Hibble, D.A.Rice, D.M.Pickup, M.P.Beer. *J. Chem. Soc., Faraday Trans.*, **92**, 2131 (1996)
206. V.E.Fedorov. *Khalkogenidy Perekhodnykh Tugoplavkikh Metallov. Kvaziodnomernye Soedineniya. (Chalcogenides of Transitional Refractory Metals. Quasi-One-Dimensional Compounds)*. (Novosibirsk: Nauka, 1988). P. 218
207. K.Wu, M.Blei, B.Chen, L.Liu, H.Cai, C.Brayfield, D.Wright, H.Zhuang, S.Tongay. *Adv. Mater.*, **32**, 2000018 (2020)
208. M.Li, J. Dai, X.C.Zeng. *Nanoscale*, **7**, 15385 (2015)
209. E.M.Dizhur, M.A.Il'ina, S.V.Zaĭtsev-Zotov. *JETP Lett.*, **86**, 132 (2007)
210. E.Dizhur, M.Il'ina, S.Zaitzev-Zotov. *Phys. Status Solidi B*, **246**, 500 (2009)
211. J.Xu, B.Yu, H.Zhao, S.Cao, L.Song, K.Xing, R.Zhou, X.Lu. *ACS Sustain. Chem. Eng.*, **8**, 15055 (2020)
212. S.Li, J.He, P.Nachtigall, L.Grajciar, F.Brivio. *J. Mater. Chem. C*, **9**, 3122 (2021)
213. S.G.Zybtsev, V.Y.Pokrovskii, V.F.Nasretdinova, S.V.Zaitsev-Zotov, V.V.Pavlovskiy, A.B.Odobesco, W.W.Pai, M.W.Chu, Y.G.Lin, E.Zupanič, H.J.P.van Midden, S.Šturm, E.Tchernychova, A.Prodan, J.C.Bennett, I.R.Mukhamedshin, O.V.Chernysheva, A.P.Menushenkov, V.B.Loginov, B.A.Loginov, A.N.Titov, M.Abdel-Hafiez. *Phys. Rev. B Condens. Matter*, **95**, 035110 (2017)
214. H.Requardt, F.Y.Nad, P.Monceau, R.Currat, J.E.Lorenzo, S.Brazovskii, N.Kirova, G.Grübel, C.Vettier. *Phys. Rev. Lett.*, **80**, 5631 (1998)
215. T.Sambongi, K.Tsutsumi, Y.Shiozaki, M.Yamamoto, K.Yamaya, Y.Abe. *Solid State Commun.*, **22**, 729 (1977)
216. J.Yang, Y.Q.Wang, R.R.Zhang, L.Ma, W.Liu, Z.Qu, L.Zhang, S.L.Zhang, W.Tong, L.Pi, W.K.Zhu, C.J.Zhang. *Appl. Phys. Lett.*, **115**, 033102 (2019)
217. A.Smontara, Z.Vučic, J.L.De Boer, J.Mazuer, F.Levy, K.Biljaković. *Synth. Met.*, **70**, 1299 (1995)
218. M.Maki, M.Kaiser, A.Zettl, G.Grüner. *Solid State Commun.*, **46**, 497 (1983)
219. R.Peierls, R.E.Peierls. In *Quantum Theory of Solids*. (Oxford: Oxford University Press, 1955). P. 227
220. D.Kartoon, U.Argaman, G.Makov. *Phys. Rev. B Condens. Matter*, **98**, 165429 (2018)
221. P.Monceau. *Adv. Phys.*, **61**, 325 (2012)
222. J. Rouxel. *Crystal Chemistry and Properties of Materials with Quasi-One-Dimensional Structures: A Chemical and Physical Synthetic Approach*. Vol. 5. (Ed. J. Rouxel). (Dordrecht: Springer, 2012). P. 1
223. A.A.Balandin, F.Kargar, T.T.Salguero, R.K.Lake. *Mater. Today*, **55**, 74 (2022)
224. L.-M.Wu, D.-K.Seo. *J. Am. Chem. Soc.*, **126**, 4676 (2004)
225. Z.Lin, M.Mao, C.Yang, Y.Tong, Q.Li, J.Yue, G.Yang, Q.Zhang, L.Hong, X.Yu, L.Gu, Y.-S.Hu, H.Li, X.Huang, L.Suo, L.Chen. *Sci. Adv.*, **7**, eabg6314 (2021)
226. M.Mao, C.Yang, Z.Lin, Y.Tong, Q.Zhang, L.Gu, L.Hong, L.Suo, Y.-S.Hu, H.Li, X.Huang, L.Chen. *JACS Au*, **1**, 1266 (2021)
227. V.Q.Dang, K.Al-Ali. *New J. Chem.*, **44**, 7583 (2020)
228. A.Sakuda, N.Taguchi, T.Takeuchi, H.Kobayashi, H.Sakaebe, K.Tatsumi, Z.Ogumi. *ECS Electrochem. Lett.*, **3**, A79 (2014)
229. S.Jeong, D.Yoo, J.-t. Jang, M.Kim, J. Cheon. *J. Am. Chem. Soc.*, **134**, 18233 (2012)
230. S.Stonemeyer, J.D.Cain, S.Oh, A.Azizi, M.Elasha, M.Thiel, C.Song, P.Ercius, M.L.Cohen, A.Zettl. *J. Am. Chem. Soc.*, **143**, 4563 (2021)
231. S.Stonemeyer, M.Dogan, J.D.Cain, A.Azizi, D.C.Popple, A.Culp, C.Song, P.Ercius, M.L.Cohen, A.Zettl. *Nano Lett.*, **22**, 2285 (2022)
232. J.C.Wildervanck, F.Jellinek. *Z.Anorg. Allg. Chem.*, **328**, 309 (1964)
233. G.F.Khudorozhko, I.P.Asanov, L.N.Mazalov, É.A.Kravtsova, G.K.Parygina, V.E.Fedorov, Y.V.Mironov. *J. Struct. Chem.*, **35**, 823 (1994)
234. K.S.Liang, S.P.Cramer, D.C.Johnston, C.H.Chang, A.J.Jacobson, J.P.deNeufville, R.R.Chianelli. *J. Non-Cryst. Solids*, **42**, 345 (1980)
235. C.-H.Lee, S.Lee, G.-S.Kang, Y.-K.Lee, G.G.Park, D.C.Lee, H.-I.Joh. *Appl. Catal., B*, **258**, 117995 (2019)
236. D.M.Schleich, M.J. Martin. *J. Solid State Chem.*, **64**, 359 (1986)
237. D.M.Schleich, H.S.Chang, Y.L.Barberio, K.J. Hanson. *J. Electrochem. Soc.*, **136**, 3274 (1989)
238. R.J.H.Voorhoeve, H.B.M.Wolters. *Z.Anorg. Allg. Chem.*, **376**, 165 (1970)
239. W.Fan, M.Jiang, G.Liu, W.Weng, J. Yang, X.Yao. *ACS Appl. Mater. Interfaces*, **14**, 17594 (2022)
240. O.Mabayoje, B.R.Wygant, M.Wang, Y.Liu, C.B.Mullins. *ACS Appl. Energy Mater.*, **1**, 4453 (2018)
241. A.B.Salem, A.Meerschaut, L.Guemas, J. Rouxel. *Mater. Res. Bull.*, **17**, (1982)
242. F.A.Trumbore, L.W.Ter Haar. *Chem. Mater.*, **1**, 490 (1989)
243. S.Artemkina, E.Grayfer, M.Ivanova, A.Y.Ledneva, A.Poltarak, P.Poltarak, S.Yarovoi, S.Kozlova, V.Fedorov. *J. Struct. Chem.*, **63**, 1079 (2022)
244. J.Murray. *Bull Alloy Phase Diagr.*, **7**, 156 (1986)
245. A.Bensalem, D.M.Schleich. *Mater. Res. Bull.*, **23**, 857 (1988)
246. H.S.W.Chang, D.M.Schleich. *J. Solid State Chem.*, **100**, 62 (1992)
247. E.Y.Oganesova, E.G.Bordubanova, A.S.Lyadov, O.P.Parenago. *Pet. Chem.*, **59**, 1028 (2019)
248. M.N.Kozlova, S.B.Artemkina, T.Y.Podlipskaya, N.A.Nebogatikova, M.R.Das, V.E.Fedorov. *Russ. Chem. Bull.*, **66**, 963 (2017)
249. V.Nicolosi, M.Chhowalla, M.G.Kanatzidis, M.S.Strano, J.N.Coleman. *Science*, **340**, 1226419 (2013)
250. C.Backes, T.M.Higgins, A.Kelly, C.Boland, A.Harvey, D.Hanlon, J.N.Coleman. *Chem. Mater.*, **29**, 243 (2017)
251. L.Niu, J.N.Coleman, H.Zhang, H.Shin, M.Chhowalla, Z.Zheng. *Small*, **12**, 272 (2016)
252. E.D.Grayfer, V.G.Makotchenko, A.S.Nazarov, S.-J.Kim, V.E.Fedorov. *Russ. Chem. Rev.*, **80**, 751 (2011)
253. E.D.Grayfer, M.N.Kozlova, V.E.Fedorov. *Adv. Colloid Interface Sci.*, **245**, 40 (2017)
254. Y.Lin, J.W.Connell. *Nanoscale*, **4**, 6908 (2012)
255. D.S.Muratov, A.R.Ishteev, D.A.Lypenko, V.O.Vanyushin, P.Gostishev, S.Perova, D.S.Saranin, D.Rossi, M.Auf der Maur, G.Volonakis, F.Giustino, P.O.Å.Persson, D.V.Kuznetsov, A.Sinitskii, A.Di Carlo. *ACS Appl. Mater. Interfaces*, **11**, 48021 (2019)

256. A.Jawaid, D.Nepal, K.Park, M.Jespersen, A.Qualley, P.Mirau, L.F.Drummy, R.A.Vaia. *Chem. Mater.*, **28**, 337 (2016)
257. L.Muscuso, S.Cravanzola, F.Cesano, D.Scarano, A.Zecchina. *J. Phys. Chem. C*, **119**, 3791 (2015)
258. J.T.Han, J.I.Jang, H.Kim, J.Y.Hwang, H.K.Yoo, J.S.Woo, S.Choi, H.Y.Kim, H.J.Jeong, S.Y.Jeong, K.-J.Baeg, K.Cho, G.-W.Lee. *Sci. Rep.*, **4**, 5133 (2014)
259. X.Yu, M.S.Prévot, K.Sivula. *Chem. Mater.*, **26**, 5892 (2014)
260. A.A.Poltarak, V.A.Logvinenko, A.N.Enyashin, S.B.Artemkina, P.A.Poltarak, M.N.Ivanova, E.D.Grayfer, V.E.Fedorov. *J. Alloys Compd.*, **851**, 156705 (2021)
261. E.V.Formo, J.A.Hachtel, Y.Ghafouri, M.A.Bloodgood, T.T.Salguero. *Chem. Mater.*, **34**, 279 (2022)
262. Z.Tian, X.Guo, D.Wang, D.Sun, S.Zhang, K.Bu, W.Zhao, F.Huang. *Adv. Funct. Mater.*, **30**, 2001286 (2020)
263. Z.Tian, C.Han, Y.Zhao, W.Dai, X.Lian, Y.Wang, Y.Zheng, Y.Shi, X.Pan, Z.Huang, H.Li, W.Chen. *Nat. Commun.*, **12**, 2039 (2021)
264. A.Müller, E.Krickemeyer, H.Bögge, H.Ratajczak, A.Armatage. *Angew. Chem., Int. Ed. Engl.*, **33**, 770 (1994)
265. A.Muller, V.Fedin, K.Hegetschweiler, W.Amrein. *J. Chem. Soc., Chem. Commun.*, **24**, 1795 (1992)
266. A.Mueller, R.Jostes, W.Eltzner, C.Nie, E.Diemann, H.Boegge, M.Zimmermann, M.Dartmann, U.Reinsch-Vogell. *Inorg. Chem.*, **24**, 2872 (1985)
267. A.Muller, E.Diemann, E.Krickemeyer, H.J.Walberg, H.Bogge, A.Armatage. *Eur. J. Solid State Inorg. Chem.*, **30**, 565 (1993)
268. S.Artemkina, A.Poltarak, P.Poltarak, E.Grayfer, D.Samsonenko, V.Fedorov. *Inorg. Chim. Acta*, **512**, 119875 (2020)
269. M.Arsentev, A.Missyul, A.V.Petrov, M.Hammouri. *J. Phys. Chem. C*, **121**, 15509 (2017)
270. H.Qin, Z.Yang, L.Chen, X.Chen, L.Wang. *J. Mater. Chem. A*, **6**, 23757 (2018)
271. Q.Zhu, Q.Xiao, B.Zhang, Z.Yan, X.Liu, S.Chen, Z.Ren, Y.Yu. *J. Mater. Chem. A*, **8**, 10761 (2020)
272. L.Luo, B.Zhao, B.Xiang, C.-M.Wang. *ACS Nano*, **10**, 1249 (2016)
273. K.Yamaya, T.H.Geballe, J.V.Acrivos, J.Code. *Physica B+C*, **105**, 444 (1981)
274. V.B.Preobrazhensky, M.V.Kolkunov. *Synth. Met.*, **43**, 3999 (1991)
275. M.Elgaml, S.J.Cassidy, S.J.Clarke. *J. Solid State Chem.*, **314**, 123436 (2022)
276. P.Afanasiev, H.Jobic, C.Lorentz, P.Leverd, N.Mastubayashi, L.Piccolo, M.Vrinat. *J. Phys. Chem. C*, **113**, 4139 (2009)
277. M.S.Whittingham. *Solid State Ion.*, **134**, 169 (2000)
278. B.Li, D.Xia. *Adv. Mater.*, **29**, 1701054 (2017)
279. J.Wu, D.Wang, H.Liu, W.-M.Lau, L.-M.Liu. *RSC Adv.*, **5**, 21455 (2015)
280. M.H.Lindic, H.Martinez, A.Benayad, B.Pecquenard, P.Vinatier, A.Levasseur, D.Gonbeau. *Solid State Ion.*, **176**, 1529 (2005)
281. H.Ye, L.Ma, Y.Zhou, L.Wang, N.Han, F.Zhao, J.Deng, T.Wu, Y.Li, J.Lu. *Proc. Natl. Acad. Sci. USA*, **114**, 13091 (2017)
282. K.Yao, M.Wu, D.Chen, C.Liu, C.Xu, D.Yang, H.Yao, L.Liu, Y.Zheng, X.Rui. *Chem. Rec.*, **22**, e202200117 (2022)
283. D.Yang, S.Zhang, P.Yu, S.Cheng, Z.Yuan, Y.Jiang, W.Sun, H.Pan, Y.Feng, X.Rui. *Small*, 2107058 (2022)
284. S.Dey, J.Lee, S.Britto, J.M.Stratford, E.N.Keyzer, M.T.Dunstan, G.Cibin, S.J.Cassidy, M.Elgaml, C.P.Grey. *J. Am. Chem. Soc.*, **142**, 19588 (2020)
285. Z.Li, S.Ding, J.Yin, M.Zhang, C.Sun, A.Meng. *J. Power Sources*, **451**, 227815 (2020)
286. L.Xing, K.A.Owusu, X.Liu, J.Meng, K.Wang, Q.An, L.Mai. *Nano Energy*, **79**, 105384 (2021)
287. S.Chandrasekaran, L.Yao, L.Deng, C.Bowen, Y.Zhang, S.Chen, Z.Lin, F.Peng, P.Zhang. *Chem. Soc. Rev.*, **48**, 4178 (2019)
288. A.B.Laursen, S.Kegnaes, S.Dahl, I.Chorkendorff. *Energy Environ. Sci.*, **5**, 5577 (2012)
289. A.Grimaud, W.T.Hong, Y.Shao-Horn, J.M.Tarascon. *Nat. Mater.*, **15**, 121 (2016)
290. E.A.Kozlova, V.N.Parmon. *Russ. Chem. Rev.*, **86**, 870 (2017)
291. X.Chen, S.Shen, L.Guo, S.S.Mao. *Chem. Rev.*, **110**, 6503 (2010)
292. T.Hisatomi, J.Kubota, K.Domen. *Chem. Soc. Rev.*, **43**, 7520 (2014)
293. O.Gorochov, A.Katty, N.Le Nagard, C.Levy-Clement, D.M.Schleich. *Mater. Res. Bull.*, **18**, 111 (1983)
294. A.M.Redon. *Electrochim. Acta*, **30**, 1365 (1985)
295. K.S.Ranjith, T.Uyar. *J. Mater. Chem. A*, **5**, 14206 (2017)
296. M.Barawi, I.J.Ferrer, E.Flores, S.Yoda, J.R.Ares, C.Sánchez. *J. Phys. Chem. C*, **120**, 9547 (2016)
297. M.Keerthana, N.K.Chandar. *Diamond Relat. Mater.*, **129**, 109353 (2022)
298. J.Singh, P.Sharma, N.Tripathi, D.Shishkina, A.Rymzhina, E.A.Boltov, V.Platonov, V.Pavelyev, V.S.Volkov, A.V.Arsenin, R.Singh, R.K.Soni, M.Talib, S.Manzoor, D.Banerjee, P.M.Z.Hasan, A.Alshahrie, R.Darwesh, M.A.Anikina, P.Mishra. *Catal. Commun.*, **162**, 106381 (2022)
299. S.Artemkina, A.Poltarak, P.Poltarak, I.Asanov, V.Fedorov. *Adv. Sci. Technol. Eng. Syst.*, **4**, 165 (2019)
300. A.Krieger, M.Wagner, S.Haschke, C.Kröckel, J.Bachmann, F.Hauke, A.Hirsch, F.Gröhn. *Nanoscale*, **12**, 22952 (2020)
301. K.S.Subrahmanyam, D.Sarma, C.D.Malliakas, K.Polychronopoulou, B.J.Riley, D.A.Pierce, J.Chun, M.G.Kanatzidis. *Chem. Mater.*, **27**, 2619 (2015)
302. D.Liu, B.Li, J.Wu, Y.Liu. *Environ. Chem. Lett.*, **19**, 1395 (2021)
303. J.Mei, C.Wang, L.Kong, X.Liu, Q.Hu, H.Zhao, S.Yang. *Environ. Sci. Technol.*, **53**, 4480 (2019)
304. A.S.Golub, Y.V.Zubavichus, Y.L.Slovokhotov, Y.N.Novikov. *Russ. Chem. Rev.*, **72**, 123 (2003)